UNIVERSITY OF MIAMI

ENERGETICS OF THE WIND AND LOOP CURRENT-DRIVEN CIRCULATION IN THE GULF OF MEXICO

By

Benjamin Jaimes

A THESIS

Submitted to the Faculty
of the University of Miami
in partial fulfillment of the requirements for
the degree of Master of Science

Coral Gables, Florida

August 2005

UNIVERSITY OF MIAMI

A thesis submitted in partial fulfillment of
the requirements for the degree of
Master of Science

ENERGETICS OF THE WIND AND LOOP CURRENT-DRIVEN CIRCULATION IN THE GULF OF MEXICO

Benjamin Jaimes

Approved:

.....
Dr. Eric P. Chassignet
Committee Chair and Professor
of Meteorology and Physical Oceanography

.....
Dr. Steven G. Ullmann
Dean of the Graduate School

.....
Dr. William E. Johns
Professor
of Meteorology and Physical Oceanography

.....
Dr. Kevin D. Leaman
Professor
of Meteorology and Physical Oceanography

.....
Dr. Gustavo J. Goni
NOAA/AOML
and Adjunct faculty member at RSMAS/UM

.....
Dr. Laurent M. Chérubin
RSMAS/UM

JAIMES, BENJAMIN (M.S., Meteorology and Physical Oceanography)

Energetics of the wind and Loop Current-driven circulation in the Gulf of Mexico

(August 2005)

Abstract of a thesis at the University of Miami.

Thesis supervised by Professor Eric P. Chassignet.
No. of pages in text (128)

The main objective of this thesis is to study the role of the wind and the Loop Current (LC) in driving the circulation of the Gulf of Mexico (GOM). To this end, the dynamical adjustment under the influence of the two forcing mechanisms is investigated for the western GOM in terms of eddy-mean flow interactions. The subject is approached from an energetic point of view, thus model outputs from the Miami Isopycnic Coordinate Ocean Model (MICOM) are decomposed into eulerian mean and eddy components, and their interaction is investigated in the energy domain. The model outputs come from a high-resolution, wind-forced simulation of the North Atlantic, which includes the GOM. This experiment incorporates the basin-scale variability into the Gulf through the Yucatan Channel, which enables to reproduce realistic dynamics within the GOM. This choice, however, imposes the computation of energy transfers in open domains. Since the conventional definition of the barotropic transfer terms cannot be applied directly in open systems because the two barotropic terms differ by the divergence of Reynolds stress, which only vanishes upon volume integration over the whole domain, the divergence term is incorporated to the definition of an energy scheme that enables to investigate eulerian "eddy, time-mean" interactions in isopycnic open systems. The energy scheme is investigated in an idealized numerical experiment, in which a steady wind drives a double-gyre ocean circulation. Energetics analysis are conducted separately for each gyre to evaluate the energy scheme in open domains.

The application of the energy scheme to investigate the circulation of the western GOM in the MICOM simulation reveals that the most energetic contribution to the circulation is the boundary flux of eddy potential energy across 89W. This energy boundary flux is mostly governed by LC intrusions and westward propagation of LC eddies. Within the basin interior, baroclinic energy transfers redistribute mass horizontally, which drains the external supply of potential energy to fed the mean and eddy horizontal flows. The LC eddies are the main source of eddy kinetic energy for the western GOM, both at surface and depth. Bands of weak rectification in the mean flow are driven in surface and sub-surface waters by the fluctuating pressure field along the margins of the GOM. However, the boundary mean flows are mostly increased in response to the pressure field created by those perturbations, rather than by energy supply. The Western Boundary Current (WBC) along the Mexican coast is mostly driven at surface and sub-surface waters by a perturbation pressure field sustained by the recirculating Western Anticyclone, which apparently is sustained by incoming LC rings, rather than by inertial dynamics. The Sverdrup balance indicates that the wind-driven return flow at the WBC represents about 64% of the net return transport in the model. At deeper waters, perturbations with characteristics of topographic Rossby waves (TRWs) are superimposed on the background flow, and the energy exchange between the two flow forms is not apparent. Therefore, TRWs cannot be accounted for driving the mean deep cyclonic flow in the model.

Acknowledgments

I would like to thank my advisor, Dr. Eric Chassignet, for his advice and for having given me the freedom to pursue my research interest.

I thank Dr. William E. Johns, Dr. Kevin D. Leaman, Dr. Gustavo J. Goni, and Dr. Laurent M. Chérubin for serving in the committee and providing considerable discussions and beneficial suggestions.

Financial support for this work was provided by the Fulbright-García Robles Commission, Consejo Nacional de Ciencia y Tecnología, Instituto Politecnico Nacional, and the National Science Foundation.

Finally, I thank my wife Sandra, my children Andrea and Victor Alexander, and my parents Clemente and Casimira, to whom this work is dedicated for their love an support.

Contents

List of Figures

Chapter 1

Introduction

1.1 Role of the Loop Current in driving the Gulf of Mexico circulation

The Gulf of Mexico (GOM) is a semi-enclosed sea, which connects with the Caribbean Sea through the Yucatan Channel and with the North Atlantic Ocean through the Florida Straits. The circulation in the basin is forced at the sea surface by the frictional stress of the wind (and in less degree by heat and freshwater fluxes), and at the Yucatan Channel by the North Atlantic Western Boundary Current System (NAWBCS), where most of the Sverdrup type transport of the North Atlantic Subtropical Gyre merges with the Meridional Overturning Circulation [*Schmitz and Richardson*, 1991], yielding a net average flux of 23.8 $\pm$1 Sv [*Sheinbaum et al.*, 2002].

The baroclinic structure of the NAWBCS within the Channel consists of the Yucatan

Current flowing into the Gulf of Mexico in upper western layers, the southerly Yucatan Counter-current beneath it, and two southerly jets on the Cuban side, one at surface and another at depth [*Sheinbaum et al.*, 2002]. In surface waters (upper 800-900 m) the Yucatan Current spreads into the southeastern Gulf, forming an anticyclonic-looping and pulsating circulation: the Loop Current (LC), the regional component of the NAWBCS and principal current within the Gulf of Mexico. The LC leaves the basin across the Florida Straits, becoming the Florida Current and then the Gulf Stream.

The transport through the Yucatan Channel has historically been recognized as the dominant mechanism driving the circulation in the Gulf. *Hurlburt and Thompson* [1980, 1982] conducted a series of idealized numerical experiments and showed for the first time that even a prescribed steady transport at the Channel, used as the only forcing, is able to induce the distinctive circulation features observed in the basin, including a realistic Loop Current cycle, consisting of an extensive northwestward intrusion followed by the shedding of an anticyclonic mesoscale vortex (Loop Current ring, LCR), and the return to the so called port-to-port configuration (direct path from the Yucatan Channel to the Florida Straits). However, the shedding exhibited an unrealistic quasi-annual regularity. In reality the LC cycle is strongly variable, with recurrent shedding events at peak periods from 6 to 11 months [*Sturges and Leben*, 2000], and frequent ring detachments and reattachments during the separation sequence [*Sturges and Leben*, 2000; *Oey et al.*, 2003]. The Loop Current cycle has been associated to dynamic variability in the Yucatan Channel [i.e. *Cochrane*, 1966; *Maul*, 1977; *Hurlburt and Thompson*, 1980, 1982; *Oey*, 1996; *Schmitz*, 1996; *Bunge et al.*, 2002; *Candela et al.*, 2002; *Sheinbaum et al.*, 2002], the Caribbean Sea [*Oey et al.*, 2003], and the Atlantic Ocean [*Murphy et al.*, 1999], to a geographic control imposed by the

Florida Straits [*Pichevin and Nof*, 1997; *Nof and Pichevin*, 2001], and more recently to a combination of the geographic control by the Florida Straits and the growth of cyclones in the deep layers beneath the LC [*Chérubin et al.*, 2005].

1.1.1 Driving of surface waters

That the LC influence can extend beyond regions under the direct path of the current was first noticed by *Ichiye* [1962], who posed the hypothesis that the anticyclonic surface circulation observed in the western GOM resulted from migrating LC rings reaching the coast and decaying there. *Elliot* [1979, 1982] provided additional elements to support *Ichiye*'s hypothesis, and several authors have reported the collision of the rings with the western continental slope-rise, where smaller mesoscale cyclonic and anticyclonic circulations originate impacting the local circulation in any season [i.e. *Brooks and Legekis*, 1982; Merrell and Vásquez, 1983; *Lewis and Kirwan*, 1985; *Smith*, 1986; *Vidal et al.*, 1992]. The interaction of LC–induced eddies with the topography might play a significant role in driving the observed Western Boundary Current (WBC) along the Mexican shelf [*Vidal et al.*, 1999], competing with the wind influence posed by *Sturges and Blaha* [1976] and *Sturges* [1993], who proposed a wind-driven Gulf of Mexico circulation analogous to that of the North Atlantic Ocean. This competition could extend to the Bay of Campeche, where a semi-permanent mesoscale cyclonic circulation is observed. Some authors suggest that this feature maybe due to local wind forcing [*Molinari*, 1978; *Vázquez de la Cerda*, 1993], though a similar structure develops in numerical models of the Gulf forced with no wind [*Oey and Lee*, 2002].

1.1.2 Driving of deep waters

But the LC cycle also affects the deep circulation of the Gulf of Mexico. Most of the numerical models [see for example *Hurlburt and Thompson*, 1980, 1982; *Sturges et al.*, 1993; *Welsh and Inoue*, 2000; *Romanou et al.*, 2004] produce a cyclone-anticyclone pair or modon [*Hurlburt and Thompson*, 1980] in deep waters underneath the LC, apparently developed during the initial stage of LCR westward-propagation. *Cushman-Roisin et al.* [1990] discuss how a similar deep structure comes out in a 2-layer idealized model in response to a non-uniform distribution of relative vorticity induced in the lower layer by a westward-propagating upper layer anticyclone in the β-plane. *Welsh and Inoue* [2000] found the modon to be guided by the bottom bathymetry as it migrates westward in tandem with the surface LCR. *Romanou et al.* [2004] report that most of the deep cyclonic eddies associated with the surface LC rings end up in the Campeche Bank. In the literature, however, there are few descriptions of the Gulf's deep circulation based on observations, and the consensus is that the global circulation reverses from anticyclonic in surface layers (where the anticyclonic signatures of the LC and LC rings dominate) to cyclonic in deep waters. *Hofmann and Worley* [1986] used an inverse technique to compute geostrophic currents from data collected during several oceanographic cruises, and inferred a deep cyclonic gyre with bottom intensification in the western GOM opposing the anticyclonic upper layer circulation. *Wienders et al.* [2004] analyzed Lagrangian observations of 17 PALACE (Profiling Autonomous Lagrangian Circulation Experiment) floats deployed during 1998-2002 at 900 m depth, and found a tendency for a cyclonic flow along the continental margin of the Gulf of Mexico that is intensified in the Bay of Campeche. Lately, *DeHaan and Sturges* [2004]

using geostrophic currents from historical *in situ* data found a mean cyclonic flow below 1000 m. Nevertheless, this conclusion was achieved with very weak mean speeds though the individual velocities are strong, yielding a very small signal-to-noise ratio. Recent model comparison studies support the hypothesis of mean cyclonic flow at mid– and deep waters [*Sturges et al.*, 2004], though the contribution of the LC and its eddies to the onset of the deep cyclonic flow is unknown.

1.1.3 The Loop Current as a wave-maker

That the Loop Current cycle acts as a wave-maker in the Gulf of Mexico has not explicitly been investigated, thus only a few studies have documented the adjustment in inner Gulf regions in response to the low-frequency horizontal redistribution of mass caused by LC eddy processes. *Hurlburt and Thompson* [1980, 1982] reported high correlation between LCR westward propagation and the first internal Rossby wave speed. *Hamilton* [1990] analyzing direct measurements of currents below 1000 m in the northeastern, central and western Gulf of Mexico found deep low-frequency fluctuations highly coherent in the vertical, exhibiting bottom intensification and westward energy propagation consistent with characteristics of topographic Rossby waves (TRWs); he suggested that major sources for these waves are the fluctuations of the Loop Current, with the most energetic events being generated during eddy shedding periods. *Oey* [1996] using a numerical model found a baroclinic Rossby basin mode at the period of about 400 days, suggesting radiation of Rossby waves by migrating LCR and LC pulsations. *Oey and Lee* [2002] using a ray-tracking technique based on the TRWs dispersion relation found that east of 91° W the source of eddy

kinetic energy in the GOM comes from the LC and the LCR shedding region, while over the western GOM additional source is from the southwestward-propagating LCR. The ray calculations of *Oey and Lee* [2002] also suggest that energy sources for TRWs are from short-scale propagating meanders (wavelengths ∼100 to 200 km and periods <100 days) around the LC and LC rings. *Sturges et al.* [2004] propose that TRWs, through a rectification process, might be one of the processes inducing the mean cyclonic circulation observed in mid– and deep waters in the Gulf.

1.2 Scope of this thesis

In summary, the Loop Current cycle predominantly influences the surface flows observed in the Gulf of Mexico, including the anticyclonic circulation associated to the LC northwestward extension in the eastern Gulf, and the anticyclonic circulation in the western region where the LC rings decay. There, the LC eddies compete with the wind in driving the WBC along the Mexican shelf and the Bay of Campeche Cyclone. Through vortex stretching and Reynolds stress, the LC extends its influence into intermediate and deep waters, where planetary and topographic Rossby waves, together with other mesoscale transient vortices (westward-propagating LC rings, modons, and cyclones) represent the low-frequency, LC-driven eddy variability that comes out during the adjustment process. A great deal of uncertainty exists, however, about the role of the LC eddies (vortex- or wave-like) on driving regional mean flows, the role of the LC in the Gulf of Mexico energy cycle, and the relative contribution of the wind in this cycle. With the aim of providing some insight on these topics, the main objective of this thesis is to investigate the differential energetic

adjustment in Gulf of Mexico interior regions in response to the LC cycle and the wind stress. The investigation focuses on the nature of the kinetic energy levels in GOM regional mean flows. In particular, in this thesis the following questions are addressed:

- What are the characteristics of the wind and Loop Current energy inputs into the Gulf of Mexico, and what is their relative contribution to the Gulf mean circulation?
- What are the energy sources and sinks, and energy fluxes and transfers building up the energy levels in the mean flow, and what is their nature?

These questions represent important issues to understand leading processes distributing mass, heat, momentum, and dissolved and suspended material throughout the Gulf. Moreover, the relevance of this topic to the climatology of Southeastern North America is through the role of the Gulf of Mexico in regulating the regional climate.

Eddy-mean flow interaction is an important part of this investigation and can be addressed with mesoscale resolution numerical general ocean circulation experiments since the numerical models resolve the main mesoscale circulation features and provide the needed temporal coverage for the oceanic mean fields to be statistically significant. Therefore, to accomplish the goals of this thesis, the Gulf of Mexico circulation is decomposed in eulerian mean (time average at fixed points) and perturbation fields (departure from the time mean) using model outputs from a wind-forced, high-resolution, MICOM isopycnic simulation of the North Atlantic Ocean, which includes the Gulf of Mexico. The main advantage of this experiment is that it incorporates the basin-scale variability into the Gulf through the Yucatan Channel. This choice, however, imposes the computation of energy conversions in open domains, because the GOM has two open boundaries that connect it with the rest

of the computational domain. The computation of energy conversions in open domains is complicated due to the fact that the mathematical expressions widely used to represent barotropic energy transfer do not cancel in open systems, thus they cannot account for energy conversion [*Rhines*, 1977; *Harrison and Robinson*, 1978]. Since the physics of the energy cycle is a central issue that must be understood before discussing the eulerian eddy-mean flow interactions within the Gulf of Mexico, it is important to present the energy cycle in idealized open and closed domains, and discuss some advantages and limitations of our current formalism in regards to eddy-mean flow interactions in the energy domain.

The outline of this thesis is as follows. In chapter 2 the formalism to investigate the eulerian energetics in open domains is introduced. First, the equation of total energy is analyzed to explain similarities and differences in the energetics in closed and open systems. The energy scheme to be investigated is defined as well. Next, the energy scheme is evaluated and discussed in terms of a numerical experiment in which a square ocean is driven by steady wind.

Using the energy scheme defined in chapter 2, the role of the Loop Current eddy processes on driving Gulf of Mexico regional mean flows is investigated in chapters 3, 4, and 5. First, in chapter 3 the numerical experiment of the North Atlantic Ocean used to obtain eulerian mean and fluctuating flows for the Gulf of Mexico circulation is described; the processing of model outputs is discussed as well. Next, in section 4 the first question is addressed by investigating the energy input into the western Gulf of Mexico due to the wind stress and the boundary fluxes across 89W. A discussion of the Sverdrup and model transport across 25N along the western boundary current is presented as well. Chapter 5

focuses on the second question. Thus the energy cycle in the whole GOM basin, and the energy pathways in different regions are investigated in terms of the prototype energy scheme. The nature of the eddies in the Gulf of Mexico, as rectification or dissipative processes, is clarified. Finally, in chapter 6 the conclusions of this investigation are presented.

Chapter 2

Energetics in open domains

2.1 Introduction

The problem of eddy-driven mean flows in the ocean has been investigated theoretically [*Rhines and Holland*, 1979], but mainly in the context of mesoscale resolution numerical general ocean circulation experiments [for example *Holland and Lin*, 1975; *Robinson et al.*, 1977; *Böning and Budich*, 1992]. A fundamental step for addressing the problem is the decomposition of the flow in mean and eddy components, in the classical Reynolds sense, which allows investigating the nature of the average flows, the effects of the perturbation motions on the mean, and the interactions between both flow forms. Given the complexity of the problem, substantial averaging in time and space is typically carried out over the total extent of the computational domain, and a single energy budget summarizes the full system dynamics. This approach, however, is prone to produce energy budgets that might

not represent any regional flow within the domain. Moreover, it might neutralize important dynamics as a result of the averaging procedure.

With the purpose of understanding the spatial inhomogeneity of a turbulent flow, *Harrison and Robinson* [1978] (HR78 from now on) investigated mean turbulent kinetic energy budgets over arbitrary open regions, and they concluded that the interpretation of open regional energy budgets is complicated by the fact that the interaction of Reynolds stresses with the mean flow does not generally produce conversion of energy between the mean flow and the eddy flow (barotropic conversion), as it does in a closed region. HR78 arrived at that conclusion after examining the barotropic interaction terms, which should couple the equation of kinetic energy of the mean flow (KM) with the equation of mean kinetic energy of the eddy flow (KE). HR78 obtained the following energy interaction terms in their equations 1a and 1b:

$$+\overline{u}_\lambda \frac{\partial}{\partial x_j} \overline{u'_j u'_\lambda} \tag{2.1}$$

$$+\overline{u'_\lambda u'_j} \frac{\partial \overline{u}_\lambda}{\partial x_j} \tag{2.2}$$

where equations (2.1) and (2.2) are the barotropic interaction terms in the KM and KE equations, respectively, $\lambda = 1, 2$, and $j = 1, 2, 3$. After using a mathematical identity and integrating over a volume of fluid, HR78 derived the following expression from equations (2.1) and (2.2):

$$\rho_0 \int_V \frac{\partial}{\partial x_j} \left(\overline{u'_\lambda u'_j} \overline{u}_\lambda \right) dV = \rho_0 \int_V \overline{u}_\lambda \frac{\partial}{\partial x_j} \overline{u'_j u'_\lambda} \, dV + \rho_0 \int_V \overline{u'_\lambda u'_j} \frac{\partial \overline{u}_\lambda}{\partial x_j} \, dV. \tag{2.3}$$

Equation (2.3) shows that upon volume integration over the whole domain the left side vanishes and, in consequence, the two barotropic interaction terms are equal and opposite,

representing an energy conversion process. Obviously, in an open domain (subregion), the left side does not necessarily vanish, and this is the principal argument for HR78 to conclude that in an open system the barotropic conversion might or might not exist, depending on the magnitude and sign of equations (2.1) and (2.2). In consequence, HR78 introduced a method to investigate subregional energetics, in which they define three types of regions in terms of the barotropic interaction terms: region type 1, where the interaction terms act roughly like a regional conversion process [equations (2.1) and (2.2) opposite and approximately equal]; region type 2, where the interaction terms does not act like a regional conversion process, but can be neglected compared to other terms in the equations; and region type 3, where the interaction terms does not act like a regional conversion process and cannot be neglected compared to other interaction terms. Moreover, *Rhines* [1977] discusses that the barotropic conversion terms written as in (2.1) and (2.2) do not satisfy the conventional definition of energy conversion, which states that the terms must be equal and opposite in their mathematical form. In fact *Rhines* [1977] noticed that (2.1) and (2.2) differ by a divergence, $\partial/\partial x_j \left(\overline{u'_\lambda u'_j}\overline{u}_\lambda\right)$, which vanishes upon integration over the whole domain, but it has to be taken into account in the investigation of energetics in open systems.

It seems pertinent therefore to review the energy cycle in closed and open domains to identify the energetic difference between the two systems, and to define an energy scheme suitable to investigate "eddy, time-mean" (ETM) interactions in open isopycnic systems by considering the mathematical transformation in equation (2.3). With these goals in mind, in the first section of this chapter we discuss the equation of conservation of total energy in closed and open systems. Next, the energy scheme to investigate the ETM interaction in isopycnic open systems is defined and discussed. Then, the energy scheme is evaluated in

an idealized numerical experiment in which an isopycnic two-layer square ocean is spun-up by a steady wind.

2.2 Total energy in closed and open systems

In general, conservation of total energy (E) is given by

$$\frac{DE}{Dt} = F + D, \tag{2.4}$$

where F and D stand for energy sources and sinks, respectively. Neglecting internal energy, $E = K + P$, where K is kinetic energy and P is gravitational potential energy. If the system is inviscid and adiabatic, or if the energy sources and sinks balance, total energy is conserved ($DE/Dt = 0$).

The conventional procedure to investigate eddy-mean flow interactions consists of decomposing the velocity, density, temperature, and pressure fields in (2.4) into mean and eddy components, and then applying a spatial or temporal averaging operator to the resulting set of equations, which produces

$$\frac{\partial E}{\partial t} = -\nabla \cdot (\mathbf{v}E) + C(E) + F(E) + D(E) \tag{2.5}$$

where,

$$E = KM + KE + PM + PE. \tag{2.6}$$

PM and PE stand respectively for the mean and eddy gravitational potential energy, and

the terms in the right side of (2.5) are respectively the sum of energy divergences (dot product), energy conversions (C), energy sources (F), and energy sinks (D) within the full system. If the system is closed, inviscid, and adiabatic (or unforced), then (2.5) becomes

$$\frac{\partial E}{\partial t} + C(E) = 0. \tag{2.7}$$

Therefore, in the absence of local and external energy sources/sinks, energy is conserved ($\partial E/\partial t = 0$) only if the sum of the conversion terms vanishes, that is

$$\begin{aligned} \sum C(E) \quad \equiv \quad & CKMKE - CKMKE + CPMKM - CPMKM \\ & + CPMPE - CPMPE + CPEKE - CPEKE = 0. \end{aligned} \tag{2.8}$$

where $CKMKE$ is conversion from KM to KE, $CPMKM$ is conversion from PM to KM, $CPMPE$ is conversion from PM to PE, and $CPEKE$ is conversion from PE to KE. Depending on the vertical coordinate choice, some conversions in (2.8) may vanish and new terms may arise. Equation (2.8) summarizes the formal definition of energy conversion, and is a consequence of the coupling between the four equations in which (2.5) can be expanded by using (2.6). Moreover, this statement is a requirement to guarantee that any energy form is not created or destroyed, but transformed, within the system. This is a fundamental concept that must be satisfied in any set of energy equations, whether the system is open or closed. Therefore, the statement of conservation of total energy in any system can be written as

$$\frac{\partial E}{\partial t} = -\nabla \cdot (\mathbf{v}E) + F(E) + D(E), \tag{2.9}$$

and the right hand side collects all remote and local energy sources/sinks in the system.

Some conclusions can be made on the basis of (2.9). If the system is open the local rate of change of E is given by the external supply of energy (boundary fluxes) and the imbalance between local energy sources and sinks. One interesting solution is obtained when the local imbalance of sources/sinks vanishes or is negligible compared with the other terms in the equation: the rate of change of total energy within the subregion is function only of the sum of energy boundary fluxes,

$$\frac{\partial E}{\partial t} = -\nabla \cdot (\mathbf{v}E)\,. \tag{2.10}$$

Therefore, the following statement must be satisfied for an open system to be energetically conservative in the absence or balance of local energy sources/sinks

$$\nabla \cdot (\mathbf{v}KM) + \nabla \cdot (\mathbf{v}KE) + \nabla \cdot (\mathbf{v}PM) + \nabla \cdot (\mathbf{v}PE) = 0. \tag{2.11}$$

That is, the total energy advected by the inflows must balance the total energy advected by the outflows. However, due to energy conversions within the subregion the distribution of the energy forms advected by the outflows can be very different from that advected by the outflows.

To understand the subregional energy budgets in the context of the whole systems, let A and B in Figure 2.1 be two subregions of a closed system, and E_A and E_B their respective total energy contents.

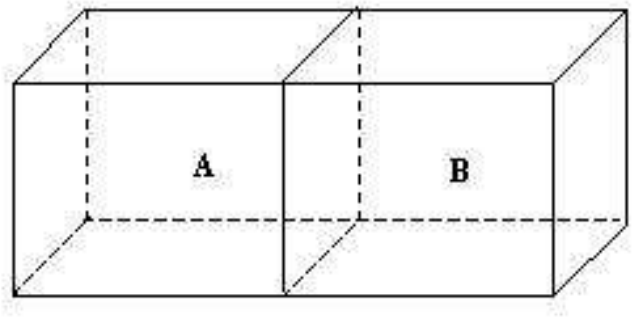

Figure 2.1: Schematics of a system split in 2 subregions.

Using (2.5) it follows that the statement of conservation of total energy in an inviscid and adiabatic, or unforced system is

$$\frac{\partial}{\partial t}\left(E_A + E_B\right) = -\nabla \cdot (\mathbf{v}E_A + \mathbf{v}E_B) + C(E_A + E_B), \tag{2.12}$$

where,

$$-\nabla \cdot (\mathbf{v}E_A) - \nabla \cdot (\mathbf{v}E_B) = 0, \tag{2.13}$$

$$C(E_A) + C(E_B) = 0. \tag{2.14}$$

That is, the energy divergence and conversion terms are equal and opposite in relation to those of the other subregion. Statement (2.14) implies that opposite physical processes must work between the two subregions to guarantee total energy conservation in the whole

system. In this scenario, the whole energy cycle is a "merry-go-round" of equal (but nonzero) conversions and flux divergences, which exactly cancel (equations 2.13 and 2.14) such that the net tendency of total energy is zero. Interesting to notice is that in this scenario of equilibrium the boundary energy exchange between the subregions cancels identically, thus the subregions look like independent closed systems. The wind-driven, double-gyre ocean experiment will help to understand how statements (2.13) and (2.14) work together to bring the whole system into a state of equilibrium.

As discussed in section 2.1, the energy interactions terms as defined in (2.1) and (2.2) do not satisfy the definition of a barotropic energy transfer in an open system [*Rhines*, 1977]. In the following section, we discuss the physics in statements (2.1), (2.2), and (2.3), and on the basis of this discussion we define an appropriate form for the barotropic transfer term to be incorporated in an energy scheme suitable to investigate ETM interactions in isopycnic closed and open systems.

2.3 Energy balance in isopycnic open systems

After *Bleck* [1985], the particular form of the system (2.5) in isopycnic coordinates including forcing and dissipation is:

$$\begin{aligned}
\underbrace{\frac{\partial}{\partial t}\left(\frac{\hat{\mathbf{v}}^2}{2}\frac{\partial \bar{p}}{\partial s}\right)}_{KM} &= \underbrace{-\nabla_s\cdot\left(\hat{\mathbf{v}}\frac{\partial \bar{p}}{\partial s}\frac{\hat{\mathbf{v}}^2}{2}\right)}_{KMDIV} \underbrace{-\hat{\mathbf{v}}\cdot\left[\nabla_s\cdot\left(\overline{\mathbf{v}'\frac{\partial p}{\partial s}\mathbf{v}'}\right)\right]}_{CKMKE} \\
&\quad \underbrace{-\nabla_s\cdot\left(\hat{\mathbf{v}}\frac{\partial \bar{p}}{\partial s}\hat{\phi}\right)}_{MPFDIV} + \underbrace{\left[\bar{\phi}\nabla_s\cdot\left(\hat{\mathbf{v}}\frac{\partial \bar{p}}{\partial s}\right)-\hat{\mathbf{v}}\cdot\frac{\partial \bar{p}}{\partial s}\hat{\alpha}\nabla_s\bar{p}\right]}_{CPMKM} \\
&\quad \underbrace{+\left[\overline{\phi^*\nabla_s\cdot\left(\frac{\partial p^*}{\partial s}\hat{\mathbf{v}}\right)}-\hat{\mathbf{v}}\cdot\overline{\frac{\partial p^*}{\partial s}\alpha\nabla_s p^*}\right]}_{CPEKM} \underbrace{-\hat{\mathbf{v}}\cdot\frac{\partial \bar{p}}{\partial s}g\frac{\partial \hat{\tau}}{\partial s}}_{MWIND} + \underbrace{\hat{\mathbf{v}}\nabla_s\cdot\left(\frac{\partial \bar{p}}{\partial s}\nu\nabla_s\hat{\mathbf{v}}\right)}_{MDIS}
\end{aligned} \tag{2.15}$$

$$\begin{aligned}
\underbrace{\frac{\partial}{\partial t}\left(\overline{\frac{\mathbf{v}'^2}{2}\frac{\partial p}{\partial s}}\right)}_{KE} &= \underbrace{-\nabla_s\cdot\left(\overline{\mathbf{v}\frac{\partial p}{\partial s}\frac{\mathbf{v}'^2}{2}}\right)}_{KEDIV} \underbrace{-\overline{\mathbf{v}'\frac{\partial p}{\partial s}\cdot(\mathbf{v}'\cdot\nabla_s)\hat{\mathbf{v}}}}_{CKEKM} \\
&\quad \underbrace{-\nabla_s\cdot\left(\overline{\mathbf{v}'\frac{\partial p}{\partial s}\phi^*}\right)}_{EPFDIV} + \underbrace{\left[\overline{\phi^*\nabla_s\cdot\left(\mathbf{v}'\frac{\partial p}{\partial s}\right)}-\overline{\mathbf{v}'\cdot\frac{\partial p}{\partial s}\alpha\nabla_s p^*}\right]}_{CPEKE} \\
&\quad \underbrace{-\overline{\mathbf{v}'\cdot\frac{\partial p}{\partial s}g\frac{\partial \tau'}{\partial s}}}_{EWIND} + \underbrace{\overline{\mathbf{v}'\nabla_s\cdot\left(\frac{\partial p}{\partial s}\nu\nabla_s\mathbf{v}'\right)}}_{EDIS}
\end{aligned} \tag{2.16}$$

$$\underbrace{\frac{\partial}{\partial t}\left(\bar{p}\hat{\alpha}\frac{\partial \bar{p}}{\partial s}\right)}_{PM} = \underbrace{-\nabla_s\cdot\left(\hat{\mathbf{v}}\frac{\partial \bar{p}}{\partial s}\bar{p}\hat{\alpha}\right)}_{PMDIV} \underbrace{-\left[\bar{\phi}\nabla_s\cdot\left(\hat{\mathbf{v}}\frac{\partial \bar{p}}{\partial s}\right)-\hat{\mathbf{v}}\cdot\frac{\partial \bar{p}}{\partial s}\hat{\alpha}\nabla_s\bar{p}\right]}_{CPMKM} \tag{2.17}$$

$$\frac{\partial}{\partial t}\underbrace{\left(\overline{p^*\alpha\frac{\partial p}{\partial s}}\right)}_{PE} = \underbrace{-\nabla_s\cdot\left(\overline{\mathbf{v}\frac{\partial p}{\partial s}p^*\alpha}\right)}_{PEDIV} \underbrace{-\left[\overline{\phi^*\nabla_s\cdot\left(\frac{\partial p^*}{\partial s}\hat{\mathbf{v}}\right)}-\hat{\mathbf{v}}\cdot\overline{\frac{\partial p^*}{\partial s}\alpha\nabla_s p^*}\right]}_{CPEKM}$$

$$\underbrace{-\left[\overline{\phi^*\nabla_s\cdot\left(\mathbf{v}'\frac{\partial p}{\partial s}\right)}-\overline{\mathbf{v}'\cdot\frac{\partial p}{\partial s}\alpha\nabla_s p^*}\right]}_{CPEKE} \tag{2.18}$$

where $s \equiv \alpha$ is the isopycnic vertical coordinate (specific density), $\mathbf{v}$ is the horizontal velocity vector, p is pressure, $\partial p/\partial s$ is the layer thickness in pressure units, $\nabla_s \equiv \partial/\partial x\,\underline{\mathbf{i}} + \partial/\partial y\,\underline{\mathbf{j}}$, $\hat{(\,)}$ denotes a temporal or spatial mass-weighted average, $(\,)'$ is the departure from the mass-weighted average, $\bar{(\,)}$ is an unweighted average, $(\,)^*$ is the departure from the unweighted average, and $\phi \equiv gz$ is the departure in density interface geopotential height respect to rest. In addition, $MWIND$ and $EWIND$ are respectively the energy inputs due to the mean and eddy wind stress acting on surface currents; $MDIS$ and $EDIS$ stand respectively for energy losses from work done by stress due to mean and eddy shears in the flow; $MPFDIV$ and $EPFDIV$ are mean and eddy geopotential flux divergencies; and $KMDIV$, $KEDIV$, $PMDIV$, and $PEDIV$ are divergence of KM, KE, PM, and PE respectively. In equations (2.15)-(2.18) all terms containing α' and $\dot{s}$ in *Bleck*'s original equations were omitted here, since they vanish in isopycnic coordinates. In this system, the only external forcing considered is wind forcing; buoyancy forcing by surface air-sea exchange is neglected.

The system of equations (2.15)-(2.18) has successfully been used to investigate eddy-mean flow interactions in closed domains [see *Chassignet and Boudra*, 1988, for an example]. However, the application of equations (2.15) and (2.16) in open systems is not straightforward, since the barotropic transfer terms in the two equations ($CKMKE$ and $CKEKM$

terms) correspond to (2.1) and (2.2) in isopycnic coordinates and do not couple the KM and KE equations as conversions terms. In both HR78 and *Bleck* [1985], the KM equation is formed by taking the scalar product of the mean velocity with the vector mean momentum equation, and the KE equation is obtained by subtracting the KM equation from that of total kinetic energy.

Rhines [1977] proposes an alternate form for the KE equation in order for the barotropic transfer term to couple the two kinetic energy equations and satisfy statement (2.8), both in closed and open systems. The method consists in using equation (2.3) to replace the barotropic transfer term in the KE equation. Therefore, in the context of *Bleck*'s equations this implies to replace

$$\underbrace{\overline{\mathbf{v}'\frac{\partial p}{\partial s}\cdot(\mathbf{v}'\cdot\nabla_s)\hat{\mathbf{v}}}}_{CKEKM} = \underbrace{\nabla_s\cdot\left(\overline{\hat{\mathbf{v}}\mathbf{v}'\frac{\partial p}{\partial s}\mathbf{v}'}\right)}_{RSFDIV} - \underbrace{\hat{\mathbf{v}}\cdot\left[\nabla_s\cdot\left(\overline{\mathbf{v}'\frac{\partial p}{\partial s}\mathbf{v}'}\right)\right]}_{CKMKE} \tag{2.19}$$

into equation (2.16), and the new form of the KE equation is

$$\begin{aligned}\frac{\partial}{\partial t}\left(\overline{\frac{\mathbf{v}'^2}{2}\frac{\partial p}{\partial s}}\right) &= -\nabla_s\cdot\left(\overline{\mathbf{v}\frac{\partial p}{\partial s}\frac{\mathbf{v}'^2}{2}}\right) - \underbrace{\nabla_s\cdot\left(\overline{\hat{\mathbf{v}}\mathbf{v}'\frac{\partial p}{\partial s}\mathbf{v}'}\right)}_{RSFDIV} + \underbrace{\hat{\mathbf{v}}\cdot\left[\nabla_s\cdot\left(\overline{\mathbf{v}'\frac{\partial p}{\partial s}\mathbf{v}'}\right)\right]}_{CKMKE} \\ &\quad -\nabla_s\cdot\left(\overline{\mathbf{v}'\frac{\partial p}{\partial s}\phi^*}\right) + \left[\overline{\phi^*\nabla_s\cdot\left(\mathbf{v}'\frac{\partial p}{\partial s}\right)} - \overline{\mathbf{v}'\cdot\frac{\partial p}{\partial s}\alpha\nabla_s p^*}\right] \\ &\quad -\overline{\mathbf{v}'\cdot\frac{\partial p}{\partial s}g\frac{\partial\tau'}{\partial s}} + \overline{\mathbf{v}'\nabla_s\cdot\left(\frac{\partial p}{\partial s}\nu\nabla_s\mathbf{v}'\right)},\end{aligned} \tag{2.20}$$

where $RSFDIV$ is the Reynolds stress flux divergence, or momentum flux divergence. Now the KM and KE equations are coupled since the barotropic terms are equal an

opposite in their mathematical form: $\pm\hat{\mathbf{v}} \cdot \left[\nabla_s \cdot \left(\overline{\mathbf{v}' \frac{\partial p}{\partial s} \mathbf{v}'}\right)\right]$. This also implies that the original perturbation flux (first term in the right side of 2.20) is altered by adding the term $RSFDIV$ which becomes the perturbation energy flux as defined by *Rhines* [1977]. The duality and inseparability of the energy transfer/flux terms has been discussed by *Plumb* [1983] among others, who on the basis of this behavior argue that energy "conversions" and "fluxes" are not particularly useful indicators of wave propagation characteristics or generation. Several observed energy conversions in wave phenomena can only be explained by analyzing the mutual evolution of the conversion and flux terms [see for example *Plumb*'s, 1983, discussion on the energetics of topographically-generated, upward-propagating quasi-geostrophic Rossby waves in a frictionless adiabatic atmosphere].

One may wonder at this point why to favor $\pm\hat{\mathbf{v}} \cdot \left[\nabla_s \cdot \left(\overline{\mathbf{v}' \frac{\partial p}{\partial s} \mathbf{v}'}\right)\right]$ to substitute the conventional form of the barotropic transfer [$CKEKM$ in equations (2.16) & (2.19)], since one could instead replace $CKMKE$ in equation (2.15). To answer this question we should rely on the physics of the two barotropic transfer terms. Since $\left(\overline{\mathbf{v}' \frac{\partial p}{\partial s} \mathbf{v}'}\right)$ represents momentum, thus $\nabla_s \cdot \left(\overline{\mathbf{v}' \frac{\partial p}{\partial s} \mathbf{v}'}\right)$ in $CKMKE$ indicates how much momentum is gained/lost. For example, if $\nabla_s \cdot \left(\overline{\mathbf{v}' \frac{\partial p}{\partial s} \mathbf{v}'}\right) < 0$ (sink of momentum) then $CKMKE < 0$ and KM increases in the absence of other energy sources/sinks [equation (2.15)]. The inverse process happens when $\nabla_s \cdot \left(\overline{\mathbf{v}' \frac{\partial p}{\partial s} \mathbf{v}'}\right) > 0$. Therefore $CKMKE$ indeed represents an energy exchange between the mean flow and the fluctuations. In contrast, $CKEKM$ represents the work done by the Reynolds stress against horizontal shears in the mean flow. This work has to be removed from the Reynolds stress flux divergence, $RSFDIV$, to evaluate the amount of momentum

transferred to/from the mean flow, as illustrated by equation (2.19) written in the form

$$\underbrace{\hat{\mathbf{v}}\cdot\left[\nabla_s\cdot\left(\overline{\mathbf{v}'\frac{\partial p}{\partial s}\mathbf{v}'}\right)\right]}_{CKMKE}=\underbrace{\nabla_s\cdot\left(\overline{\hat{\mathbf{v}}\mathbf{v}'\frac{\partial p}{\partial s}\mathbf{v}'}\right)}_{RSFDIV}-\underbrace{\overline{\mathbf{v}'\frac{\partial p}{\partial s}\cdot(\mathbf{v}'\cdot\nabla_s)\hat{\mathbf{v}}}}_{CKEKM}. \tag{2.21}$$

If there is not a horizontal shear in the mean flow $CKEKM = 0$, and the Reynolds stress flux is non-divergent ($RSFDIV = 0$) in the absence of other energy sources/sinks, then there is no barotropic energy transfer ($CKMKE = 0$). As long as a horizontal shear develops in the mean flow in general $CKEKM \neq 0$, the Reynolds stress flux converges/diverges ($RSFDIV \neq 0$), and barotropic transfers take place ($CKMKE \neq 0$). Therefore, the common practice of using (2.2) or $CKEKM$, to sum up the mutual interaction of mean with fluctuations is incomplete [*Rhines*, 1977].

The theory of eddy-mean flow interaction has mostly been developed in atmospheric sciences in terms of the investigation of the interaction of waves and zonal-mean flows. There are however, both in the ocean and atmosphere, many situations for which the ETM separation is more appropriate. This is particularly true in the Gulf of Mexico and the western boundary currents, where a predominant zonal circulation is not observed. Under the ETM separation the values in hat in the set of equations (2.15), (2.17), (2.18), and (2.20) stand for an eulerian background mean field, and the primed variables are the perturbation circulation superimposed on it. The energy transfer terms –and likely $RSFDIV$–, provide the pathway for the two flow forms to exchange energy.

Before proceeding to develop the energy scheme to be investigated here, some simplifications can be made in equations (2.15), (2.17), (2.18), and (2.20). By considering the hydrostatic balance in isopycnic coordinates, $\partial\phi/\partial s = -\alpha\partial p/\partial s$, the sum of $MPFDIV$

and $PMDIV$,

$$MPFDIV + PMDIV = -\nabla_s \cdot \left[\hat{\mathbf{v}} \frac{\partial \bar{p}}{\partial s} \left(\hat{\phi} + \bar{p}\hat{\alpha} \right) \right], \tag{2.22}$$

vanishes since $\hat{\phi} + \bar{p}\hat{\alpha} = 0$. In addition, $PEDIV$ can be written as

$$PEDIV = -\nabla_s \cdot \left[\overline{(\hat{\mathbf{v}} + \mathbf{v}') \frac{\partial p}{\partial s} p^* \alpha} \right], \tag{2.23}$$

therefore, in analogy to (2.22) the perturbation part of (2.23) balances $EPFDIV$, and $PEDIV$ reduces to

$$PEDIV = -\nabla_s \cdot \left(\overline{\hat{\mathbf{v}} \frac{\partial p}{\partial s} p^* \alpha} \right). \tag{2.24}$$

Therefore, the dynamically important component of the equation of conservation of total energy is

$$\frac{\partial E}{\partial t} \equiv \frac{\partial}{\partial t}(KM) + \frac{\partial}{\partial t}(KE) + \frac{\partial}{\partial t}(PM) + \frac{\partial}{\partial t}(PE) = 0, \tag{2.25}$$

where

$$\begin{aligned}
\frac{\partial}{\partial t}(KM) &= KMDIV + CKMKE + CPMKM + CPEKM + MWIND + MDIS, \\
\frac{\partial}{\partial t}(KE) &= KEDIV - CKMKE + CPEKE + EWIND + EDIS, \\
\frac{\partial}{\partial t}(PM) &= -CPMKM, \\
\frac{\partial}{\partial t}(PE) &= PEDIV - CPEKM - CPEKE.
\end{aligned}$$

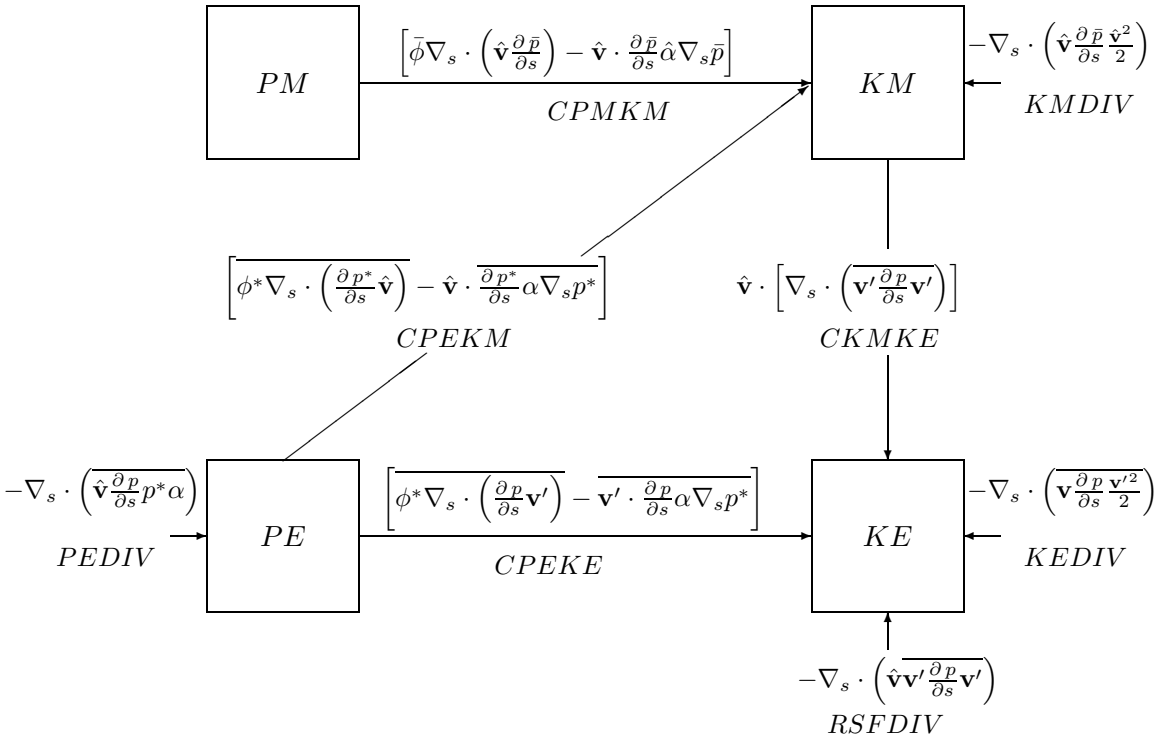

Figure 2.2: Energy diagram in isopycnic open systems [adapted from *Bleck*, 1985]. The direction of the arrows is controlled by the sign of the energy terms. Terms beginning with C stand for energy transfers, while terms ending in DIV represent energy boundary fluxes. For simplicity, energy inputs and energy dissipation in each box are omitted.

Due to the fact that the definitions of $CPEKM$ and $CPEKE$ discussed here are not robust in generalized vertical coordinates because they break down in isobaric coordinates where $s \equiv p$ and $p^* \equiv 0$, it has been a common practice to avoid decomposing the potential energy into mean and perturbation fields [*Bleck and Boudra*, 1986; *Chassignet and Boudra*, 1988]. In this work, however, these definitions are kept because they work fine in isopycnic coordinates, but most important, because with them it is possible to get a direct pathway between PE and KM, and between PE and KE, which are of great interest during the study of eddy-mean flow interactions. $CPEKM$, for example, when positive represents the rectification in the mean flow due to density interface oscillations, while $CPEKE$ provides

the way for PE to degenerate into KE during the energy cascade (dissipation process). Nevertheless, the price to pay for decomposing the pressure field into mean and perturbation components is that the pathway between PM and PE vanishes in isopycnic coordinates [*Bleck*, 1985], and the interaction between these energy forms during the baroclinic transfer is only possible through KM as depicted in Figure 2.2, which summarizes the energy diagram to be investigated here [adapted from *Bleck*, 1985].

2.4 Double-gyre numerical experiment

Model outputs from the isopycnic model of *Bleck and Boudra* [1986] were used to test the prototype energy diagram in Figure 2.2, and to verify statements (2.13) and (2.14). The model configuration consists of a 2-layer isopycnic square ocean with dimensions of $L \times L$, where $L = 2000$ km, as illustrated in Figure 2.3. The grid interval is chosen as 20 km, and the initial layer thickness $h_1 \sim 1000$ m and $h_2 \sim 4000$ m. No-slip boundary condition is used. The model was integrated from rest during 10 years at time steps of 20 min, which satisfies the stability criterion (CFL condition). A trial-and-error process suggested a horizontal eddy viscosity coefficient of 3.40×10^6 cm^2 s^{-1} for the model to converge into a steady solution. The lateral viscosity is proportional to the Laplacian of the velocity. There is no interfacial or bottom friction. The layer densities are $\sigma_\theta = 25.0$ and $\sigma_\theta = 27.0$ for upper and lower layers respectively. The pattern of the surface wind stress forcing $\tau = \tau_0(\tau_x, \tau_y)$ is steady, and chosen such that a 2-gyre circulation arises: $\tau_x(y) = \tau_0 \cos(2\pi/L)$; $\tau_y = 0$; and $\tau_0 = 1$ dyn/cm^2.

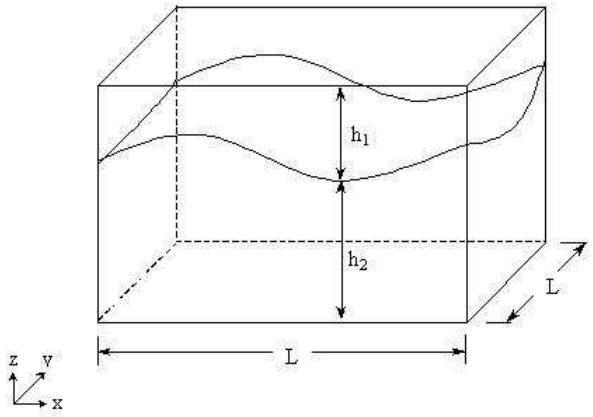

Figure 2.3: Schematics of the double-gyre square ocean experiment.

The formalism described in section 2.3 is used to calculate energy conversions and energy boundary fluxes for two diagnostics conducted using the same model outputs. In the first, the whole extension of the square ocean was used to compute the energetics in a closed system. In the second diagnostic the square ocean was split into two subregions, one for the cyclonic gyre and another for the anticyclonic gyre. The energy equations were translated into finite differences in a c-grid computational representation, as described in *Bleck* [1978]. Standard averaging and differentiation operators were used, which conserve total energy in the fluid [*Bleck*, 1978]. Two criteria are used to define mean and fluctuations for the experiment: one for the spin-up period, and another for steady state or equilibrium. In the first case the reference state is rest, and the fluctuations are the departures form this state. In the second case the mean is computed for the last 500 days of the experiment, and the fluctuations are the departures from this mean. In the following section the discussion mostly focus on the diagnostic for the open system.

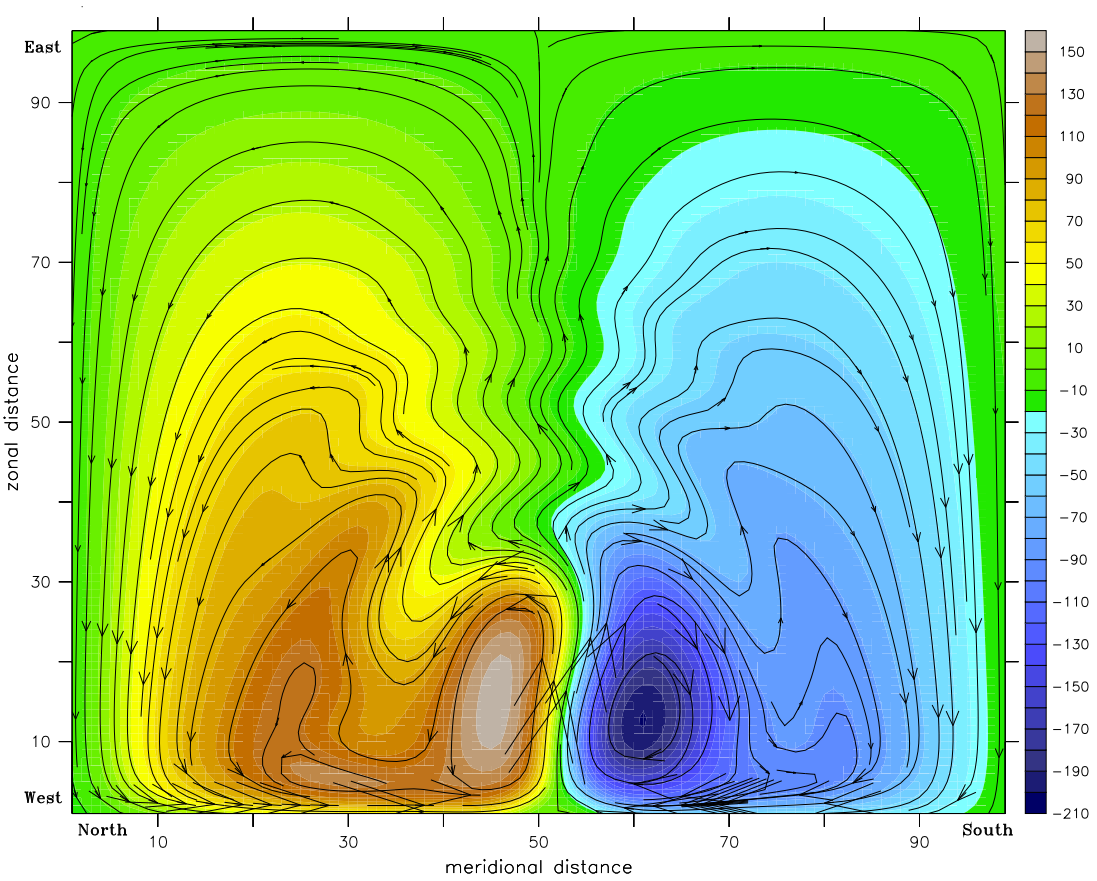

Figure 2.4: Double-gyre surface mean circulation. Color is the departure in depth (m) of the density interface respect to 1019 m.

2.5 Results

The double-gyre idealized experiment mimics the large-scale circulation features observed in the subtropical gyre (anticyclone) and the subpolar gyre (cyclone) in the North Atlantic. The gyres are separated in the model by an eastward flow which resembles the Gulf Stream after leaving the western boundary (Figure 2.4). In the experiment the eastward flow meanders along a zonal imaginary line that separates the two gyres.

2.5.1 Double-gyre spin-up

In response to the wind stress acting on the sea surface the first 1200 days of the spin-up process are characterized by a gradual increase in available potential energy (APE) in the two gyres (Figure 2.5). However, opposite dynamics operates between the gyres, since in the anticyclone the wind stress drives an Ekman sinking which pushes lighter water downward, whereas in the subpolar gyre denser water is lifted by Ekman pumping. As a result of the increased pressure gradients the kinetic energy intensifies gradually in the upper layer of the two gyres (Figure 2.6), and by day 1200 the content of kinetic energy in the anticyclone is twice larger than in the cyclone, since the pressure gradients are stronger in the anticyclone (Figure 2.4). In contrast, the deep circulation in the two gyres is very weak (Figure 2.6).

2.5.2 The onset of the deep circulation

By day 1300 the vertical shears have grown sufficiently for the large-scale flow in the cyclonic gyre to become baroclinically unstable, as indicated by the sudden drop in APE (Figure 2.5) and the intense burst of KE in deep waters of the cyclone (Figure 2.6). Thus, vigorous mesoscale eddies arise to redistribute mass horizontally and the deep flow is put in motion. The onset of the deep circulation is delayed in the anticyclone (Figure 2.6), since this gyre is less effective to build up APE. The differential adjustment between the two gyres has to do with the way the wind is prescribed in a layer model (over the top layer), since surface velocities are stronger in the cyclonic gyres than in the anticyclonic gyres [*Chassignet and Gent*, 1991]. Figure 2.7 illustrates the onset of the baroclinic instabilities

in the deep waters of the cyclonic gyre. The positive peaks of $CPEKE$ between days 1300-1500 confirm that the baroclinic instability indeed drains PE to feed the perturbation kinetic energy of the deep flow. At the same time that the baroclinic instability is in progress, the horizontal shears trigger barotropic instabilities which are much weaker (not shown). Figures 2.6 and 2.7 illustrate the fact that the deep circulation is totally driven by the eddies. When the viscosity is increased in the experiment to suppress the eddies (no baroclinic instabilities, $CPEKE \sim 0$), the deep circulation vanishes (Figure 2.8).

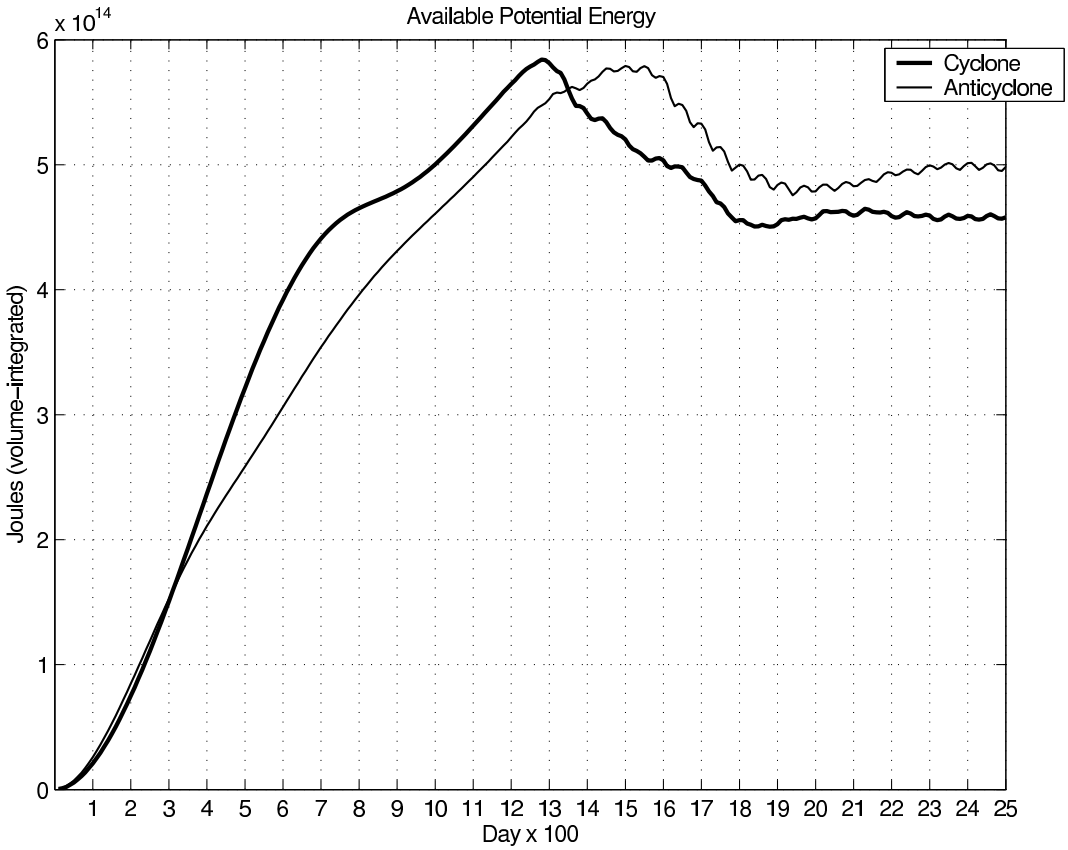

Figure 2.5: Available potential energy in the two gyres.

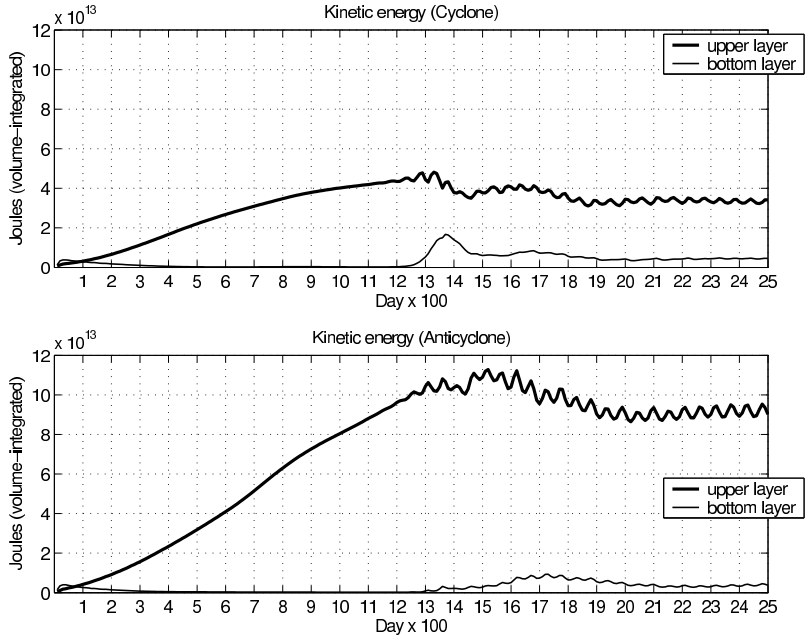

Figure 2.6: Kinetic energy in the two gyres.

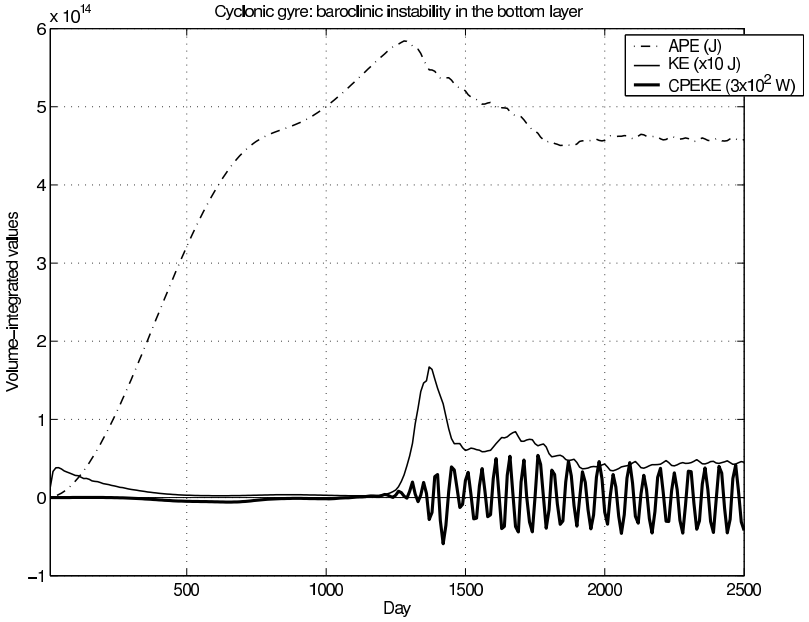

Figure 2.7: Onset of the baroclinic instability in the bottom layer of the cyclonic gyre.

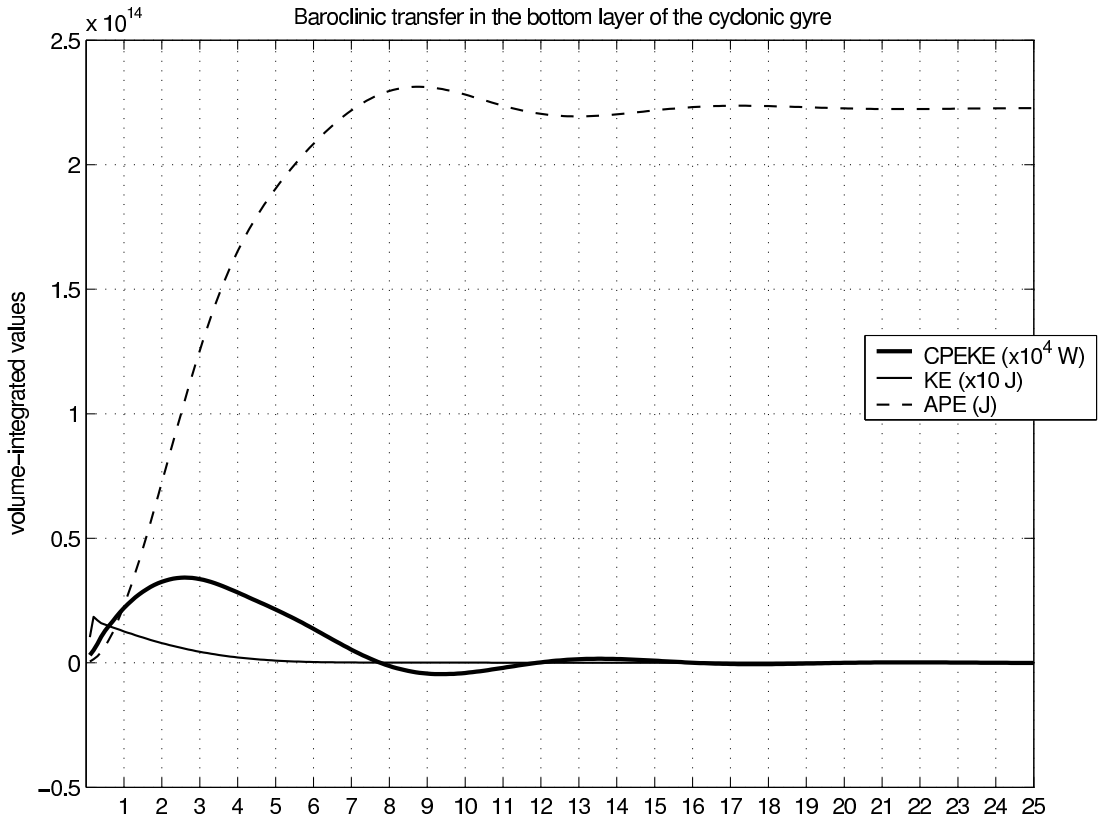

Figure 2.8: Baroclinic transfer ($CPEKE$) in the two gyres with a viscosity 10 times higher than in the main experiment.

2.5.3 The equilibrium

The transition to equilibrium (days 1300-2000) is characterized by the release of APE (Figure 2.5), the decrease(increase) of kinetic energy in the surface(bottom) layer (Figure 2.6), and the growing of bottom-intensified baroclinic instabilities (Figure 2.9). This scenario suggest that the eddies in this experiment act to redistribute mass horizontally, limit the amplitude of the mean flow in the surface layer, and fill the deep layer with kinetic energy, in agreement with early findings of *Holland and Lin* [1975].

After 2000 days the system reaches the equilibrium. At this stage the amplitude of the

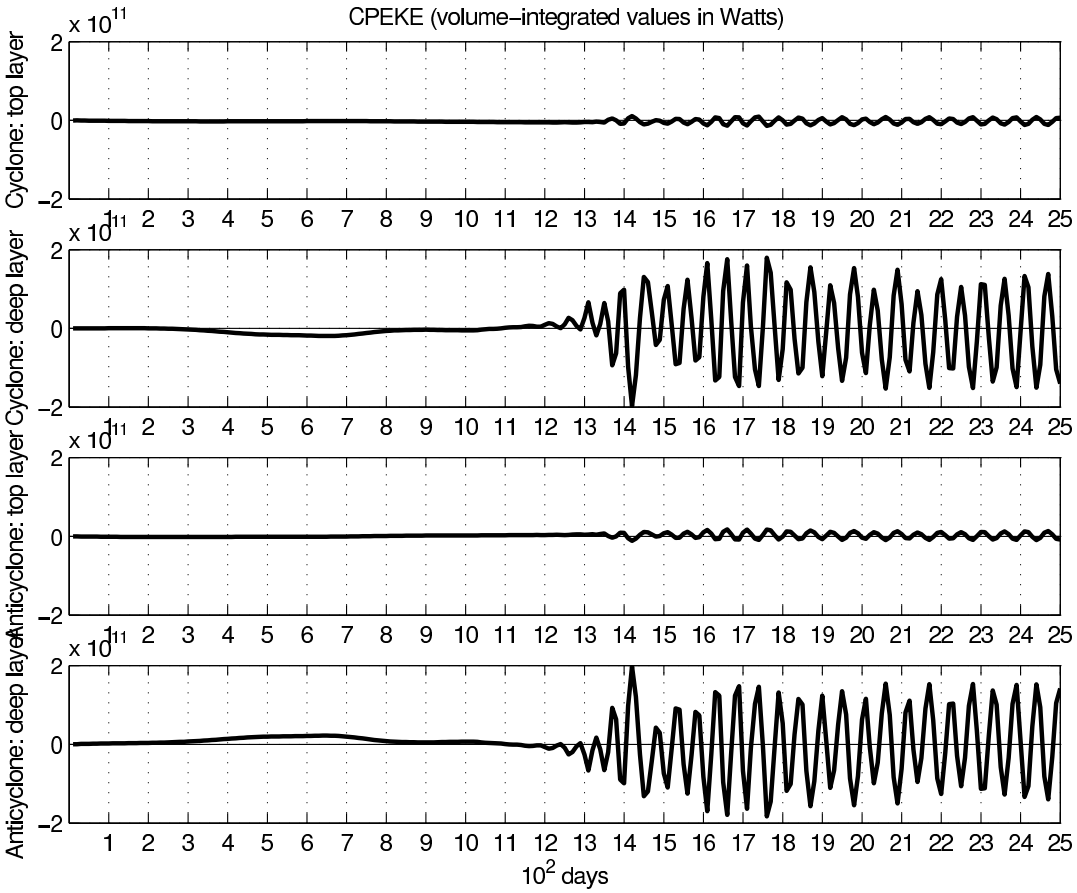

Figure 2.9: Baroclinic transfer ($CPEKE$) in the two gyres.

baroclinic transfer signal is stable, and the levels in potential and kinetic energy oscillate smoothly and quasi-periodically around an average value in the two gyres (Figure 2.10). In this scenario, the whole energy cycle is a "merry-go-round" of equal (but nonzero) conversions and flux divergences, which exactly cancel (equations 2.13 and 2.14) such that the net tendency of total energy is zero. Figure 2.11 shows that the magnitude of $PEDIV$ (the leading boundary flux) is negligible compared to the magnitude of the baroclinic transfer, suggesting that during equilibrium the two subregions behave as independent closed systems, since the exchange of mass between the gyres vanishes. However, opposite individual baroclinic transfers take place between the two gyres to maintain the energy equilibrium

of the whole system (Figure 2.11). Although the most energetic baroclinic instabilities are developed in the cyclonic gyre region during the transition to equilibrium, during the equilibrium the baroclinic transfers are similar in magnitude in the two gyres, and there is a net baroclinic transfer to the eddies in both gyres.

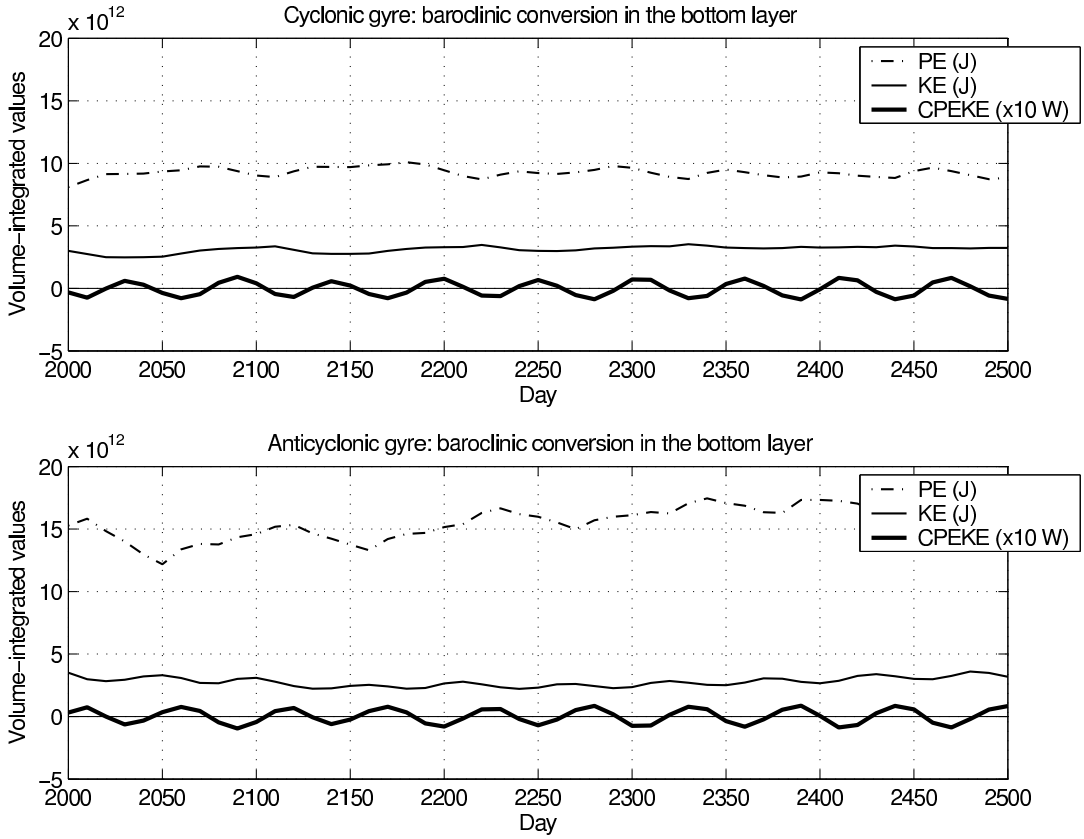

Figure 2.10: Baroclinic transfer ($CPEKE$) in the bottom layer during equilibrium. Upper panel: cyclonic gyre. Bottom panel: anticyclonic gyre.

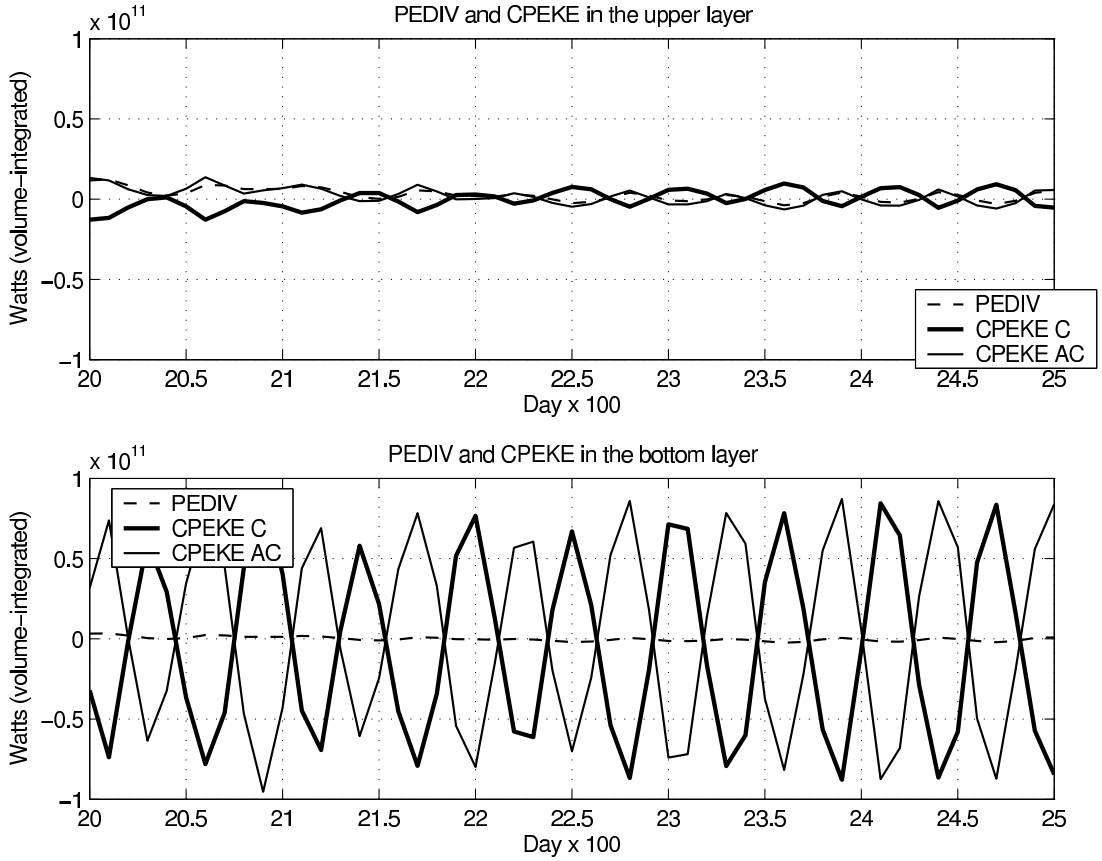

Figure 2.11: $PEDIV$ (dashed line) and ($CPEKE$) during the equilibrium in the upper layer (upper panel) and the bottom layer (bottom panel). Thicker(thinner) line is $CPEKE$ in the cyclonic(anticyclonic) gyre.

2.6 Discussion

2.6.1 Advantages of the method

The main advantage of the computation of energetics in open domains is that the method enables to investigate the energy cycle in specific portions of the large-scale flow, permitting to identify the regional adjustment in response to local and remote forcing. For example, the separated energetic diagnostic of the two gyres revealed the different physics working in

each gyre. Therefore we identified that the most energetic baroclinic instabilities occur in the cyclonic gyre during the transition to equilibrium, since this subregion is more efficient to build up APE during the experiment. The application of the method to the different layers of the idealized ocean shows that the deep circulation is driven by eddies triggered by bottom-intensified baroclinic instabilities.

In addition, the investigation of subregional energetics provides a better assessment of the relative contribution of barotropic and baroclinic instabilities during the triggering of eddies. A common practice during the investigation of energetics is to summarize the energy cycle in energy schemes similar to the one in Figure 2.2. For example, Figure 2.12a shows the energy budget for the whole domain of the double-gyre experiment (closed system). On the basis of this scheme one may conclude that the barotropic transfer represents $\sim 15\%$ of the source of kinetic energy for the fluctuations, and the rest is provided by baroclinic transfers. However, a closer look on the time evolution of the two processes (Figure 2.13, upper panel) shows that $CPEKE$ is much more energetic than $CKMKE$. Nevertheless, when a separate energy budget is conducted for each gyre, the box diagrams (Figures 2.12b and 2.12c) are more consistent with the dynamic evolution of the gyres, since the subregions are dynamically homogeneous (Figure 2.13, intermediate and lower panels). Therefore, one should define homogeneous circulations when investigating subregional energetics.

Figure 2.13 also illustrates how the global energy balance hides the opposite dynamics that has to work in the subregions to maintain the energy equilibrium of the whole system. Therefore, one should be cautious when interpreting energy boxes in general, but specially those for closed systems composed by heterogeneous dynamic subregions.

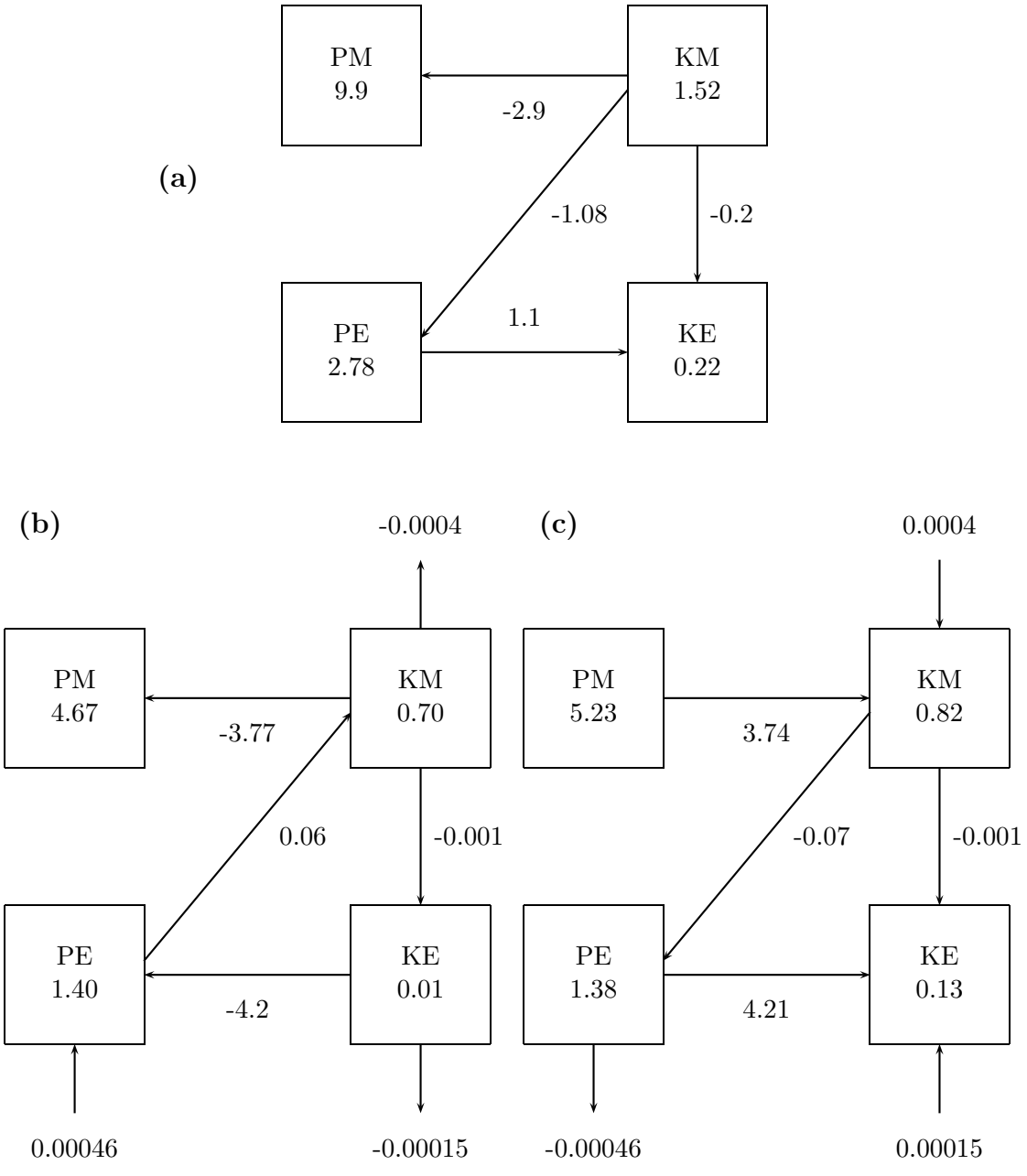

Figure 2.12: Double-gyre energy balance (volume-integrated values). (a) Whole system, (b) cyclonic gyre, and (c) anticyclonic gyre. Energy levels in the boxes are in $10^{13}J$; Energy conversions and divergencies (arrows) are in $10^{6}W$ in (a), and in $10^{8}W$ in (b) and (c).

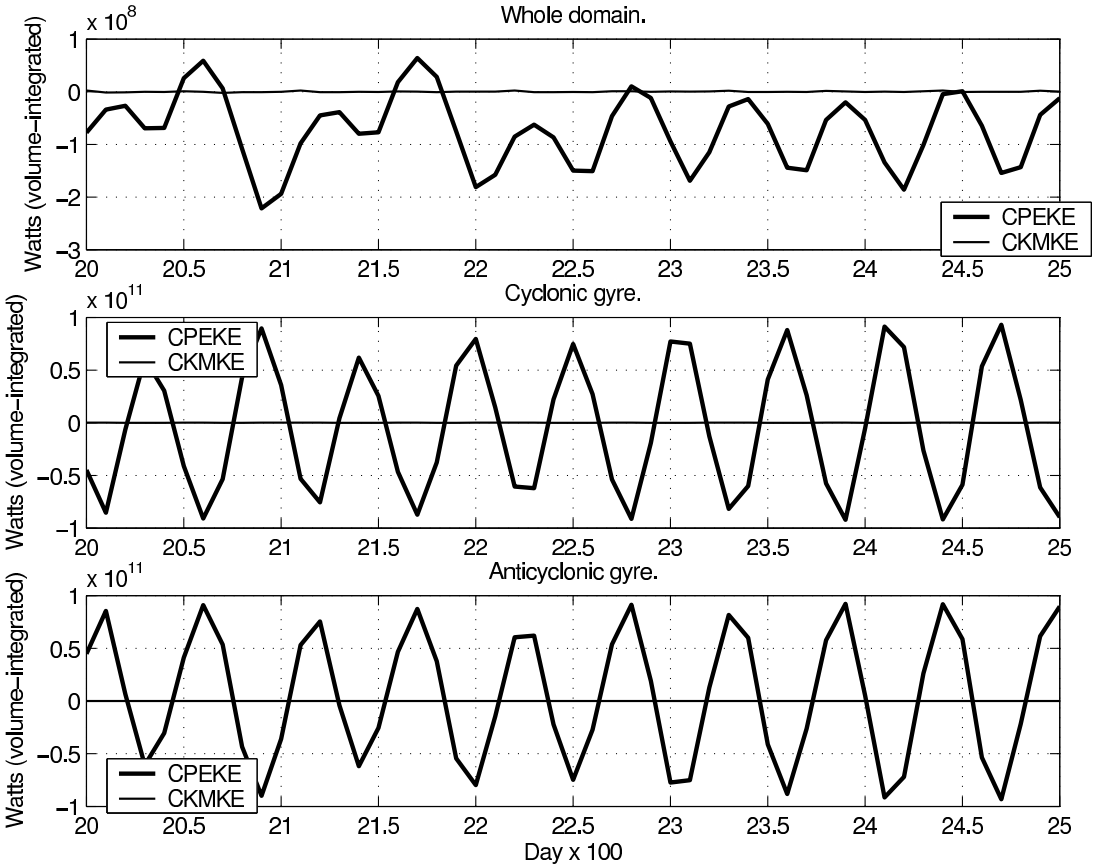

Figure 2.13: $CPEKE$ (thicker line) and $CKMKE$ (thinner line) during the equilibrium in the double gyre experiment. Upper panel is for the whole system, and intermediate and lower panels are for the cyclonic and anticyclonic gyres, respectively.

One should notice that the regularity in amplitude of the eddies during the equilibrium is due to the steady nature of the wind forcing and its balance with the dissipation during the steady state.

2.6.2 Limitations

The theory of eddy-mean flow interaction has mostly been developed by investigating the interaction of waves and zonal-mean flows in the atmosphere. The theory consist of two parts. The first deals with the propagation of the waves in non-uniform background zonal-mean flows, including a description based on wave-conservation laws such as the Eliassen-Palm theory. The second part treats the nonlinear rectified effects of the waves on the zonal flow, including the Charney-Drazin "nonacceleration" theorem [*Andrews*, 1990]. There are however, both in the ocean and the atmosphere, situations for which the "eddy, time-mean" separation, such as the one followed in this investigation, is more appropriate. Nevertheless, in these situations most of the theory developed to understand zonal-mean problems is not directly applicable [*Plumb and Ferrari*, 2005]. Thus, much theoretical effort has been recently focused on the development of an analogous theory for ETM interaction, and a number of conservation laws for waves on time-mean flows have been derived under various assumptions, although their application to observations or model outputs remains limited [see *Andrews*, 1990, and references therein]. Less progress has been made on the second part of the theory, and the forcing of the time-mean by the transient eddies is a topic with several theoretical open issues [*Andrews*, 1990]. The absence of a mature theory limits the understanding of the ETM interaction and, currently, we have to rely on heuristic approaches to try to clarify eddy-triggering and rectification mechanism during the ETM interaction.

In regard to the analysis of energetics in open systems the main limitation of the technique is associated to the duality and inseparability of the barotropic energy transfer and the Reynolds stress flux term, which may prevent to identify unequivocally purely barotropic energy conversion processes, since in open domains the Reynolds stress flux does not necessarily vanish at the open boundaries. The duality/inseparability arises because both terms come from the same non-linear terms in the momentum equations when the equations are transformed into flux form and the averaging operator is applied on them. Thus, both energy terms account for the interaction between different scales of motion in the flow. Therefore additional analysis techniques, such as vorticity balances for example, should be conducted to verify the results of the energy analysis.

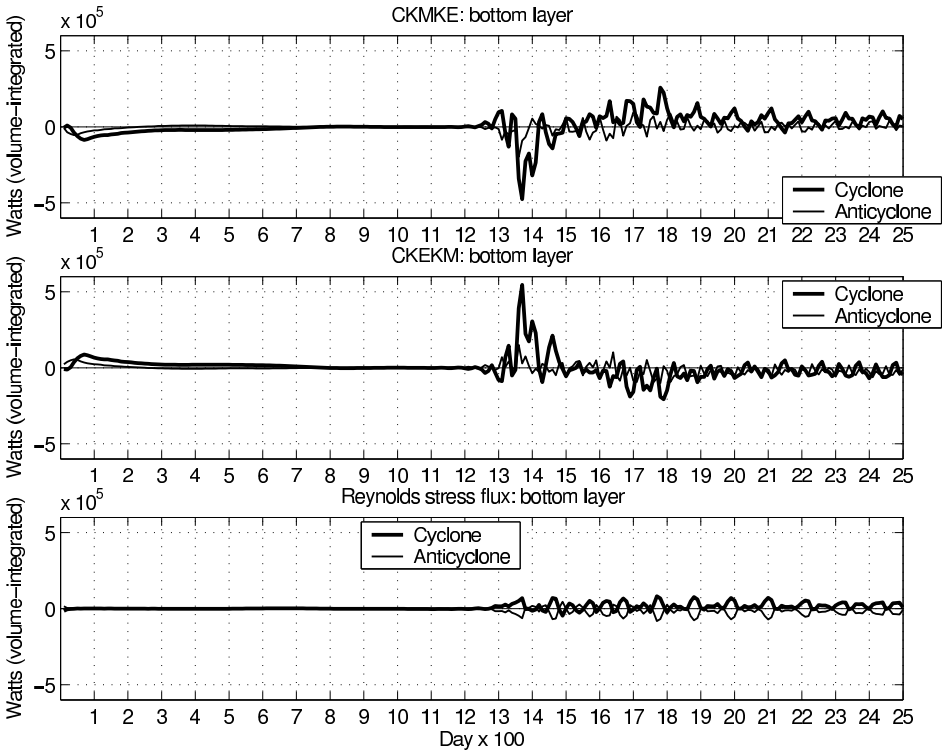

Figure 2.14: Barotropic transfer ($CKMKE$), Reynolds stress work ($CKEKM$), and Reynolds stress flux divergence $RSFDIV$ in the bottom layer of the two gyres.

Figure 2.14 shows the complication to interpret the barotropic transfer in open systems. As a result of the intensifications in the horizontal shears (intermediate panel) the Reynolds stress flux becomes divergent/convergent during steady state (lower panel), whereas the tendency in the other energy fluxes is to become non-divergent (for example $PEDIV$, Figure 2.11).

Finally, one should notice that the result of the averaging procedure for the final statistical state is highly dependent on the choice of the averaging interval, since the energy transfers are stable in amplitude and quasi-periodic. Consider for example Figure 2.10. If one do the average for days 2050-2480 the mean value of $CPEKE$ would be zero or close to zero. If however the average is conducted for days 2000-2500 the mean value would mostly be determined by the extremes of the series since the interior values would cancel identically, and the mean could be positive or negative. Therefore, one should be cautious to define the averaging interval. Perhaps the best choice is to start with the beginning of an energy cycle, and finish at the end of other energy cycle (days 2050-2480 for example).

2.6.3 The physics of the conversion terms

To investigate the mechanism of the eulerian baroclinic energy transfer in isopycnic coordinates let us expand $CPEKE$ from equation (2.18) and, for simplicity, consider a purely zonal flow

$$CPEKE = \underbrace{\overline{\phi^* \frac{\partial U'}{\partial x}}}_{DIV} \underbrace{-\overline{U' \alpha \frac{\partial p^*}{\partial x}}}_{WORK} \tag{2.26}$$

where $U' \equiv u' \partial p / \partial s$ is the fluctuating zonal flow and $\partial p^* / \partial x$ is the perturbation pressure gradient tangent to the density surface in the x-direction. DIV in (2.26) is a divergence

term representing advection of layer thickness anomaly by the fluctuating flux, and $WORK$ stands for the work done by the fluctuating flux against the pressure tangent to the density interfaces. Therefore, the transfer $CPEKE$ is driven by the pressure gradient. If $\partial p^*/\partial x$ is zero in a local volume, the work done by U' on the density surfaces is zero. Thus U' is unaltered and the divergence term vanishes, $CPEKE$ is zero.

Let us now consider an originally non-divergent fluctuating flow, U', which propagates eastward and at certain point it faces a westward propagating wave in the β-plane, as illustrated in Figure 2.15a. At the front of the wave, say point A, U' acts against the pressure gradient force (PGF), which tends to redistribute mass horizontally in opposite direction to U'. Therefore U' does work against the density surface ($WORK < 0$), the wave front is slowed down and the wave grows in amplitude. Thus U' loses energy to the potential energy of the wave ($CPEKE < 0$). In the eastern side of the wave (point B) the mechanism is opposite, since U' progresses in the direction in which the wave tends to redistribute mass and, therefore, the release of PE accelerates U', that is, $CPEKE$ is positive. Figure 15b shows the analogous mechanism that takes place when U' encounters the trough of the wave. In general, $CPEKE$ is positive when the background velocity is in the direction of the PGF.

The propagation of the wave over a weak background flow (small U') can drive weak baroclinic conversions. Consider again Figure 2.15a. At $t = 0$ there is lighter water at point A, and denser water at point B. As the wave propagates westward the conditions in A and B change. After a while, denser water gets onto A and, in consequence the center of mass ascends and PE increases at expenses of the kinetic energy of the wave. Therefore $CPEKE$ is negative and the front of the wave is decelerated. In the back of the wave lighter

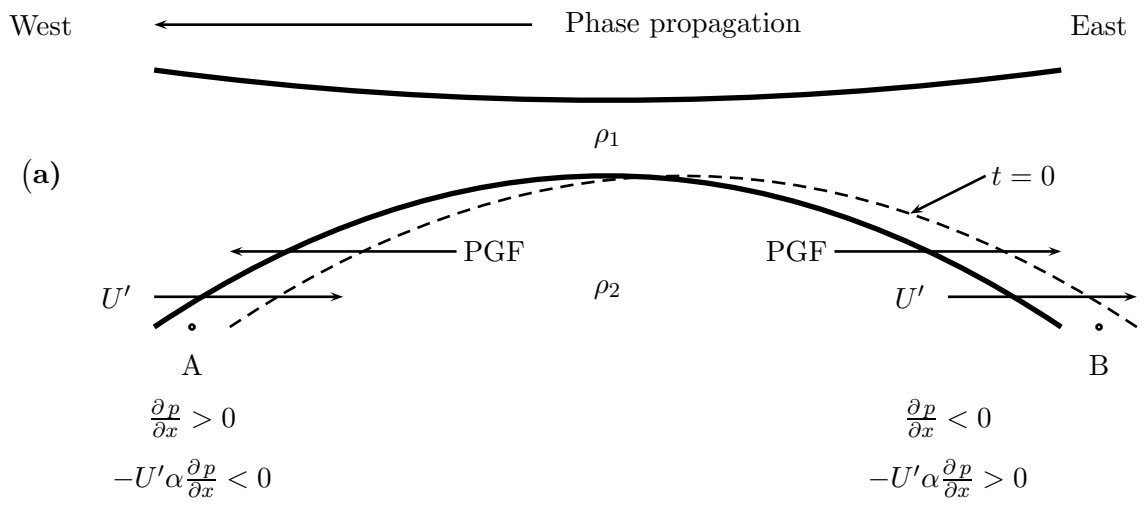

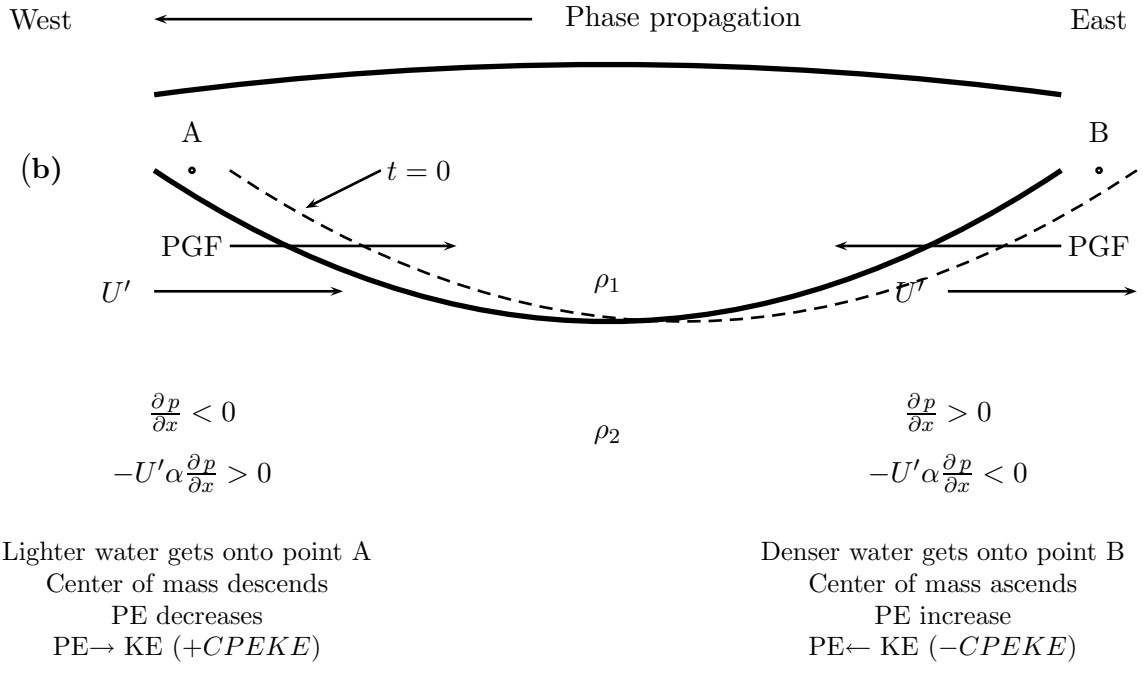

Figure 2.15: Mechanism of the baroclinic conversion, $CPEKE$, in isopycnic coordinates during the interaction of a fluctuating eastward flux with a westward propagating wave. (a) Cyclonic part of the wave (crest). (b) Anticyclonic part of the wave (trough).

water gets onto B, the center of mass descends and PE is fed into KE. Whether the wave interacts or not with a background field the truth is that at the face of the wave $CPEKE$ is negative, and positive at the back. This is also true for $CPEKM$, but the background mean velocity replaces the fluctuating velocity in equation (2.26).

Given the theoretical limitations for the investigation of the ETM interaction we need to identify what can we learn from the energy scheme proposed here in regards of mean flow rectification due to waves (positive $CPEKM$) and wave generation (negative $CPEKE$). To simplify the discussion let us look for a relation between the energy transfer terms and some kind of wave activity, say Rossby wave activity. QG theory states that planetary waves have an associated northward flux of eastward momentum, given by [*Gill*, 1982]

$$\rho\overline{u'v'} = -\frac{1}{2}\rho kl(g\eta_0/f_0)^2, \tag{2.27}$$

which has sign opposite to that of the energy flux since ω (wave frequency) and k (wavenumber in the x-direction) have opposite signs in the Rossby waves dispersion equation. Therefore, westward momentum is carried away from a source in the direction of group propagation. This result is of great interest for the purpose of our investigation, since for example, when the westward momentum flux varies because, say, the planetary wave is dissipated, there must be a corresponding westward acceleration of the mean flow [*Gill*, 1982], which in the context of energy conversion should manifests as positive $CPEKM$ (rectification).

Equation (2.27) shows that the sign of the Reynolds stress is determined by the components of the wavenumber vector, $\mathbf{K} = k\mathbf{i} + l\mathbf{j}$. Since Rossby waves exist due to gradients in planetary vorticity and topography, thus it is convenient to orientate the Reynolds stress

with respect to the gradient of ambient potential vorticity, ∇Q_a [*Bower and Hogg*, 1992]. In this new reference frame the "north" is directed up the gradient ∇Q_a, and since the geostrophic flow runs along the isopleths of Q_a, then the wavevector is perpendicular to the geostrophic velocity [*Pedlosky*, 2003], such that if the flow is purely geostrophic, $\mathbf{v}\cdot\nabla Q_a = 0$, there are no waves. If $Q_a = f/H$, where f is the planetary vorticity and H is the local water depth, then

$$\nabla Q_a \equiv \nabla\left(\frac{f}{H}\right) = -\left(\frac{f}{H}\frac{\partial H}{\partial x}\right)\mathbf{i} + \left(\beta - \frac{f}{H}\frac{\partial H}{\partial y}\right)\mathbf{j}. \tag{2.28}$$

In the new coordinate system, $\mathbf{X}(\mathbf{i}', \mathbf{j}')$ (Figure 2.16), fluid motions associated with a wave packet traveling from SE to NW will produce a negative Reynolds stress (fluid motion polarized in the second and fourth quadrants of the new coordinate system), and fluid motions associated with waves propagating from NE to SW will produce positive Reynolds stress. In particular, if u' and v' are the fluctuation velocities in a "north/east" coordinate system, the fluctuation velocities in the new coordinate system are

$$\begin{aligned} u_r{}' &= u'\sin\theta - v'\cos\theta \\ v_r{}' &= u'\cos\theta + v'\sin\theta, \end{aligned} \tag{2.29}$$

where θ is the orientation of ∇Q_a respect to the east (Figure 2.16). The rotation of the Reynolds stress in the new coordinate system enables to determine properly the direction of energy propagation over sloping topography, both for incident as for reflected waves [*Bower and Hogg*, 1992]. In the flat-bottom double-gyre experiment the equation (2.28) reduces to $\nabla Q_a = \beta\mathbf{j}$.

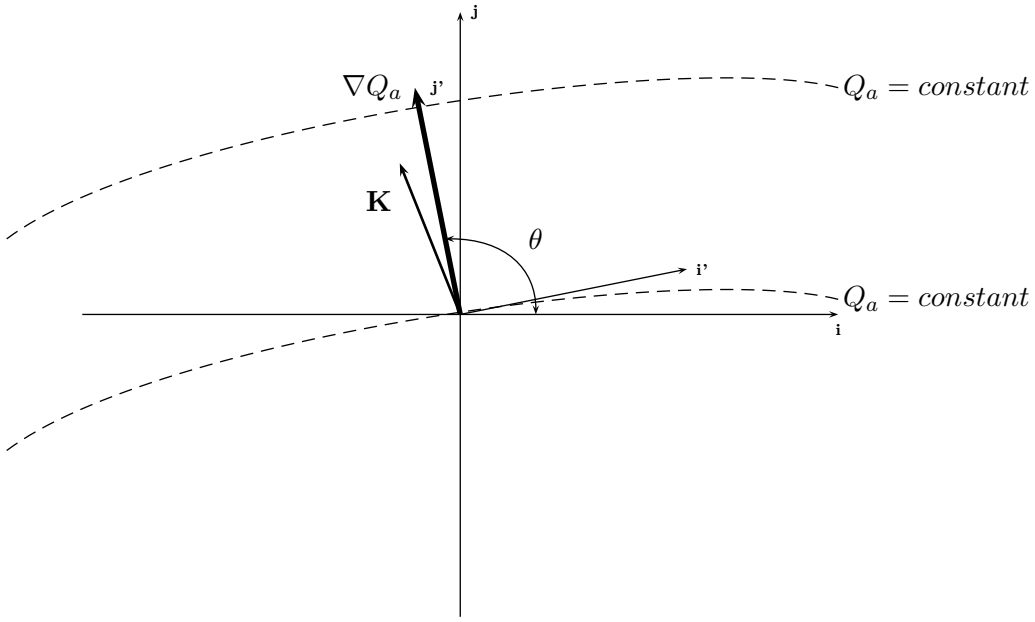

Figure 2.16: The relation between the gradient of ambient potential vorticity (∇Q_a) and the wavenumber vector (**K**) in a coordinate system orientated respect to ∇Q_a.

Figure 2.17 shows the spatial distribution of $CPEKE$, the Reynolds stress ($u'v'$), and the relative vorticity (ξ) for the upper layer of the model ($\sim$1000 m) at day 1810 of the double-gyre experiment. At this point the system has already reached the steady state, thus forcing and dissipation cancel identically. Figure 2.17a shows a region of strong baroclinic transfers ($CPEKE > 0$) along the Gulf Stream extension, associated to the formation of a front that separates negative and positive values of relative vorticity associated respectively to the Gulf Stream and the eastward return flow for the northern Gyre. The front evidences strong shears in the flow. Away from the region of strong baroclinic transfers, most of the eastern region is covered by alternate bands of $CPEKE$ and ξ in the zonal direction, suggesting Rossby waves with $(+,-)\xi$ indicating the (crests,troughs) of the waves. In the map, the waves exhibit wavelengths of $\sim$300 km.

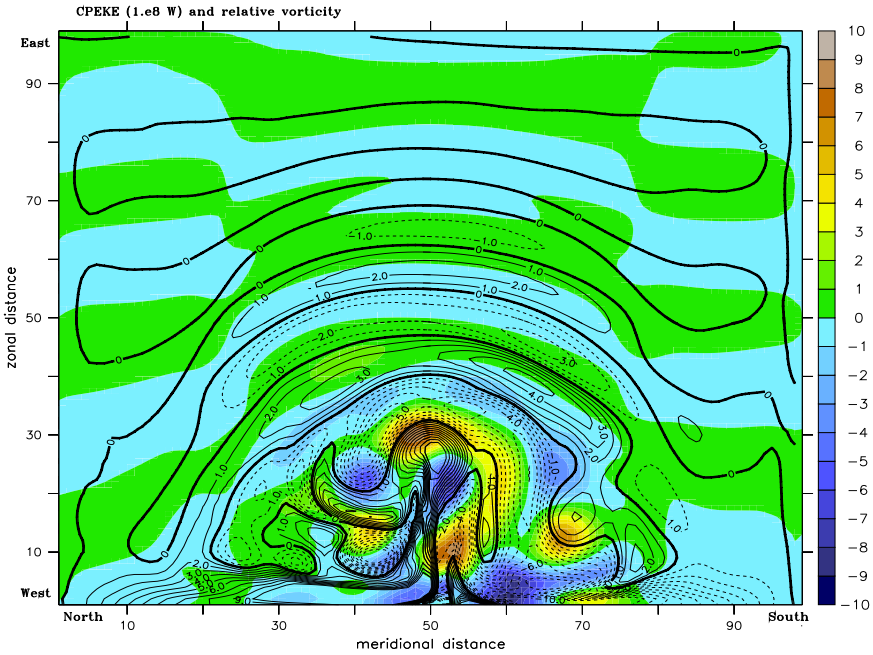

(a)

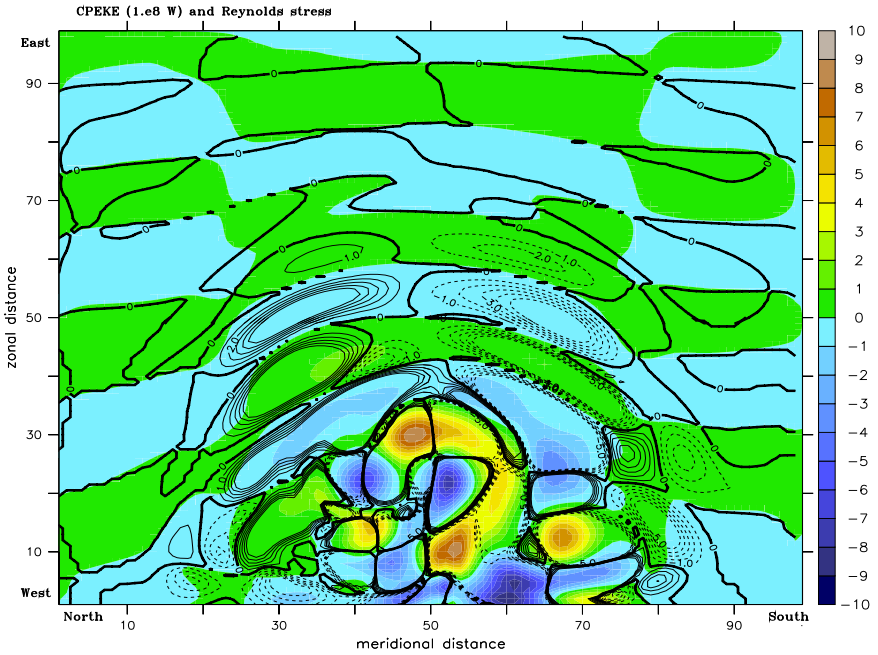

(b)

Figure 2.17: Spatial distribution of $CPEKE$ (color) at day 1810 of the double-gyre experiment. (a) Contours of relative vorticity, $\xi = \partial v'/\partial x - \partial u'/\partial y$. (b) Contours of Reynolds stress, $u'v'$.

Figure 2.17b verifies the presence of Rossby waves in the model. In the southern gyre the negative Reynolds stress indicates that the long waves are formed in the SE by the wind stress. Shorter waves with positive Reynolds stress are closer to the western boundary current (WBC), suggesting eastward-propagating Rossby waves reflected by the wall. In the northern gyre the positive values of Reynolds stress indicate that the long waves are formed in the NE; negative values are associated to shorter waves reflected in the western wall. The approach and reflection of the Rossby waves at the western boundary are easily observed in a movie of Reynolds stress. In the WBC the fluctuation velocities build up an intense pressure gradient ($CPEKE < 0$) in the two gyres, that is stronger in the southern gyre. The correlation of ($CPEKE < 0$) with the Reynolds stress of the shorter waves suggests that reflected waves sustain the pressure gradient required to maintain the WBC. Figure 2.18 shows patches of positive $CPEKM$ along the WBC, specially in the northern gyre. The patches coincide with values of Reynolds stress associated to short waves. This pattern suggest that the shorter Rossby waves at the western boundary rectify the mean flow. This result is supported by the smaller magnitudes of the Reynolds stress along the WBC, suggesting that the waves have lost momentum to the mean currents. A close observation on Figure 2.17 shows that in mid-latitudes there is a tendency for $CPEKE < 0$ to lay on the front of the waves, while in the back the tendency is for $CPEKE > 0$. In fact, this pattern mimics the sketch in Figure 2.15.

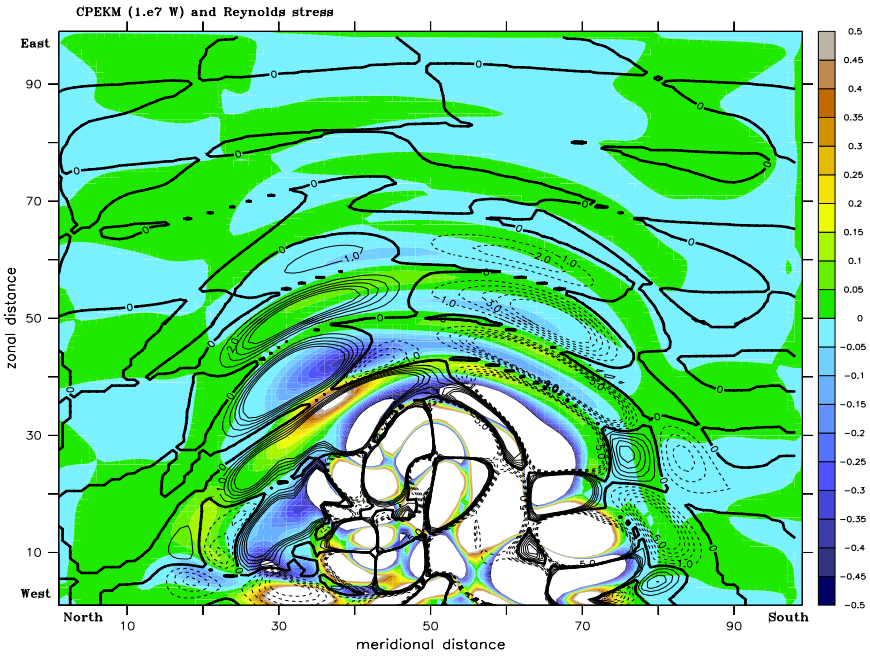

Figure 2.18: Spatial distribution of $CPEKM$ (color) at day 1810 of the double-gyre experiment; contours are Reynolds stress ($u'v'$).

2.7 Summary and conclusions

In this chapter we investigated the energetics in open systems, both analytically and numerically. The investigation of the equation of conservation of total energy revealed that in the absence of any source/sink of energy, the sum of all the energy conversions must be zero for the system to be energetically conservative. This is a stringent statement that must be satisfied in any set of energy equations in order to satisfy the principle of conservation of energy, whether the system is closed or open.

When the equation of kinetic energy of the eddy flow is derived by subtracting the equation of kinetic energy of the mean flow from the equation of total kinetic energy, the resulting barotropic transfer terms cannot be used directly in open systems, since the

barotropic transfer terms differ by the divergence term, $\partial/\partial x_j \left(\overline{u'_\lambda u'_j}\overline{u}_\lambda\right)$, which vanishes upon volume integration over the whole domain, but has to be taken into account during the analysis of energetics in open systems. The divergence term was incorporated to the definition of an energy scheme that enables to investigate "eddy, time-mean" interactions in isopycnic open systems. Although this scheme allows to investigate the differential energetic adjustment in heterogeneous ocean circulations, the introduction of the divergence term complicates to identify barotropic energy conversion from the perturbation energy flux. However, these terms are likely to be negligible compared to the baroclinic transfer terms.

When a subregion is exposed to external forcing from other subregions of the system, under inviscid and adiabatic conditions the subregion conserves energy only when the total energy content in the inflows balances the total energy content in the outflows. Opposite dynamics must work in the different subregions for the whole system to satisfy this condition and become energetically conservative.

The subregional analysis showed that during the spin-up of the ocean circulation a wind-driven cyclonic gyre is more efficient in building up available potential energy. Therefore, during the transition to equilibrium the cyclonic gyre triggers the most energetic instabilities for the center of mass of the water column to return to an equilibrium position. The equilibrium state is reached and kept as long as the energy transfers operate oppositely in the two gyres. This statement was verified in the double-gyre experiment, which showed that when a baroclinic transfer is taking place in the cyclonic region ($CPEKE > 0$), in the anticyclone the fluctuating flow builds up a pressure gradient ($CPEKE < 0$), and viceversa.

The investigation of energetics in open systems revealed that the box diagrams commonly used to summarize the energetics in a closed system can be misleading, preventing to asses properly the relative contribution of the barotropic and baroclinic energy transfers during the onset of instabilities in the flow.

We were able to reproduce the important dynamics of the double-gyre, wind-driven ocean experiment early reported by *Holland and Lin* [1975]. The energy scheme investigated here produces energy conversions consistent with the results of those authors. A technique was developed in which the baroclinic transfer terms $CPEKM$ and $CPEKE$, in conjunction with the Reynolds stress, enable a description of "eddy, time-mean" interactions in isopycnic coordinates. The technique was applied to identify sources of Rossby waves in the double-gyre experiment, as well as regions where the mean flow is rectified by the eddies. A more robust approach to the problem is needed, but currently the theory of "eddy, time-mean" interaction is incipient.

Chapter 3

Numerical experiment of the North Atlantic Ocean

3.1 Introduction

Having defined the energy scheme to study eddy-mean flow interactions in isopycnic open domains, now the scheme is used to investigate the influence of Loop Current eddy processes on driving Gulf of Mexico regional mean circulations. This section describes the numerical experiment of the North Atlantic Ocean used to obtain the mean and eddy flows for the Gulf of Mexico circulation. The processing of model outputs, and how they compare with observations are discussed as well.

The simulation was conducted with MICOM, the Miami Isopycnic Coordinates Ocean Model. MICOM is a primitive-equation model with density-following vertical coordinate, which contains 4 prognostic equations, one for the horizontal velocity vector, a mass continuity or layer thickness tendency equation, and two conservation equations for salt and heat [*Bleck and Chassignet*, 1994]. The fundamental reason to simulate the ocean circulation in density coordinates is that this system suppresses the diapycnal component of numerically caused dispersion of material and thermodynamic properties that has been proven to occur in models framed in Cartesian coordinates [*Chassignet et al.*, 1996]. This characteristic allows isopycnic models to prevent the numerical warming of deep waters. In addition, the association of vertical shear with isopycnal packing and tilting in the ocean makes isopycnic models appropriate for studies of strong baroclinic currents such as the Loop Current.

3.2 Model configuration

The MICOM simulation used here is an ECMWF (European Center for Medium-Range Weather Forecasts) wind forced run of the North and equatorial Atlantic Ocean (28^oS to 70^oN), including the Caribbean Sea and the Gulf of Mexico. The horizontal grid is defined on a Mercator projection with resolution of $1/12 \times 1/12^o\, cos(\varphi)$ ($\sim$8.5 km within the Gulf), where φ is the latitude. The vertical density structure within the Gulf consists of 14 isopycnic layers, topped by an active bulk Krauss-Turner surface mixed layer that exchanges mass and properties with the isopycnic layers underneath. The model uses a diapycnal mixing parametrization based on a Richardson number dependent diapycnal mixing, plus entrainment parametrization as in *Hallberg* [2000]. The vertical resolution was chosen to provide

maximum resolution in the upper part of the ocean. The ECMWF atmospheric forcing is from the 1979-1999 reanalysis. After a six-year spin up with monthly climatological forcing the model was integrated using surface boundary conditions based on ECMWF 6-hourly atmospheric data from 1979 to 1986. Open ocean boundaries are treated as closed, but are outfitted with 3^o buffer zones in which temperature and salinity are linearly relaxed toward their seasonally varying climatological values [*Levitus*, 1982], with damping/relaxation time from 5 days at the wall to 30 days at the inner edge of the buffer zone. Bottom topography is derived from the ETOPO 2.5 quality-controlled data set.

3.3 Processing of model outputs

In the Gulf of Mexico the circulation is spatially non-homogeneous, thus basin energetics analysis and budgets can be physically misleading, preventing an understanding of the differential adjustment driven by the LC cycle and the wind. Therefore, a regional dynamical approach is followed, where vertical and horizontal distributions of the energetic processes are used to define regions clearly identified with some part of the mean flow. After analyzing the baroclinic structure of the Gulf mean circulation it was found convenient to divide the model outputs in four vertical sections (Table 3.1), and nine horizontal subregions (Figure 3.1). In Figure 3.1 the subregional mean flows are : LTX (Louisiana-Texas shelf), MAF (Mississippi-Alabama-Florida shelf), WBC (Western Boundary Current), WAC (Western Anticyclone), CGN (Central Gulf North), CGS (Central Gulf South), LPC (Loop Current region), BCC (Bay of Campeche Cyclone), and CBK (Campeche Bank). Table 3.1 describes the density layers included in each vertical section.

Table 3.1: Description of vertical sections.

Section	average vertical extension (m)	MICOM density layers (σ_θ)
Surface	0–500	24.70, 25.28, 25.77, 26.18, 26.52, 26.80
Sub-surface	500–1000	27.03, 27.22, 27.38, 27.52, 27.64
Intermediate	1000–2000	27.74
Deep	>2000	27.82

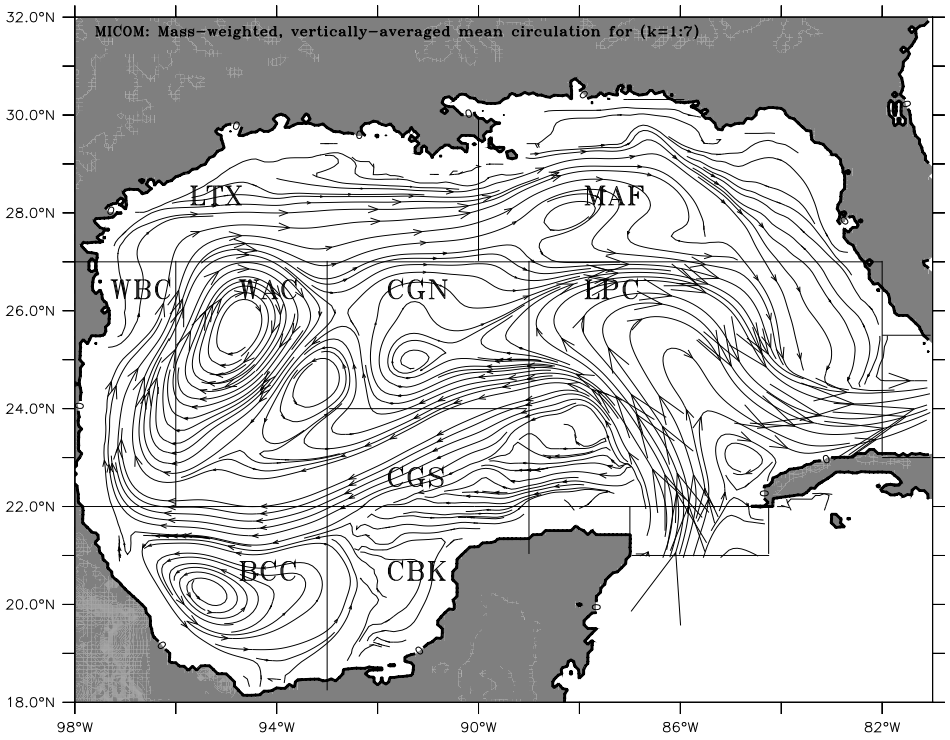

Figure 3.1: Flow lines for the 7-years time-averaged circulation in Gulf of Mexico surface waters. The boxes delimit regional circulations. See text for description of acronyms.

The time-averaged circulation is calculated using mass-weighted averages of the velocity field for a time span of ∼7 years. The averaging is computed between port-to-port configurations. This approach allows covering five complete LC cycles, which guarantees that the averaging procedure starts and finishes at comparable energetic levels within the basin. In addition, time-averaged circulations are computed for each individual LC cycle, and for the four annual seasons.

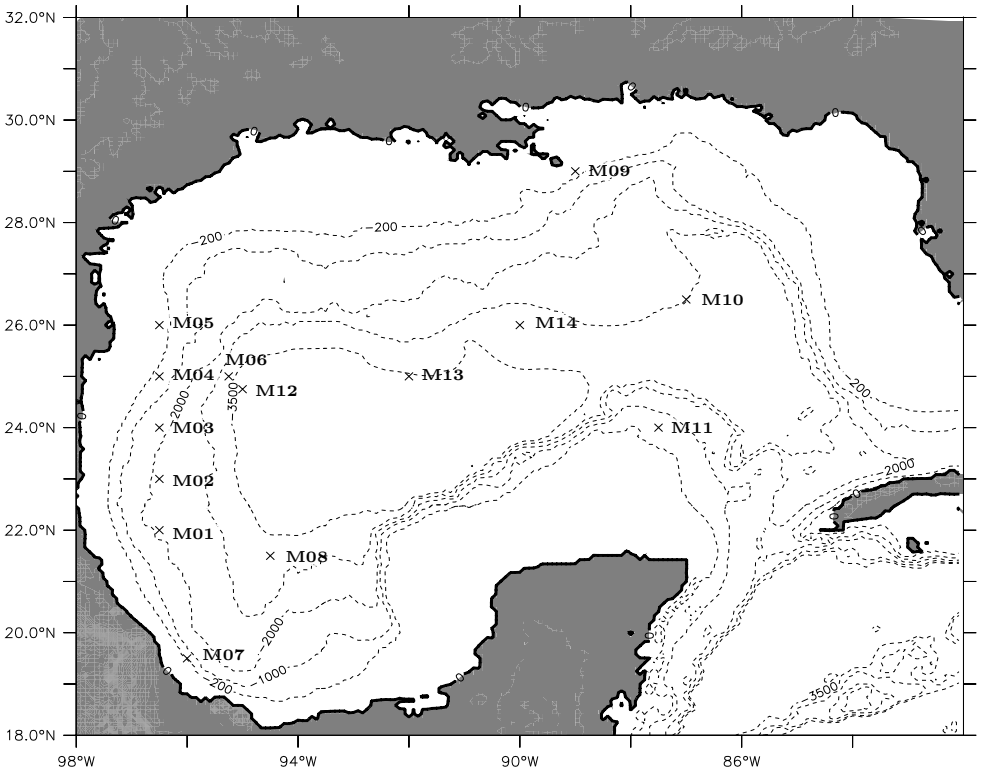

Figure 3.2: Location of the model "moorings".

The formalism described in section 2.3 is used to calculate mean/eddy boundary fluxes of kinetic/potential energy across selected imaginary walls bounding the subregions. Time-series of energy conversions, fluxes, and Reynolds stresses are computed for subregion boxes and for selected model "moorings" (Figure 3.2). The ambient potential vorticity gradient for the Gulf of Mexico (Figure 3.3) is computed with equation (2.28), then the perturbation velocities are rotated to be orientated respect to it [equation (2.29)]. Finally, the Reynolds stress is computed at each grid point in the new coordinate system.

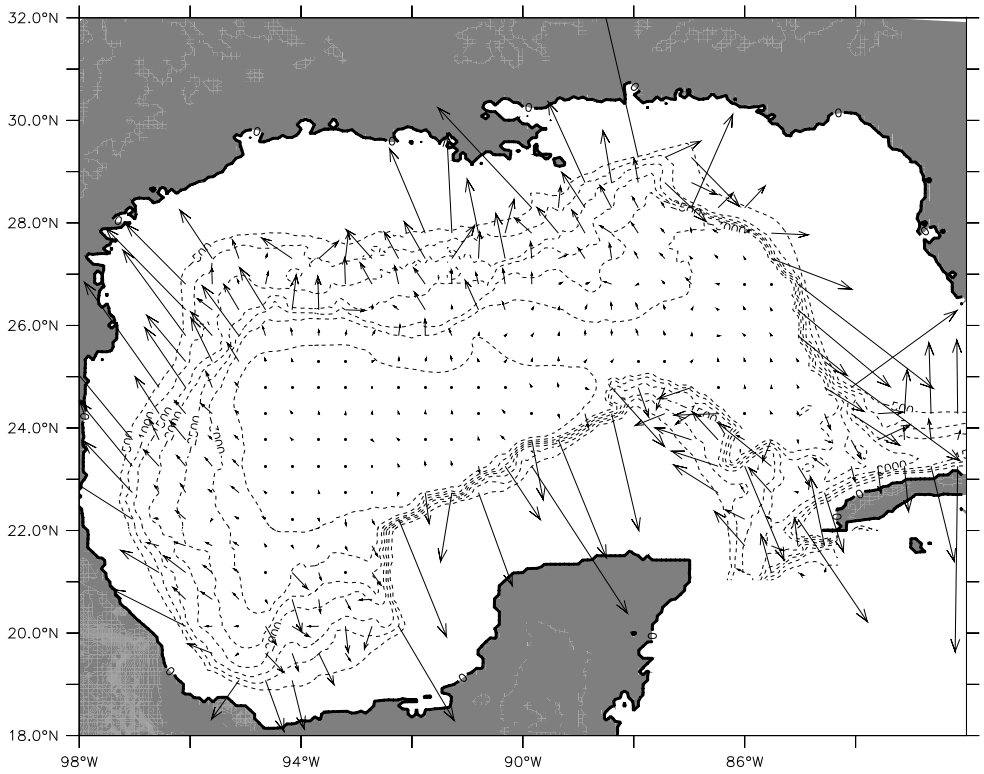

Figure 3.3: Ambient potential vorticity gradient, $\nabla Q_a \equiv \nabla(f/H)$, in the GOM. The arrows point to the local "β-north". Bottom topography (H) is derived from the ETOPO 2.5 quality-controlled data set.

3.4 Comparison of model outputs and observations

The model reproduces realistically the most important characteristics of flow in the Gulf of Mexico, including Loop Current northwestward extensions, LCR shedding and southwestward propagation, LCR detachments and reattachments, the anticyclonic circulation in the western Gulf where the LCR decay, a Western Boundary Current along the Mexican shelf, and the Bay of Campeche cyclone. In surface waters the model exhibits an overall mean anticyclonic circulation (Figure 3.1). In sub-surface waters the global mean circulation still anticyclonic (not shown), though observations and other models indicate mean cyclonic flow [*Sturges et al.*, 2004]. Intermediate waters display a transition regime and the model preserves the anticyclonic global circulation as in sub-surface waters. In deep waters the model produce a mean cyclonic circulation, consistent with observations and other models of the Gulf of Mexico [*Sturges et al.*, 2004].

Figure 3.4a shows the mean flow structure across the Yucatan Channel at 21.83^{o}N. The distribution of inflows and outflows is consistent with observations reported by *Sheinbaum et al.* [2002] (Figure 3.4b). In MICOM, however, the mean meridional velocity is weaker in the southerly Yucatan Counter-current (2 cm s^{-1} compared with 6 cm s^{-1}). In contrast, in MICOM the counter-current in the Cuban side is stronger than observations.

Sheinbaum et al. [2002] obtained a mean transport of 23.8±1 Sv across the Yucatan Channel from a 10 months current meter moorings record during the CANEK program; the transport values range from 13.5 to 31.7 Sv. Moreover, *Johns et al.* [2002] obtained a 28 Sv net transport by estimating the budget of the Atlantic inflow into the Caribbean Sea through the Antilles passages. *Romanou et al.* [2004] calculated a 27 Sv mean transport

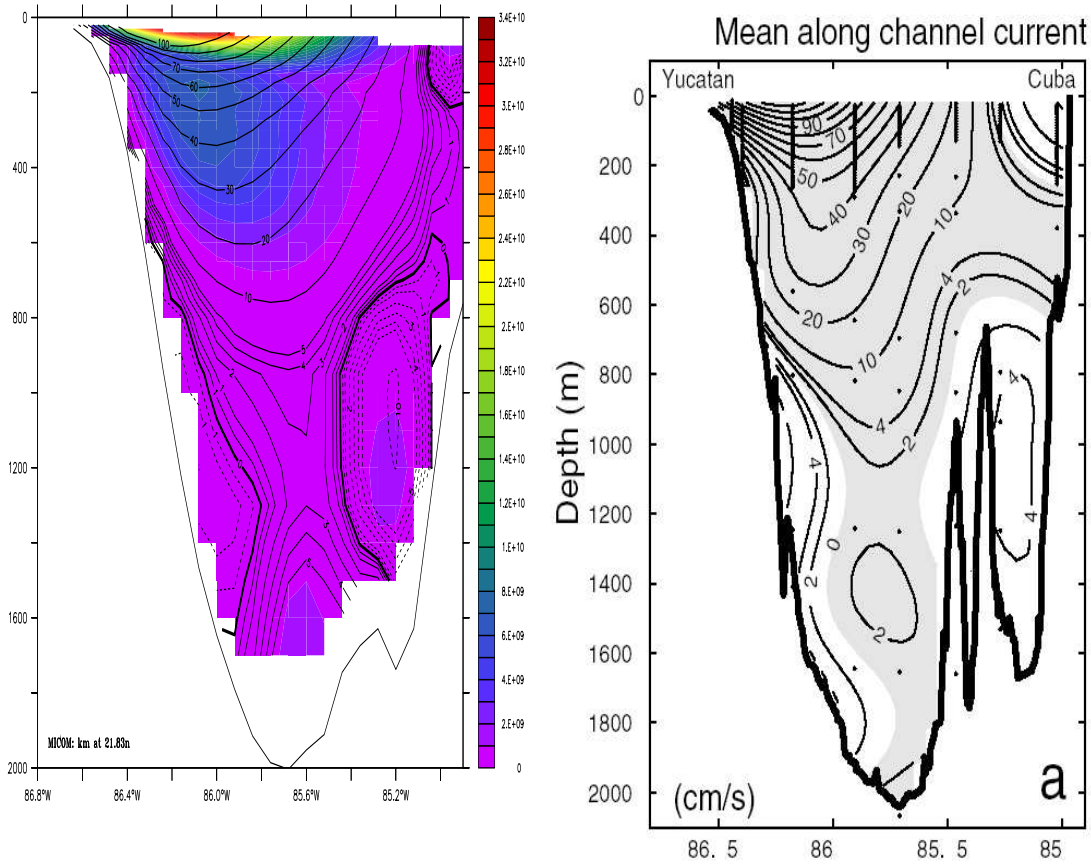

(a) (b)

Figure 3.4: Time-averaged flow structure at the Yucatan Channel. (a) MICOM: solid(dashed) contours are for northward(southward) meridional velocities; color is kinetic energy of the mean flow (Joules). (b) Structure of the mean along-channel velocity field from observations (10-months time-average) [Sheinbaum at al., 2002].

across the Yucatan Channel in a COADS-forced simulation with the same MICOM configuration reported here, with values ranging from 18 to 32 Sv over a 5 years analysis, in good agreement with the results of *Johns et al.* [2002]. *Chérubin et al.* [2005] obtained a net transport of 27.17 Sv with the same ECMWF-forced MICOM simulation used in this thesis. The values range between 13.5 and 33.7 Sv, indicating stronger variations than those in the simulation of *Romanou et al.* [2004], due to the less smoothed wind forcing.

Romanou et al. [2004] concluded that the COADS-forced version of the simulation investigated here is able to produce a quite realistic surface circulation for the North and equatorial Atlantic, and the smaller-scale, basin-wide dynamics variability within the Gulf of Mexico. For example, *Romanou et al.* [2004] report that the LCR diameters range between 140 and 500 m, the life span is about 1 year, and the translation speeds are 2-3 km d^{-1}, in good agreement with observations. The vertical structure of the temperature and salinity of each modeled LCR, from the moment it is shed until it disintegrates in the western Gulf, is in agreement with the few available observations. *Romanou et al.* [2004] computed the LCR orbital speeds, and noticed that the speed is linearly increasing from about 10-20 cm s^{-1} at the center of the eddy to 60-110 cm s^{-1} at 92-100 km away from the eddy center; older LCR that have advanced farther west in the Gulf have reduced maximum speeds with the location of the maximum speed at 60-70 km from the eddy center.

Figure 3.5 shows the distribution of eddy kinetic energy in the Gulf of Mexico obtained from geostrophic currents due to the sea surface anomaly, both from satellite imagery and the ECMWF-forced MICOM simulation. In the two cases the most energetic eddy circulations within the Gulf's interior occur along the path of the westward-propagating LCR. However, the geostrophic currents are 3-4 times more energetic in the model, probably due to the smoothing of the satellite data during the interpolation toward higher spatial resolution.

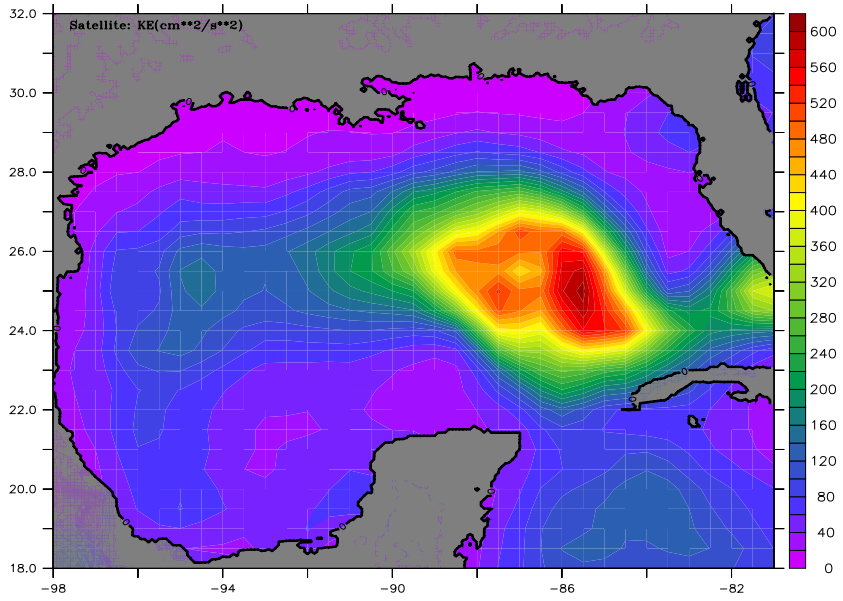

(a)

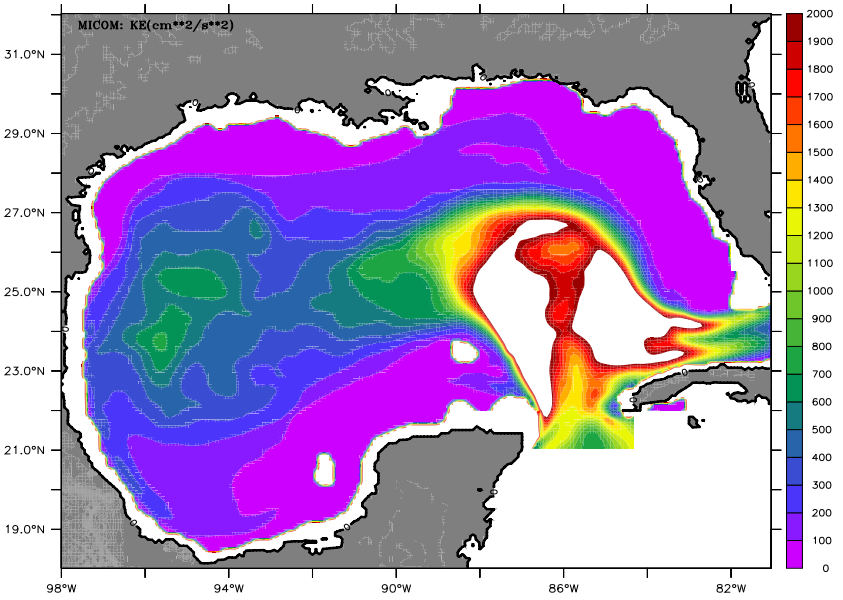

(b)

Figure 3.5: Time-averaged eddy kinetic energy from geostrophic currents. (a) Satellite data from CNES-AVISO: Nov/1992 - Dec/2004. (b) ECMWF-forced MICOM simulation: Mar/1980 - Dec/1986. In the two cases the geostrophic currents are computed with $V_s = \frac{g}{f}\frac{\partial \eta}{\partial x}$ and $U_s = -\frac{g}{f}\frac{\partial \eta}{\partial y}$, where η is the sea surface anomaly. KE is in cm^2 s^{-2}.

Chapter 4

Energy input into the Gulf of Mexico

4.1 Introduction

There is a long history in trying to quantify the relative contribution of the wind stress and the Loop Current in driving the Gulf of Mexico circulation in order to identify the leading processes distributing mass, heat, momentum, and dissolved and suspended material throughout the Gulf. The interest on the competition between the two forcing mechanisms initiated when *Ichiye* [1962] posed the hypothesis that the anticyclonic surface circulation observed in the western Gulf of Mexico resulted from migrating LC rings reaching the western coast and decaying there. *Sturges and Blaha* [1976] based on data of *Hellerman*

[1967], used the Sverdrup wind-driven ocean circulation theory to pose a second hypothesis, which explains the existence of the anticyclonic circulation in terms of the anticyclonic wind stress acting on the Gulf. On the basis of this hypothesis *Sturges and Blaha* [1976] suggested that there should be a western boundary current to return the flow for the interior transport. Continuing this line *Sturges* [1993] studied the annual cycle of the western boundary current and found that the flow is ∼200 km wide, and it extends beyond regions driven by local long-shore winds, thus he concluded that the observed flow must be a large scale feature associated with the wind stress curl and Ekman pumping. However, *Elliot* [1979, 1982] provided additional elements to support *Ichiye*'s hypothesis, and *Vidal et al.* [1999] suggested that the interaction of the LC eddies with the topography might play a significant role in driving the observed WBC along the Mexican shelf. The LC/wind competition could extend everywhere in the Gulf. For example to the Bay of Campeche, where a semi-permanent mesoscale cyclonic circulation is observed. Some authors suggest that this feature may be due to local wind forcing [*Molinari*, 1978; *Vázquez de la Cerda*, 1993], though a similar structure develops in some numerical models of the Gulf forced with no wind [*Oey and Lee*, 2002].

With the aim of providing new elements for a better understanding of the LC/wind competition in driving the Gulf of Mexico circulation, in this chapter the following question is addressed: What are the characteristics of the wind and Loop Current energy inputs into the GOM, and what is their relative contribution to the Gulf mean circulation?

Since we are interested in elucidating the remote influence of the Loop Current in driving interior Gulf's circulations, it is appropriate to focus on the adjustment to the west of 89W, since this longitude in the model represents the average threshold for the LC to force the

basin interior (see the western edge of the LC in Figure 3.1). In particular in this chapter the relative energy inputs of the wind stress into the western Gulf, and the boundary fluxes across 89W are assessed. Thus the $MWIND$ and $EWIND$ terms [equations (2.15) and (2.16)] and the energy divergence terms in equations (2.15), (2.17), (2.18), and (2.20) are investigated here to estimate the contribution of the two forcing mechanisms to the energy budget in the Gulf of Mexico. In addition, the hypothesis of *Sturges and Blaha* [1976] is investigated by computing the Sverdrup circulation in the basin. The meridional Sverdrup transport across a transect at 25N, 95W-89W is calculated to infer the return transport across the WBC. This transport is compared with the transport in the model's WBC.

4.2 Wind input

Figure 4.1 shows the seasonal cycle of the mean wind input into the Gulf of Mexico. The time averages for each season were calculated using the last 7 years of the simulation. In MICOM, the direct wind influence vanishes at the bottom of the mixing layer (top layer). With exception of winter, the mean wind stress is mostly westward in central regions, anticyclonic in the northern Gulf, and cyclonic in the Bay of Campeche. In consequence, the wind strengthens the mean surface currents along the Campeche Bank and at the Western Anticyclone region, as shown by positive values of the $MWIND$ distribution: maxima in wind input occur in the western side of the LC region, and to a lesser degree along the Campeche Bank and the WAC box. During spring and summer the western boundary current is locally wind-intensified, while the western portion of the Bay of Campeche Cyclone is strengthened all year around. In contrast, the mean wind stress does work against the

Table 4.1: Seasonal mean wind energy input into the western GOM ($MWIND, 10^5$ Watts).

	spring	summer	autumn	winter	7-years
Positive work	0.75	0.95	0.82	0.87	0.65
Negative work	-0.36	-0.26	-0.59	-0.68	-0.35
Net work	0.39	0.69	0.23	0.19	0.30

surface flow in the northern and northeastern Gulf, including the eastern portion of the Loop Current, where the maximum in negative work is observed. In fact, a pool of maximum negative work is observed in the LCR shedding area in the 7-years mean (not shown), similar in intensity, extension, and position to that for spring (Figure 4.1a). Table 4.1 summarizes the time-averaged, area-integrated wind input into the west of 89W. The surface flow in the western GOM is wind-intensified all year around, with maximum and minimum net inputs during summer and winter respectively. The decision for presenting absolute values (area or volume-integrated) was taken with the purpose of comparing horizontal energy inputs (wind) with boundary fluxes computed across vertical sections (transport across 89W).

4.3 Energy input across 89W

Figure 4.2a shows the baroclinic structure of the mean flow and its kinetic energy across 89W. A westward flow –which represents the time-averaged forcing into the inner Gulf– intrudes between 24.5-26.5N. Otherwise the mean flows are mostly eastward, though the westward flow is stronger. KM shows three maxima in the upper 400m –two of them associated to the LC extension (southern part)–, and two bottom intensified maxima below 1400m related to the deep cyclonic circulation. KE is also bottom-intensified below 1000m (Figure 4.2b). The surface sources of KM and KE at 89W are associated to the LC

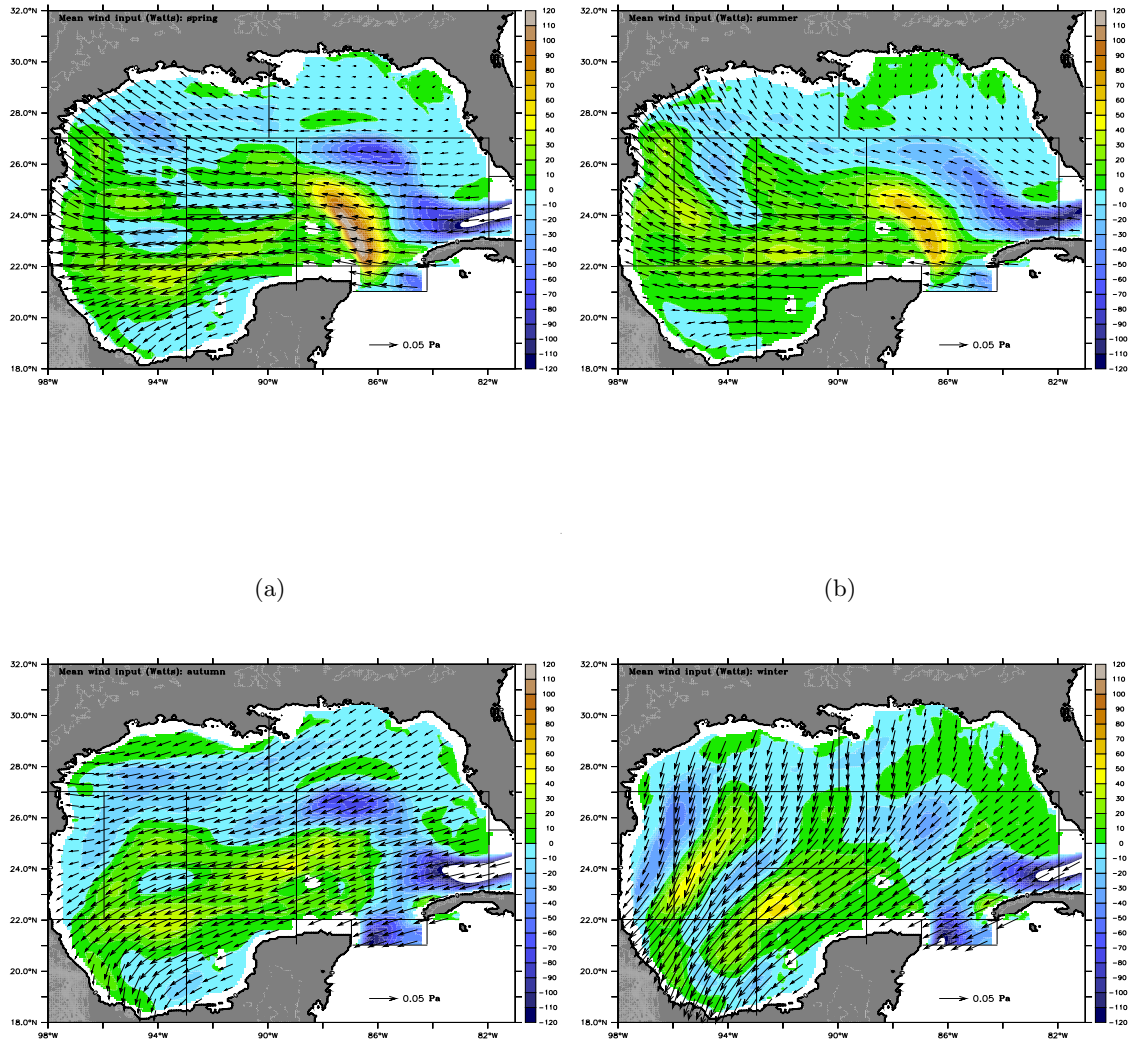

(a) (b)

(c) (d)

Figure 4.1: Seasonal wind input into the Gulf of Mexico for the 7-years of the experiment. Vectors are mean wind stress (Pa) computed from the ECMWF dataset (1980-1986); the color scale (Watts) is time-averaged work done by the wind on surface currents [$MWIND$, equation (2.15)]. Green-yellow-red colors are positive work, and represent regions where the mean surface flow is locally wind-intensified. Blue tones stand for areas where the mean surface currents do work against the wind stress. (a) Spring, (b) summer, (c) autumn, (d) winter.

extension and its eddies. At depth, however, it is not evident what is the source for the two forms of kinetic energy. Several authors have explained the deep pool of kinetic energy in the deep Gulf of Mexico in terms of topographic Rossby waves [*Hamilton*,1990; *Oey and Lee*, 2002]. In chapter 5 the sources for the deep KM and KE are investigated.

On the basis of the energy scheme in Figure 2.2, three dynamically important energy boundary fluxes are possible across 89W in the isopycnic system: $KMDIV$, $KEDIV$, and $PEDIV$. Therefore, the mean flow is mostly responsible for advecting the three forms of energy. In $KMDIV$, KM is advected by the mean flow. In $KEDIV$ one portion of KE is advected by the mean flow and the rest by the perturbation flow. Finally, in $PEDIV$, PE is advected by the mean flow. The divergence terms can be translated into boundary fluxes with the Gauss theorem

$$\int_V \nabla \cdot (\Psi)\, dV = \int_S \Psi \cdot \mathbf{n}\, dA, \tag{4.1}$$

where Ψ is any of the energy divergence terms, S is the closed surface surrounding an open domain and V is the volume inside it, dA is an element of area and $\mathbf{n}$ is a unit vector normal to it. By definition, $\mathbf{n}$ in equation (4.1) is positive in the outward direction, thus negative(positive) values in the divergence terms indicate a convergent(divergent) system. However, all the divergence terms in our system of equations appear with a minus sign, which was included with the terms during their computation. Therefore, the convention in this thesis is that positive(negative) values in the divergence terms indicate that the local levels of a particular energy form are increasing(decreasing).

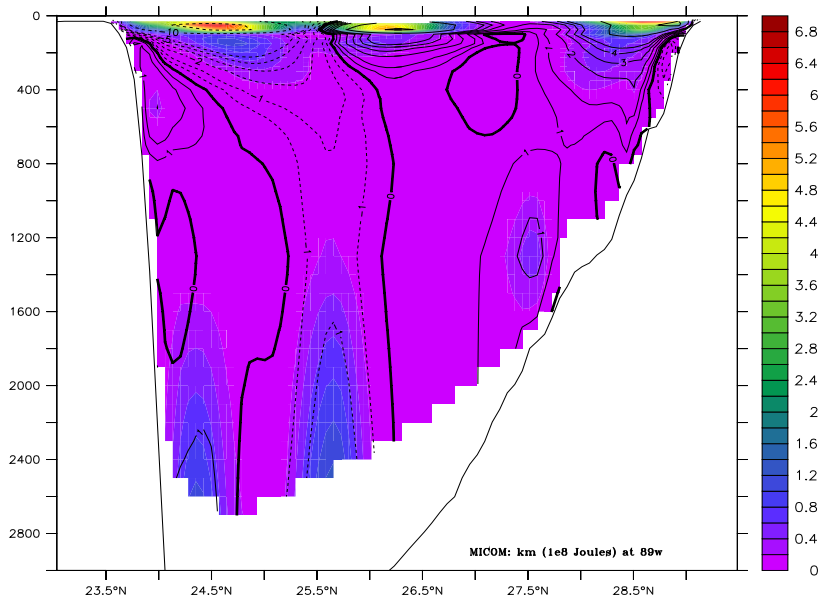

(a)

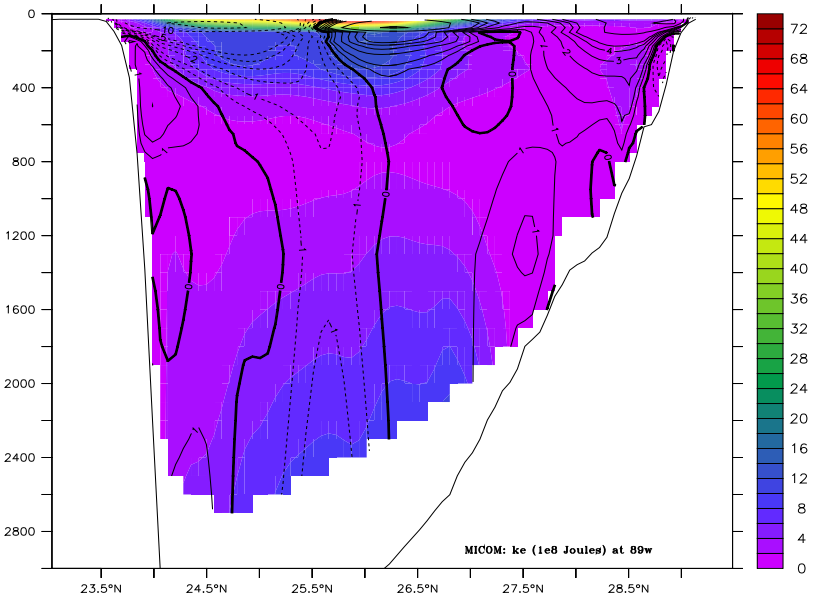

(b)

Figure 4.2: Time-averaged flow structure at 89W. Solid(dashed) contours are for eastward(westward) zonal velocities (cm/s). Color is volume-integrated kinetic energy (10^8 Joules) in (a) the mean flow, and (b) the eddy flow.

Table 4.2: 7-years mean energy boundary fluxes across 89W (Watts).

	KM_{flux}	KE_{flux}	PE_{flux}
In	3.03x10^5	50.71x10^5	8.17x10^8
Out	2.92x10^5	13.40x10^5	5.73x10^8
Gain	0.01x10^5	37.31x10^5	2.44x10^8

Table 4.2 shows the boundary fluxes across 89W. The main energetic contribution into the western Gulf is mean advection of eddy potential energy (PE_{flux}), that is, the mean flow carries the PE that will be released in the interior in the form of baroclinic transfer ($CPEKE > 0$), or to intensify the mean flow ($CPEKM > 0$). Figure 4.3 shows the variability of PE_{flux} in surfaces waters across a transect at 89W, 24-27N. About 30% of the energy flux concentrates at periods of 20-100 days, with the most energetic fluxes occurring during shedding events (red dashed vertical lines, panels a & b). In addition, more than one third of the PE_{flux} variability occurs at periods of 101-300 days, with maxima at shedding events as well (panel c). The last band (301-500 days, panel d) mimics the growing of the LC extension, since minima occur at port-to-port positions (PTP from now on, blue solid vertical lines), and maxima at points around the time when the LC is about to shed a ring in the model (when the LC extension intrudes beyond 25N, green dashed vertical lines). This band was chosen because in the model the minimum and maximum shedding periods are 312 and 480 days, respectively (Table 4.3). Almost 20% of the (PE_{flux}) variability takes place at periods larger than the maximum ring shedding period in the model (not shown). At depth (Figure 4.4), the PE energy flux is more energetic in the bands of 101-300 (61.8%) and 301-500 (25.5%) days, which together concentrate ~87.3% of the energy supply to the deep western Gulf.

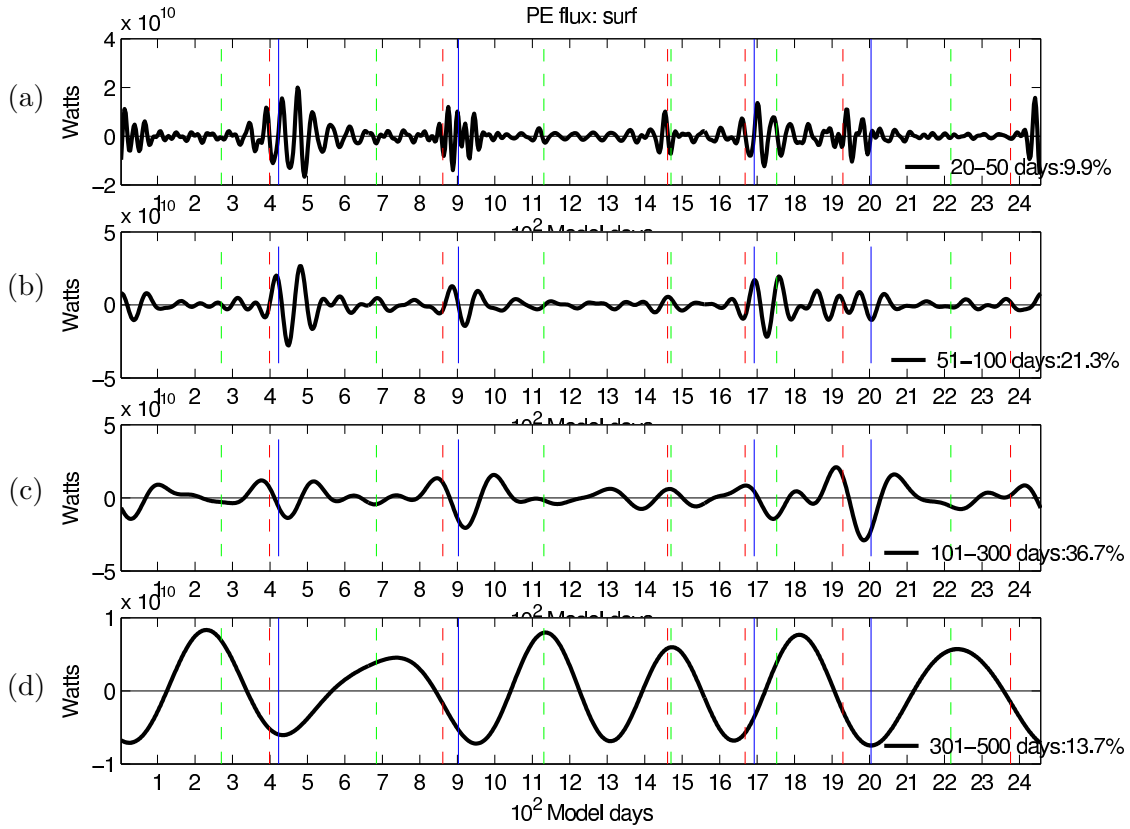

Figure 4.3: Variability of the potential energy flux (PE_{flux}) across 89W in surface waters (upper 500m in average). Blue solid vertical lines represent a LC port-to-port position; green dashed vertical lines represent LC intrusions beyond 25N; red dashed vertical lines represent ring shedding events. (a) band 20-50 days: 9.9%; (b) band 51-100 days: 21.3%; (c) band 101-300 days: 36.7%; (d) band 301-500 days: 13.7%. About 20% of the variability occurs at periods larger than 500 days (not shown).

Table 4.3: Shedding interval of LC rings in the model.

Ring	months
1	14.1
2	16.0
3	13.3
4	12.9
5	10.4
6	15.5
Mean	13.7

Table 4.4: Energy balance for the 7-years period in the western Gulf of Mexico.

$MWIND + EWIND$	DIS	$KMDIV$	$KEDIV$	$PEDIV$	Balance
0.46x10^5	-6.9x10^5	0.01x10^5	37.31x10^5	2.44x10^8	2.47x10^8

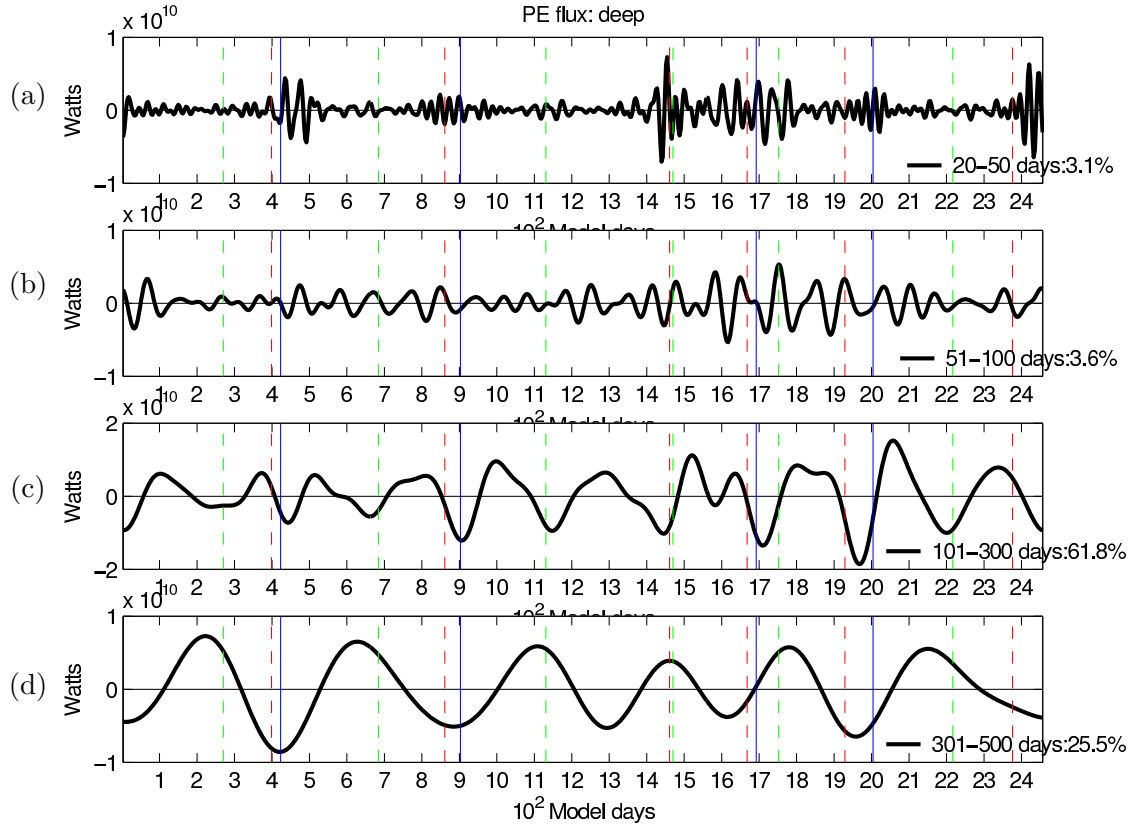

Figure 4.4: Variability of the potential energy flux (PE_{flux}) across 89W in deep waters (>2000m in average). Blue solid vertical lines represent a LC port-to-port position; green dashed vertical lines represent LC intrusions beyond 25N; red dashed vertical lines represent ring shedding events. (a) band 20-50 days: 3.1%; (b) band 51-100 days: 3.6%; (c) band 101-300 days: 61.8%; (d) band 301-500 days: 25.5%.

4.4 Wind/Loop Current competition

Table 4.4 summarizes the energy sources/sinks into the western Gulf of Mexico, which on the basis of equation (2.25) represent in a good approximation the energy budget in the subregion. The local wind input ($MWIND + EWIND$) is 46 times larger than the boundary flux of KM advected by the mean flow ($KMDIV$). However, the dissipation in the region is ∼15 times larger than the joint contribution of the wind and $KMDIV$. This

indicates that in the absence of other energy inputs the circulation in the region would spin-down to a zero velocity field. Nevertheless, the boundary fluxes of $KEDIV$, but mostly $PEDIV$, both associated to the eddy nature of the LC, supply the energy to sustain the circulation in the basin against the large dissipation. The local dissipation is larger than the local wind input because the dissipation is proportional to the Laplacian of the velocity field, which in turn is function of the wind input and mean and eddy boundary fluxes across 89W.

If the LC had a steady nature similar to that in Figure 3.1 (no ring shedding nor intrusions), $KEDIV$ and $PEDIV$ would be zero and the circulation in the western GOM would be entirely driven by the wind since $KMDIV$ is much smaller than $MWIND$. However, Table 4.4 shows that the energetic wind contribution is negligible when the eddy nature of the LC ($KEDIV$ and $PEDIV$) is incorporated to the energy balance. Chapter 5 contains a discussion about how the energy supply of $PEDIV$, the leading energy source, is fed into KM and KE to guarantee energy balance within the western Gulf.

Another approach to compare the wind and LC-driven circulation is in terms of the hypothesis of *Sturges and Blaha* [1976] (Sverdrup theory or vorticity balance). Therefore the western boundary current is a good place to evaluate the relative contribution of the forcing mechanisms. If we consider the Sverdrup theory alone, the WBC should represent the return flow for the meridional interior transport integrated along a zonal distance to be determined [*Sturges and Blaha*, 1976]. The meridional Sverdrup transport at any point in the ocean is

$$V_s \equiv \int_{-H}^{0} v dz = \frac{1}{\rho_0 \beta} \nabla \times \tau. \tag{4.2}$$

If $\mathbf{V_s} = U_s\,\mathbf{i} + V_s\,\mathbf{j}$, and $\nabla \cdot \mathbf{V_s} = 0$, there is a function $\psi(x, y)$ such that

$$U_s = \frac{\partial\,\psi}{\partial y}, \qquad\qquad V_s = -\frac{\partial\,\psi}{\partial x}, \tag{4.3}$$

which are first order partial differential equations that accept only one boundary condition. Then, with (4.2) and (4.3) the total meridional transport at point x is

$$\psi(x) = \psi(x = 0) - \frac{1}{\rho_0 \beta} \int_{x=0}^{x} (\nabla \times \tau)\, dx, \tag{4.4}$$

where $\psi(x = 0) = 0$, and $x = 0$ is the east boundary. Now the questions are where to put the east boundary in the Gulf of Mexico, where to stop the integration since (4.4) is valid only in the ocean interior away from the WBC, and at what latitude the integration should be conducted. Assuming that the WBC is ∼200 km wide [*Sturges*, 1993] then the integration can stop at 95W. The choice of the position of the east boundary is, however, not so clear since one may chose to put it at the Florida Straits or at the western edge of the Loop Current. Nevertheless, the second option appears more appropriate because the Loop Current is a dynamical barrier canceling the wind transport from east to west in the region to the east of 89W. Therefore the integration is conducted from 89W to 95W, which indeed is consistent with the area where the energy balance is investigated.

Figure 4.5a shows the mean Sverdrup transport streamfunction for the western GOM. This is how a purely wind-driven barotropic circulation may look if the model is run with a steady wind in the absence of dissipation, nonlinear interactions, and other forcing. The wind used to compute the mean wind stress curl that drives the Sverdrup circulation is the same used to drive the circulation in the model. There are two wind-driven gyres,

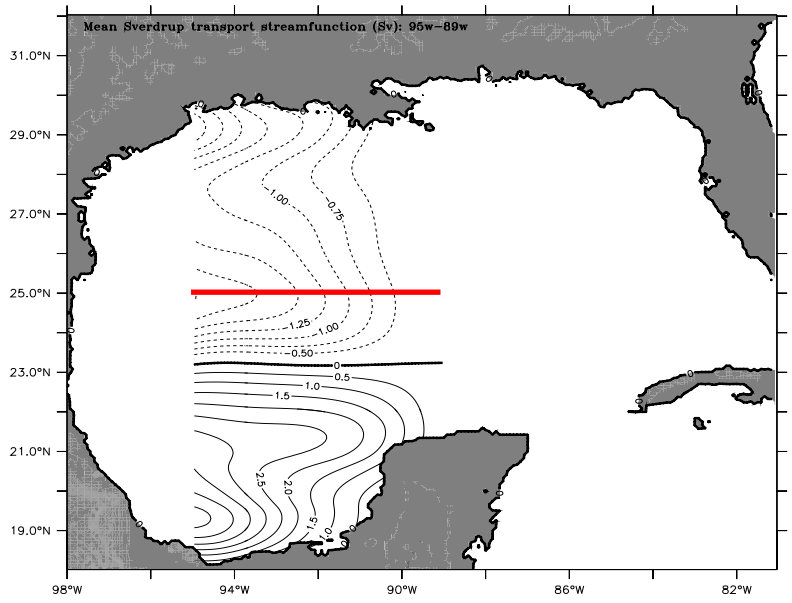

(a)

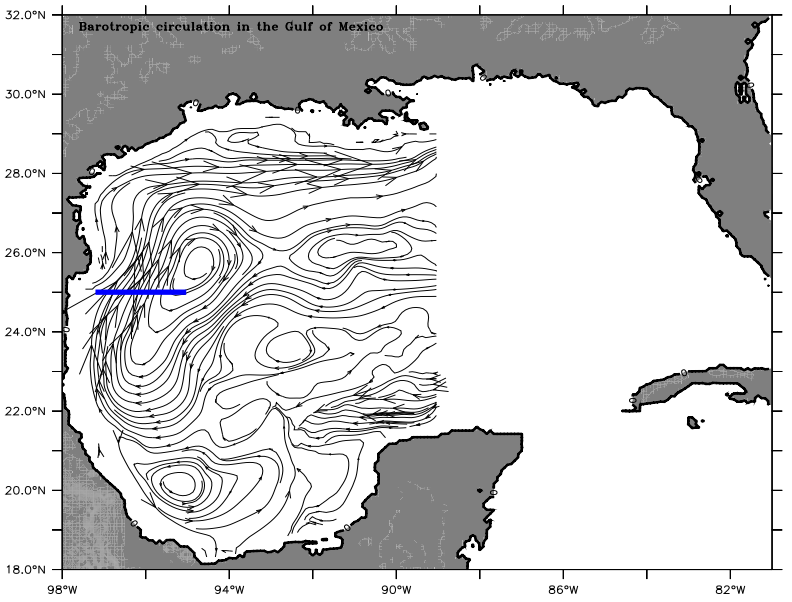

(b)

Figure 4.5: Barotropic circulation in the western Gulf of Mexico. (a) Sverdrup transport streamfunction (Sv) from 89W to 95W, calculated from the mean wind stress from the ECMWF dataset (1980-1986). Dashed lines represent an anticyclonic circulation, and solid lines stand for a cyclonic gyre; the contour interval is 0.25 Sv. (b) Flow lines for the barotropic circulation in the model.

Table 4.5: Mean transport at the western boundary current (25N).

Sverdrup transport Sv	model transport (97W-95W) Sv	model transport (97W-93W) Sv
2.41	10.11	3.78

one anticyclonic in the north, and the other cyclonic in the south, which is stronger. The Maximum transport in the anticyclone is ∼2.4 Sv at about 25N. Therefore we can chose this latitude to infer the return transport at the anticyclonic gyre's WBC. The red line in Figure 4.5a shows the extension of the transect where the meridional Sverdrup transport is integrated to infer the return transport at the WBC. In contrast, the blue line in Figure 4.5b shows the extension of the transect where the transport at the WBC is calculated from the model outputs. The Sverdrup circulation produces a return transport of 2.41 Sv across the WBC at 25N, while in the model the transport at the WBC (97W-95W) is 10.11 Sv (Table 4.5). Therefore, by considering these two values the Sverdrup transport is about 24% of the model transport at the WBC.

However, the most notorious difference between Figures 4.5a and 4.5b is the anticyclonic recirculation in the mean barotropic flow produced by MICOM in the western GOM, suggesting that the flow along the WBC has to recirculate in the region before rejoining the interior, which should allow dissipation to set the vorticity balance as predicted by the classical boundary layer nonlinear problems. Therefore, to take into account the transport due to the recirculation, we have to estimate the transport in the model across a transect covering the full zonal extension of the recirculation, for example at 25N from 97W-93W. This computation produces a net transport of 3.78 Sv across the WBC in the model (Table 4.5). Thus, by taking into account the recirculation the Sverdrup transport is about 64% of the net transport in the model across the WBC.

The pattern of the recirculation depends on the type of dissipation (lateral mixing or bottom friction), and the magnitude of dissipation compared to the inertial effects and to the boundary conditions, which in turn determine a priori the mechanism of global vorticity balance [*Pedlosky*, 1996]. Since the MICOM simulation uses no-slip boundary conditions thus lateral dissipation should be solely responsible for the vorticity balance in the boundary layer. Therefore it is convenient to evaluate the ratio of inertial effects to lateral dissipation within the boundary layer to asses the role of the two mechanisms on the onset of the western recirculation in the GOM.

The thickness of the inertial (δ_I) and Munk (δ_M) boundary layers are, respectively,

$$\delta_I = (U/\beta)^{1/2}, \tag{4.5}$$

and

$$\delta_M = (A_H/\beta)^{1/3}, \tag{4.6}$$

where β is the planetary vorticity gradient and A_H is the horizontal turbulent viscosity, given in MICOM by

$$A_H = max\left\{u_d \Delta x, \lambda\left[\left(\frac{\partial u}{\partial x} - \frac{\partial v}{\partial y}\right)^2 + \left(\frac{\partial v}{\partial x} + \frac{\partial u}{\partial y}\right)^2\right]^{1/2} \Delta x^2\right\}, \tag{4.7}$$

u_d is a bottom diffusion velocity and λ a constant. In MICOM, we put $u_d = 2$ cm s^{-1} and $\lambda = 1$.

Table 4.6: Boundary layer parameters in the western Gulf of Mexico.

U (cm s^{-1})	$\beta(24N)$ (cm^{-1} s^{-1})	A_H (cm^2 s^{-1})	δ_I (cm)	δ_M (cm)	δ_I/δ_M
43	2.0915 x10^{-13}	5 x10^8	1.43 x10^7	1.33 x10^7	1.08
"	"	1 x10^9	"	1.68 x10^7	0.85

Table 4.6 summarizes the boundary layer parameters for the western Gulf of Mexico in the MICOM simulation. By considering the time and volume-averaged, and maximum dissipation in the experiment (5 x10^8 and 1 x10^9 cm^2 s^{-1}, respectively), the ratio δ_I/δ_M is ∼0.85–1. Therefore, the recirculation in the model WBC does not represent a typical wind-driven inertial boundary layer since dissipation is as important as nonlinear dynamics. For instance, *Bryan* [1963] used no-slip boundary conditions on the eastern and western boundaries in a numerical experiment of a single-gyre, wind-driven ocean in a rectangular basin. His calculations showed that for $\delta_I/\delta_M \sim 1$ the solution of the wind-driven problem is similar to the linear Stommel solution. *Bryan* [1963] showed that in the case of low Reynolds numbers, $Re = (\delta_I/\delta_M)^2$, the generation of anticyclonic vorticity by the beta term in the northward flowing boundary current is closely balanced by its destruction through viscosity, and in this case the boundary flow can rejoin the interior flow directly north of the point of maximum wind curl. As the Reynolds number becomes greater, and the viscosity correspondingly less, the anticyclonic vorticity acquired by the boundary current must be diffused over a longer path before it is reduced to a value matching the interior regime, thus an inertial recirculation is produced [*Bryan*, 1963].

Obviously, in the MICOM experiment, and different to *Bryan* [1963] results, at $Re \sim 1$ the barotropic circulation is far away from the linear Stommel solution (Figure 4.5b), which indicates that in addition to the wind other mechanism should contribute in driving

the recirculation. That the western recirculation is not a result of a wind-driven inertial boundary layer is also observed in Figure 4.5, since the southern most extension of the recirculation (∼21N, Figure 4.5b) exceeds the zero wind curl contour (∼23N, Figure 4.5a). *Cessi et al.* [1987] developed a model to investigate inertial recirculations driven by potential vorticity anomalies, and found that in the subtropical gyre the recirculating gyre might be driven by anomalous values of low potential vorticity carried northward by the WBC. Therefore, an issue to investigate in the future is the contribution of LCR-driven potential vorticity anomalies on the onset of the recirculation in the western GOM.

4.5 Discussion

4.5.1 Boundary forcing in surface waters

Figure 4.3 shows that the variability in the bands of 101-300 and 301-500 days is strongly associated to LC northward extensions and shedding events. The energy in those bands counts for about 50% of the total forcing into the western Gulf. At higher frequencies, however, there is continuous forcing in the bands of 20-50 and 51-100 days, which together sum up to 30% of the forcing onto the western Gulf. Therefore the question is what causes such a variability. Figure 4.6 shows the 7-years, time-averaged baroclinic energy transfers taking place in surfaces waters of the LC (upper 500m in average). Between 25.5-27N, 89-86W there is a pool of $CPEKE < 0$, which means that in that region the perturbation velocity is building up a pressure gradient. A second region of $CPEKE < 0$ develops

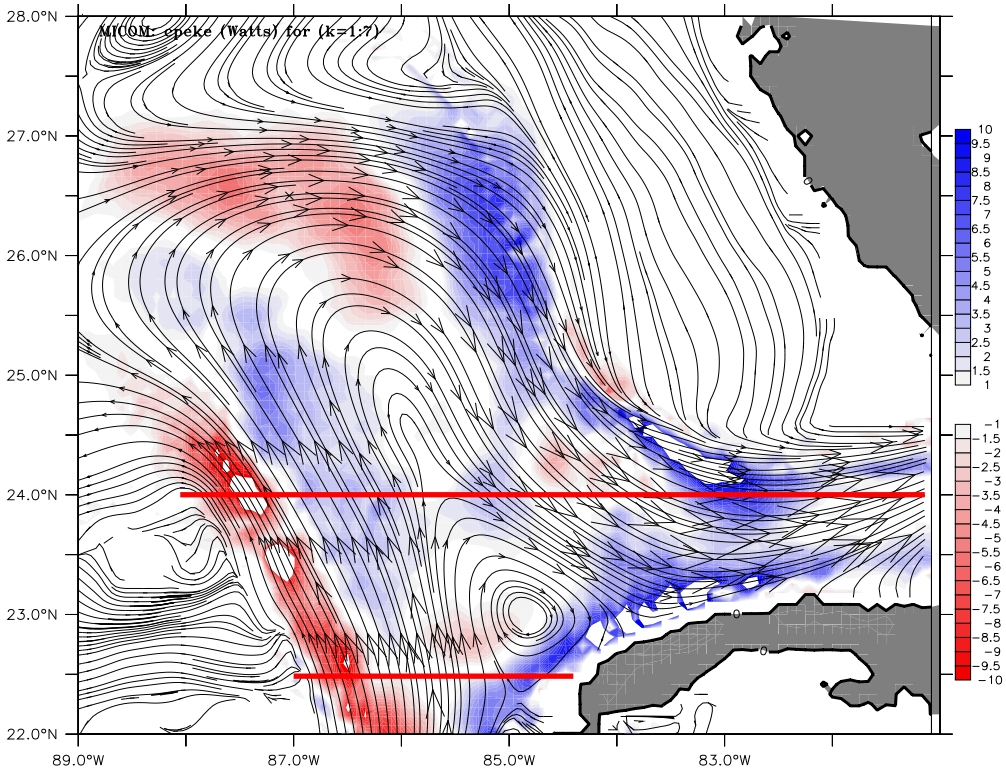

Figure 4.6: Volume-integrated baroclinic energy transfer in surface waters in the Loop Current region ($CPEKE$). Red scale stands for intensification of the pressure gradient by the fluctuating velocity field ($CPEKE < 0$), while blue scale stand for baroclinic conversion ($CPEKE > 0$). Values are in 10^7 Watts. Vertical distributions of $CPEKE$ for the transects in red are presented in Figure 4.7.

along the eastern edge of the Peninsula of Yucatan between 22-24.5N, 88-86W. Therefore it is of interest to determine what causes the alternate bands of positive/negative values in $CPEKE$ (Figure 4.6), and the temporal scales at which the perturbation velocity pushes up the density interfaces along most of the western and northern edges of the LC.

Figure 4.7 shows the vertical distribution of $CPEKE$ at two different latitudes in the Loop Current region. Figures 4.7a and 4.7b show alternate patterns of positive/negative values in $CPEKE$ even in regions where the flow is unidirectional and the density interfaces do not show significant changes in slope. Moreover, $CPEKE$ is bottom-intensified. These

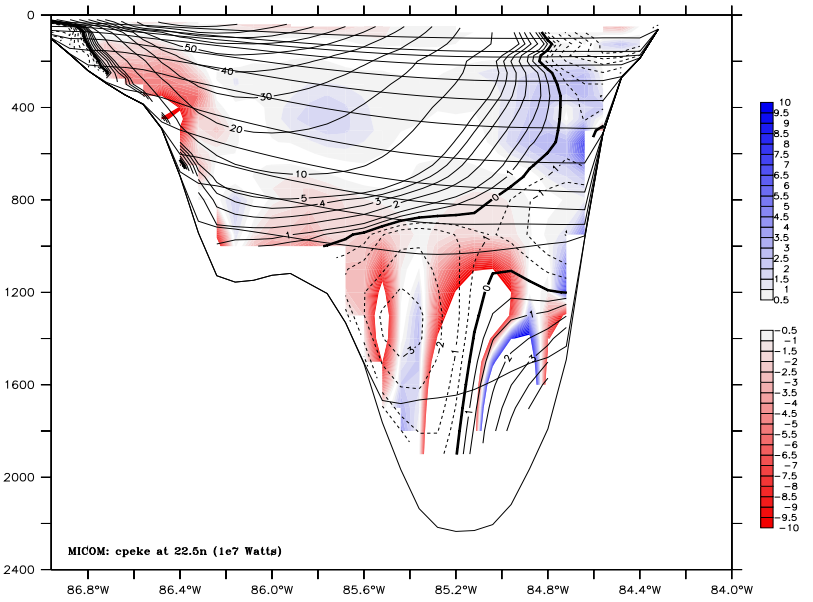

(a)

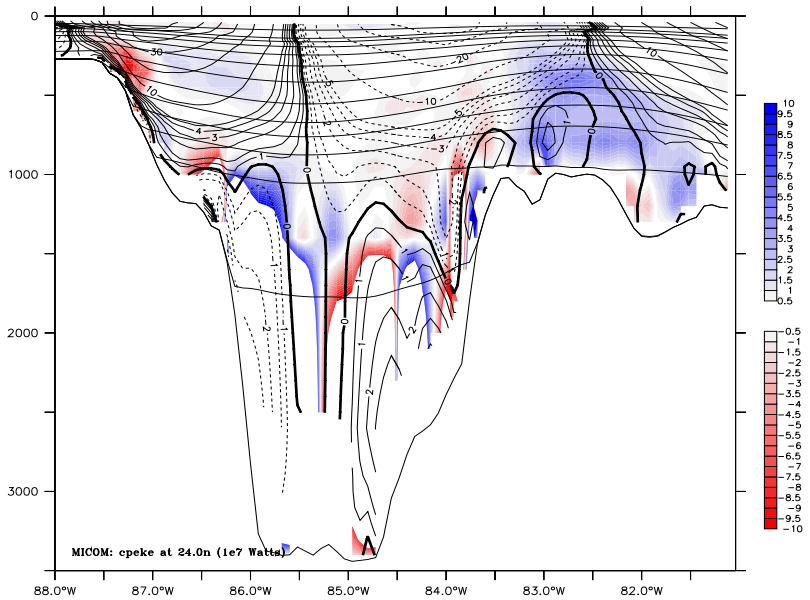

(b)

Figure 4.7: Vertical distribution of $CPEKE$ in the Loop Current region (color scale in 10^7 Watts). The labeled contours stand for the mean meridional velocity with positive values being northward velocities. The semi-horizontal contours (non-labeled) are the density interfaces. (a) 22.5N, and (b) 24N. The transects correspond to the red lines in Figure 4.6.

characteristics suggest standing topographic Rossby waves (TRWs) superimposed on the mean flow. These waves may result from the interaction of the LC with the topography due to east-west vacillations of the current's meridional axis. As a result of the longitudinal vacillations in the current's meridional axis, displaced fluid parcels along the topography gradient react to their new environment by developing either cyclonic or anticyclonic vorticity. *Chérubin et al.* [2005] identified that the longitudinal variations of the Yucatan Current maximum are correlated with the variations of the inflow transport in the Gulf of Mexico. In their results, each of the inflow peaks corresponds to an eastward shift of the Yucatan Current maximum, whereas the slowest transports correspond to a westward shift of the inflow. Similarly, the strongest deep outflows, in phase with the inflow transport variations, correspond to an eastward shift of the Yucatan Current maximum.

Figure 4.8 shows the energy spectra for the two baroclinic transfer terms at mooring M10, located at about 200m under the sea surface in the northern pool of $CPEKE < 0$ (26.5n, 87W). The spectra for $CPEKE$ reveals that most of the variability occurs between 20-115 days. This result indicates that the PE advected by the mean flow across 89W (PE_{flux}) in the band of 20-100 days may result from perturbations of the pressure field driven by the fluctuating velocity within the LC. The spectra for mooring M11 (not shown) located at 24N, 87.5W also shows high variability in the band of 20-100 days, though in this location there is more activity at higher frequencies, probably due to the vicinity to the Peninsula of Yucatan. The activity in the band of 20-100 days in mooring M11 supports the idea of TRWs triggered by the vacillations in the LC's meridional axis. The spectra for $CPEKE$ in Figure 4.8 also shows some variability at periods larger than 500 days. However, it is not clear what causes such a low-frequency signal.

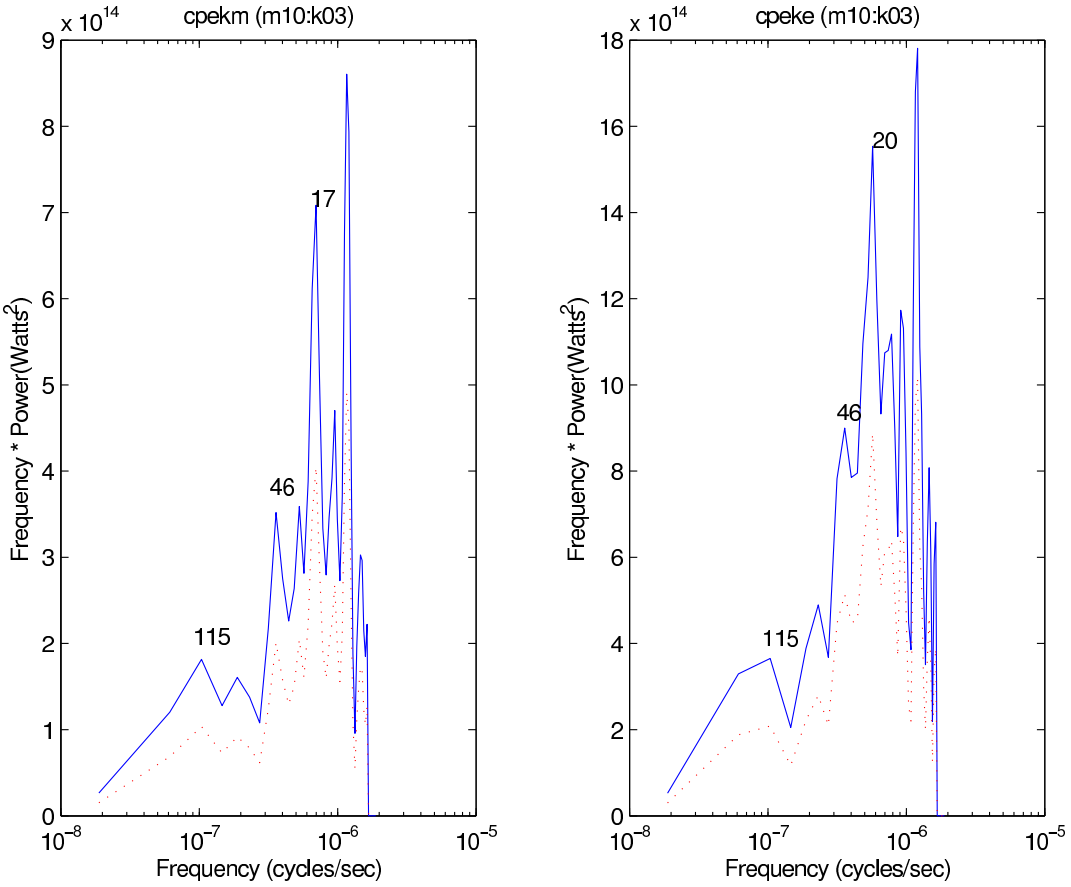

Figure 4.8: Spectra for $CPEKM$ and $CPEKE$ at mooring M10 (26.5N,87W, $z \sim$200m). The numbers in the spectra are days. The red dotted line represents the lower limit of the 95% confidence level with 18 degrees of freedom.

4.5.2 Boundary forcing in deep waters

Most of the boundary forcing (∼87%) applied into the deep Gulf of Mexico occurs at the bands of 101-300 and 301-500 days (Figure 4.4). The variability at 301-500 days shows a strong relation with the growing of the LC extension, and the band of 101-300 days appears to be related to shedding events as well. An intensification in the boundary fluxes across 89W is observed during the separation of the rings in the two bands. This is in agreement with findings by *Chérubin et al.* [2005], who report that at the end of each cycle of ring formation a sudden deepening of the LC deepest layers occurs together with an intensification of the transport and of the currents in the deep layer beneath the LC. This process is connected with the growth of the cyclones in the deep layers, which result from bottom-intensified instability of the LC ring and contribute to its separation from the LC [*Chérubin et al.*, 2005].

Figure 4.9 shows why the deep flows of PE across 89W are related with the LC cycle in waters above. At intermediate layers (∼1000-2000m depth) the fluctuating velocity builds up an intense pressure gradient beneath the NE and east edges of the LC ($CPEKE < 0$, Figure 4.9a). In response, the mean flow in the deeper layer is intensified by the fluctuating pressure gradient ($CPEKM > 0$, Figure 4.9b). Thus the deep circulation in the western Gulf of Mexico appears to be driven indirectly by dynamics underneath the Loop Current.

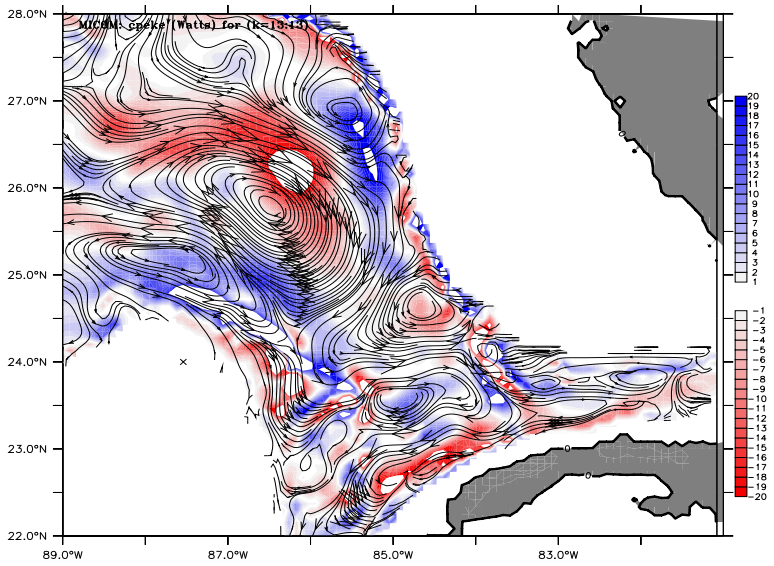

(a)

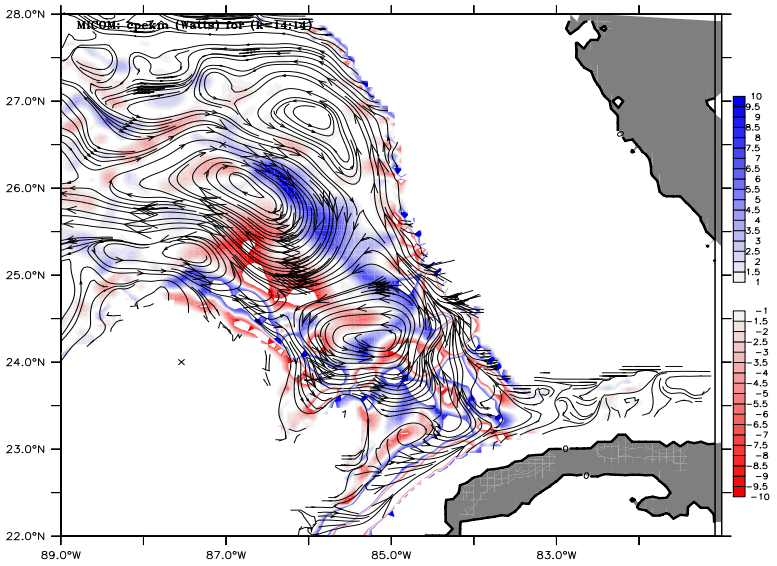

(b)

Figure 4.9: Volume-integrated baroclinic transfers in intermediate and deep waters underneath the Loop Current. (a) $CPEKE$ at layer 13; red scale indicates that the fluctuation velocity is building up a pressure gradient ($CPEKE < 0$), while blue scale indicates baroclinic transfers ($CPEKE > 0$). (b) $CPEKM$ at layer 14; red scale stands for intensification of the pressure gradient by the mean flow ($CPEKM < 0$), while blue scale stand for intensification of the mean flow due to the release of PE ($CPEKM > 0$). Values are in 10^7 Watts.

4.5.3 The relative unimportance of the wind

Table 4.4 indicates that $PEDIV$ is the most energetic contribution to the western Gulf of Mexico. In fact, this energy boundary flux is three orders of magnitude larger than the energy wind input. Therefore, in the energy domain the wind contribution into the western GOM is negligible. That the energy boundary fluxes across 89W should lead the energy cycle in the western GOM is not a surprising result, since early investigations of *Hurlburt and Thompson* [1980, 1982] revealed that a steady transport at the Yucatan Channel is enough to reproduce the dominant circulation features in models of the Gulf of Mexico forced with no wind. Table 4.5 indicates, however, that in terms of the Sverdrup balance (vorticity balance) the wind forcing may produce a return transport across the WBC in the order of 64% of the net transport in the model, which suggests that about 1/3 of the net transport across the WBC is driven by the LC eddies. In fact, the O(1) ratio of nonlinear to viscous effects in the boundary layer, together with the results of *Bryan* [1963] and *Cessi et al.* [1987] indicate that the LC eddies might be the leading mechanism driving the recirculation in the western GOM.

Given the limitations in the energy scheme discussed in section 2.6.2, and that the energetic analysis is a diagnostic tool instead of a mechanistic approach, the energy results discussed here should be taken as qualitative rather than quantitative results. In contrast, the analysis in terms of the Sverdrup balance in the interior and the closing of the circulation in the boundary layer by a mixing of viscous and nonlinear effects, seems to produce a more realistic picture of the circulation in the Gulf of Mexico, since the vorticity budgets provide a pure mechanistic approach to identify balances in the forces imparting spin (vorticity).

In the light of the relative unimportance of the wind input in the Gulf of Mexico energy cycle, one may wonder if it is possible to describe the Gulf's energy cycle without the wind. Some insight can be gathered in Figure 4.1. Interesting to notice is the west-southwest orientation of the area of positive wind work along the Campeche Bank during the four seasons, coinciding with the observed path of westward-propagating LC rings. This suggests that the wind may have some influence in determining the LCR trajectory during their propagation on waters far away from the topography. *Dewar and Flierl* [1987] demonstrated that the wind stress acting on surfaces flows produces a drag on a ring, and they suggest that a sizeable fraction of the observed motion of warm rings is in response to a connection between wind stress and ring sea surface temperature anomalies.

Figure 4.10 shows the mean surface circulation (upper layer) for 4 Loop Current cycles. The final statistical state for each cycle was obtained by time averaging between two consecutive PTP positions. Thus the time average is LCR oriented and summarizes the LCR life spans. Figure 4.10a (LC cycle 1) shows a distribution of positive wind work along the path of the LCR over the Campeche Bank. In fact, maxima in positive wind input are observed in the southern side of the LCR in the Bay of Campeche and in the WAC. The pattern replicates in each individual LC cycle: The LCR appear to propagate in the direction of the wind stress vector, and in any single ring the maximum in positive work occurs in its southern side. This pattern suggests that the wind arrests the LC rings. Therefore, even if the direct wind input may be negligible in the Gulf's energy cycle, it may play an important role in distributing the LC-driven forcing in the Gulf interior. This issue requires a deeper investigation.

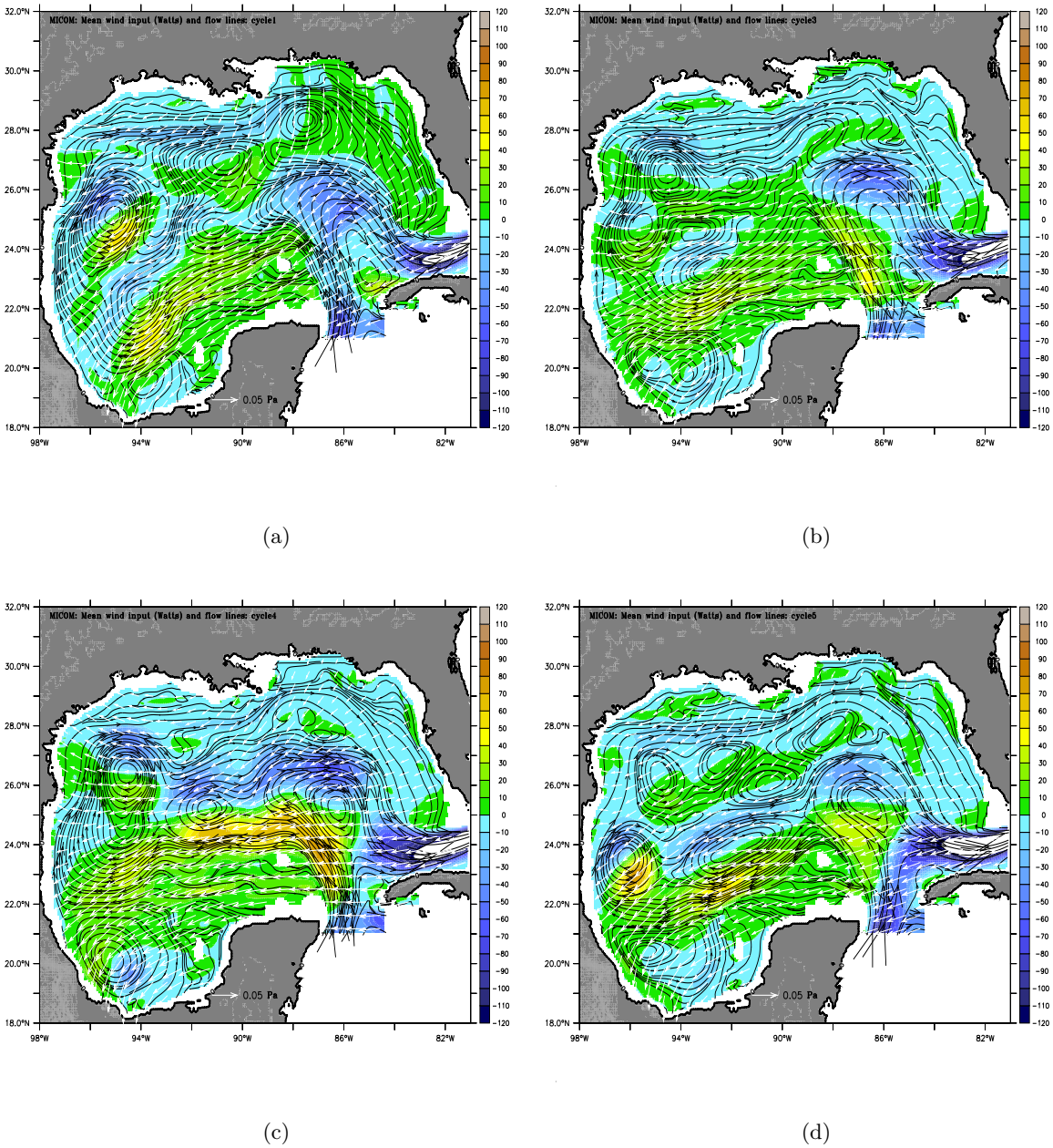

(a) (b)

(c) (d)

Figure 4.10: Time-averaged wind input into the Gulf of Mexico during four Loop Current cycles (Watts). Vectors are mean wind stress (Pa) computed from the ECMWF dataset (1980-1986); the color scale (Watts) is time-averaged work done by the wind on surface currents [$MWIND$, equation (2.15)]. Green-yellow-red colors are positive work, and represent regions where the mean surface flow is locally wind-intensified. Blue tones stand for areas where the mean surface currents do work against the wind stress. Flow lines are surface currents within the mixing layer. (a) cycle 1, (b) cycle 3, (c) cycle 4, (d) cycle 5.

4.6 Summary and conclusions

The wind and LC-driven forcing mechanisms were investigated in terms of energy budgets and the Sverdrup balance (vorticity balance), to evaluate their relative contribution in driving the circulation in the western Gulf of Mexico.

The energetic analysis revealed that mean advection of eddy potential energy ($PEDIV$) is the leading energy contribution to the western Gulf of Mexico. At surface waters, 50% of the variability of the PE flux across 89W is associated to the growing of the LC extension and LCR shedding; other 30% of the variability is associated to baroclinic transfers triggered within the Loop Current at periods between 20-100 days. At deep waters, $\sim$87% of the variability of the PE flux is related to the growing of the LC extension and LCR shedding.

The energy budget in the western Gulf of Mexico indicates that the energy wind contribution is negligible compared with the advection of eddy potential energy across 89W. However, the Sverdrup balance indicates that the wind-driven return flow at the WBC represents about 64% of the net return transport in the model, since the Sverdrup relation produces a return transport of 2.41 Sv for the interior, whereas in the model the net return transport is 3.78 Sv. In the light of the discussion in section 2.6.2 the results from the energy analysis should be taken as qualitative rather than quantitative.

In the model boundary layer the nonlinear and viscous effects are equally important, indicating that the anticyclonic recirculation in the western Gulf of Mexico might be driven by the LC rings. A vorticity analysis is required to evaluate the contribution of the eddy fluxes of vorticity to the vorticity balance in the boundary layer.

Even if the direct wind input is negligible in the Gulf of Mexico energy cycle, the wind stress may play a significant role in distributing the LC-driven forcing throughout the Gulf, by arresting the LCR and determining the place and rate of release of PE. This issue requires further investigation.

Chapter 5

Eddy-mean flow interaction in the Gulf of Mexico

5.1 Introduction

The kinetic energy of the geostrophic flow field in the ocean is dominated by mesoscale eddies with spatial scales of 50-500 km in sub-tropical latitudes. Several numerical experiments with eddy-resolving ocean circulation models have been conducted to understand the influence of the eddies on the large-scale transport of heat and momentum. *Holland and Lin* [1975] showed that mesoscale eddies spontaneously arise due to instabilities in the ocean currents, producing a transient oceanic circulation that eventually reaches the statistical equilibrium. *Holland and Lin* [1975] investigated the mean-flow interaction for the final statistical state, and they found that the eddies act to limit the amplitude of the mean flow in the upper ocean, are responsible for a downward energy propagation that fills the deep

sea with eddy energy, and create a downward momentum flux via Reynolds stress which is responsible for the creation of deep, time-mean, abyssal gyres. In fact, in *Holland and Lin* [1975] experiments the eddies are due to baroclinic instability, and reach a statistically steady state in which, on the average, the Reynolds stress tends to slow the upper layer mean flow and accelerates the lower layer mean flow and, in fact, the deep mean circulation is driven entirely by the eddies. Thus, the energy is extracted from the mean potential energy stored in the large-scale density field and fed into the eddies. The eddies in turn affect the mean flow by producing regions of positive and negative eddy viscosity.

The mean circulation, and the Gulf of Mexico eddies in their different forms (vortex or wave-like), have progressively been well documented from observations and numerical experiments. However, the role of the eddies in driving the Gulf of Mexico circulation has not been investigated, though it has been hypothesized that they may induce the observed deep mean cyclonic circulation, in particular via rectification driven by topographic Rossby waves [*Sturges et al*, 2004]. Moreover, the interaction of the LC rings with the topography in the western Gulf may have a substantial contribution during the onset of the observed western boundary current [*Vidal et al.*, 1999]. The translation of the LC eddies in surface and deep waters, and their decay via baroclinic transfer, should be important mechanisms redistributing heat and momentum within the Gulf.

With the aim of providing new insights on the role of mean-flow interactions in driving the Gulf of Mexico circulation, this section addresses the following question: What are the energy sources and sinks, and energy fluxes and transfers building up the energy levels in the mean flow in the Gulf of Mexico, and what is their nature? To answer the question, in this section the energy cycle in the whole basin, and the energy pathways in different regions, in

particular at the Western Boundary Current and the northern Gulf shelf, are investigated in terms of the prototype energy scheme (Figure 2.2) and the Reynolds stress analysis described in section 2.6.3. The goal is to evaluate the contribution of the eddies (vortex- or wave-like) in driving the circulation in the Gulf. To understand the differential baroclinic energetic adjustment within the Gulf the study is carried out separately for different waters depths.

5.2 Basin energetics

5.2.1 The energy cycle in the western Gulf of Mexico

The leading energy source for the western Gulf of Mexico is the potential energy advected by the mean flow across 89W ($PEDIV$, Table 4.4). Figure 5.1 illustrates how this energy flux influences the mean flow in the western GOM. Maxima in $PEDIV$ take place around the time when the Loop Current sheds a ring, since in the β-plane the rings propagate westward to conserve vorticity. In fact, about 50% of the variability in $PEDIV$ concentrates at periods associated to LC northwestward intrusions and shedding events (Figure 4.3). Thus, maxima in APE are highly correlated with maxima in the boundary flux of potential energy (Figure 5.1). Between maxima in $PEDIV$ the energy boundary flux drops below the time-mean value, although the energy flux oscillates smoothly around a stable level. However, the energy levels in APE reduce drastically, indicating an energy transfer ($CPEKE$ or $CPEKM$) to the velocity field within the basin interior since $PEDIV$ is

nearly non-divergent. In fact, Figure 5.1 shows that $CPEKM$ is positive during most of the time when APE is drained, which suggest that APE is fed to the mean flow. Nevertheless, the amplitude of $CPEKM$ is at least 50% smaller than $PEDIV$. Therefore, there should be an additional energy transfer to drain the residual PE for $PEDIV$ to be nearly non-divergent.

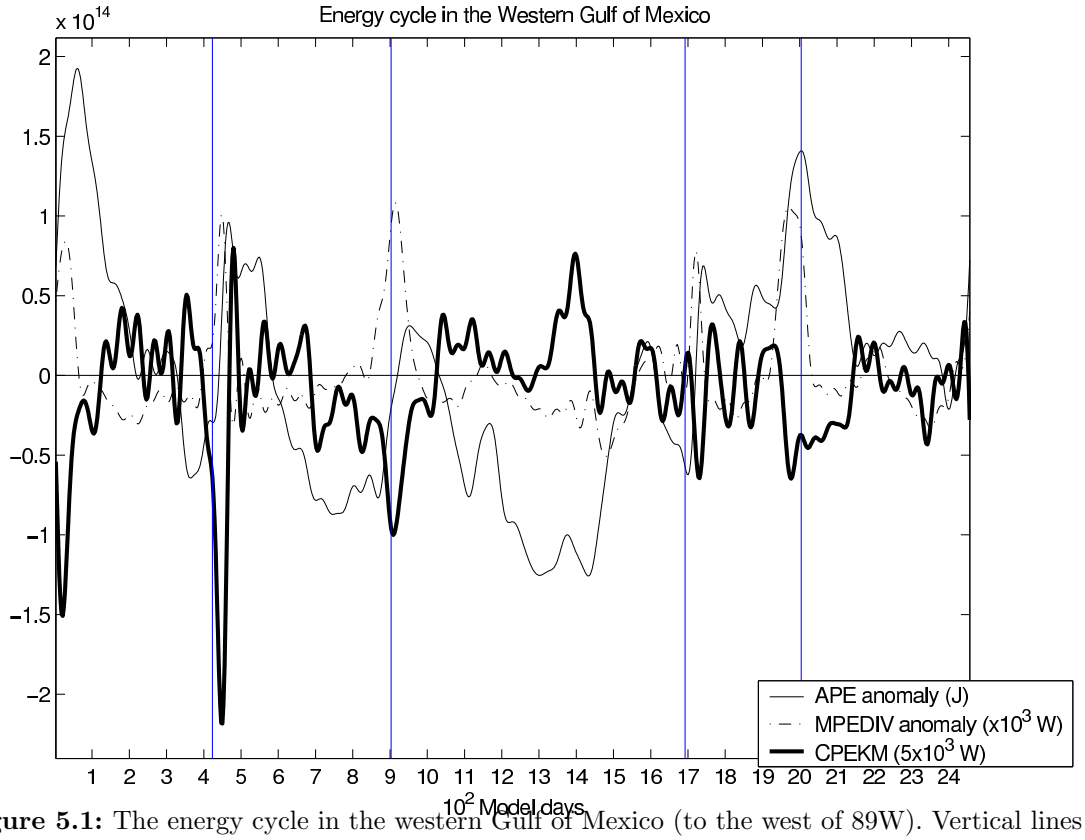

Figure 5.1: The energy cycle in the western Gulf of Mexico (to the west of 89W). Vertical lines separate Loop Current cycles. Values are volume-integrated quantities.

Figure 5.2 shows the baroclinic energy transfers in the western Gulf of Mexico. Between ring shedding events APE is fed into the kinetic energy of the fluctuating flow ($CPEKE > 0$), thus the energy levels in KE are larger than those in APE since $CPEKE > 0$ increases the horizontal mixing of momentum. $CPEKE$ is $\sim$10 times more energetic than $CPEKM$ (compare Figures 5.1 and 5.2), thus the increased horizontal mixing of momentum is the

leading process redistributing mass horizontally during the energetic adjustment remotely driven by the LC and its rings in the western Gulf of Mexico. The color picture in the upper left corner in Figure 5.2 shows the distribution of APE during a maximum level: a recently shed LCR is intruding into the western Gulf of Mexico across 89W, whereas the residuals of two old LC rings are located at about 24N/96W and 27N/95W. The color picture in the lower right corner in Figure 5.2 shows the distribution of APE for a minimum level: after 300 days the LCR is located at about 22N/95W and has lost ∼80% of its available potential energy; the two old rings have practically vanished. Therefore, the increased horizontal mixing of momentum erodes the LCR and strengthen the fluctuating flow for the western Gulf of Mexico to be energetically conservative.

5.2.2 The kinetic energy of the mean flow

The kinetic energy levels of the mean flow, KM, are larger along the topographic contours in the Gulf of Mexico (Figure 5.3). The most energetic flow in the western GOM is the WBC along the Mexican shelf, which in the model covers the upper 13 layers (∼upper 2000m); in the top 1000m the current is surface intensified. A deep western boundary counter-current (WBCC) develops below ∼2000m, and its intensity is comparable to that of the surface currents in the upper 500m (Figures 5.3a and 5.3d). In the northern shelf a bottom-intensified eastward jet develops along the topographic contours (Figures 5.3b and 5.3c), and eventually merges with the Loop Current at surface and mid-depths. In contrast, in deeper waters a central jet progresses westward below ∼2000m as part of the deep cyclonic circulation (Figure 5.3d).

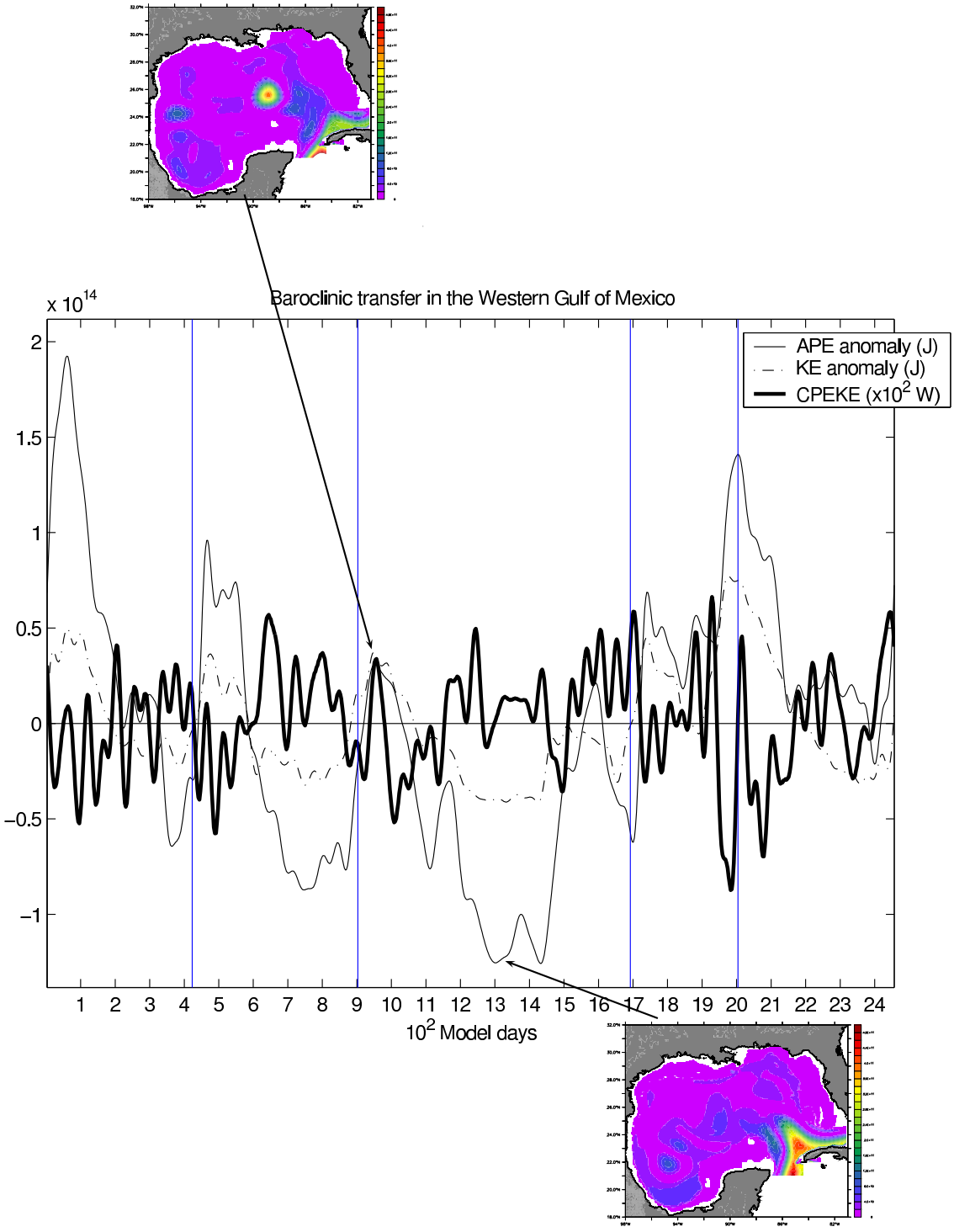

Figure 5.2: The baroclinic transfer in the western Gulf of Mexico. Vertical lines separate Loop Current cycles. Values are volume-integrated quantities. The upper Figure is a distribution of volume-integrated APE for a maximum level in potential energy, whereas the lower figure is a distribution for a minimum level.

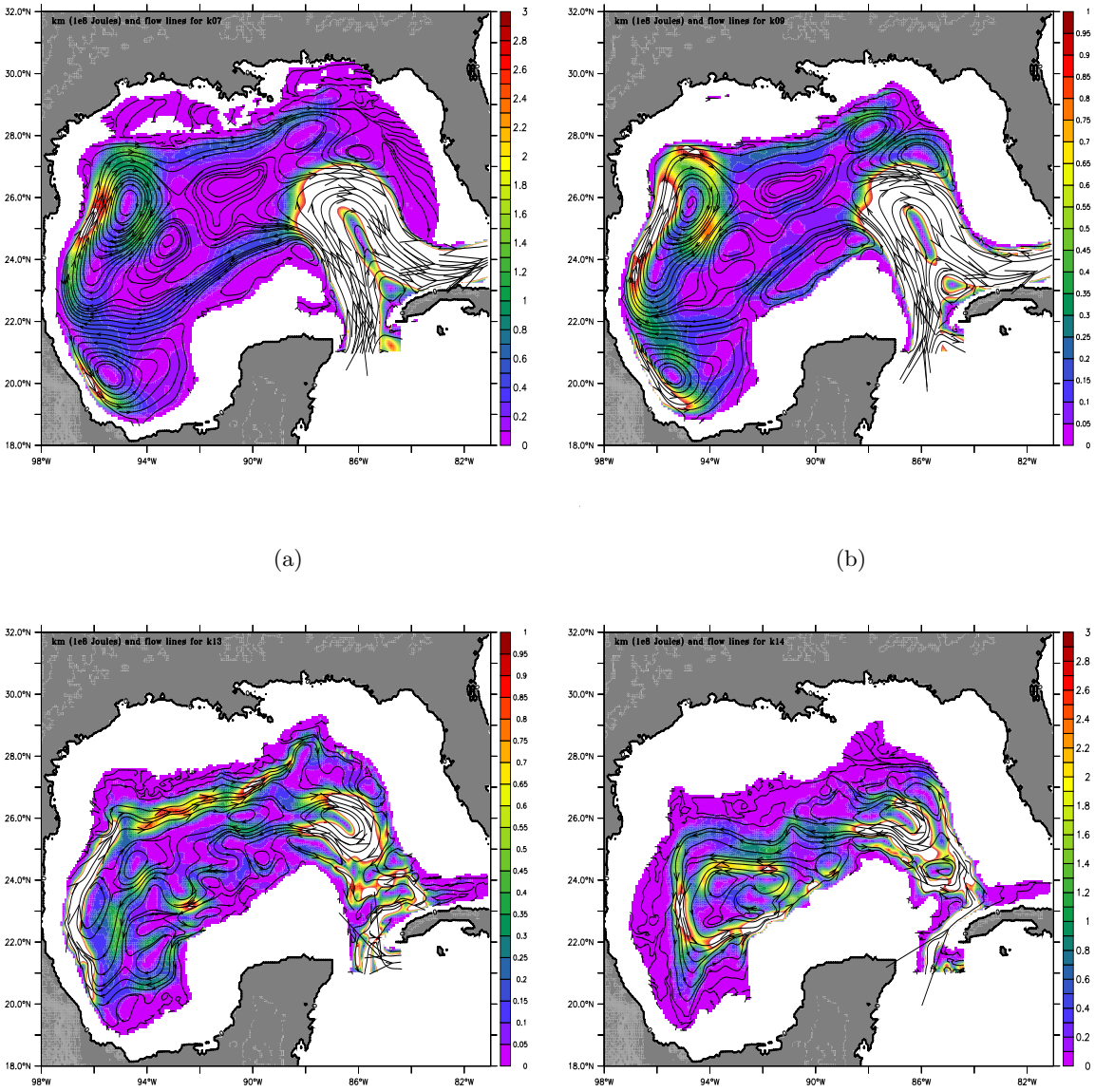

(a) (b)

(c) (d)

Figure 5.3: 7years-averaged, volume-integrated kinetic energy of the mean flow, KM, at four model layers (10^8 Joules). (a) Layer 7 (∼300m depth), (b) layer 9 (∼700m depth), (c) layer 13 (∼1700m depth), and (d) layer 14 (below 2000m in average).

5.2.3 The kinetic energy of the eddy flow

Figure 5.4 shows the distribution of the mean kinetic energy of the eddy flow at four different model layers, which are representative of surface, sub-surface, intermediate, and deep waters, respectively. At surface waters (layer 7, Figure 5.4a) most of the KE is concentrated along the path followed by the westward-propagating LC rings; secondary maxima are observed along the WBC and the Campeche Bay, and to lesser degree along the northern shelf. In sub-surface waters (layer 9, Figure 5.4b), the high KE tongue, which extends from the LC to the western GOM vanishes at about 92W. However, high concentrations of KE occur along the Mexican shelf and the northern shelf, the first being more energetic. The KE distribution in Figure 5.4b suggest a local source for the KE patch along the Mexican shelf. Moreover, KE increases with depth from surface to sub-surface waters in the northern boundary, where several authors have identified TRWs [*Hamilton*, 1990; *Oey and Lee*, 2002]. At intermediate waters (layer 13, Figure 5.4c), the KE band along the margins is less energetic than at sub-surface waters, with exception of a small patch along the WBC (24-25N). Despite that, an intense pool of KE extends between 22-25N/90-95W in a region dominated by several smaller vortex and a fluctuating westward jet. Finally, at deep waters a KE tongue extends in the central Gulf –away from the margins–, from the LC region to the western GOM, including the WBCC (Figure 5.4d).

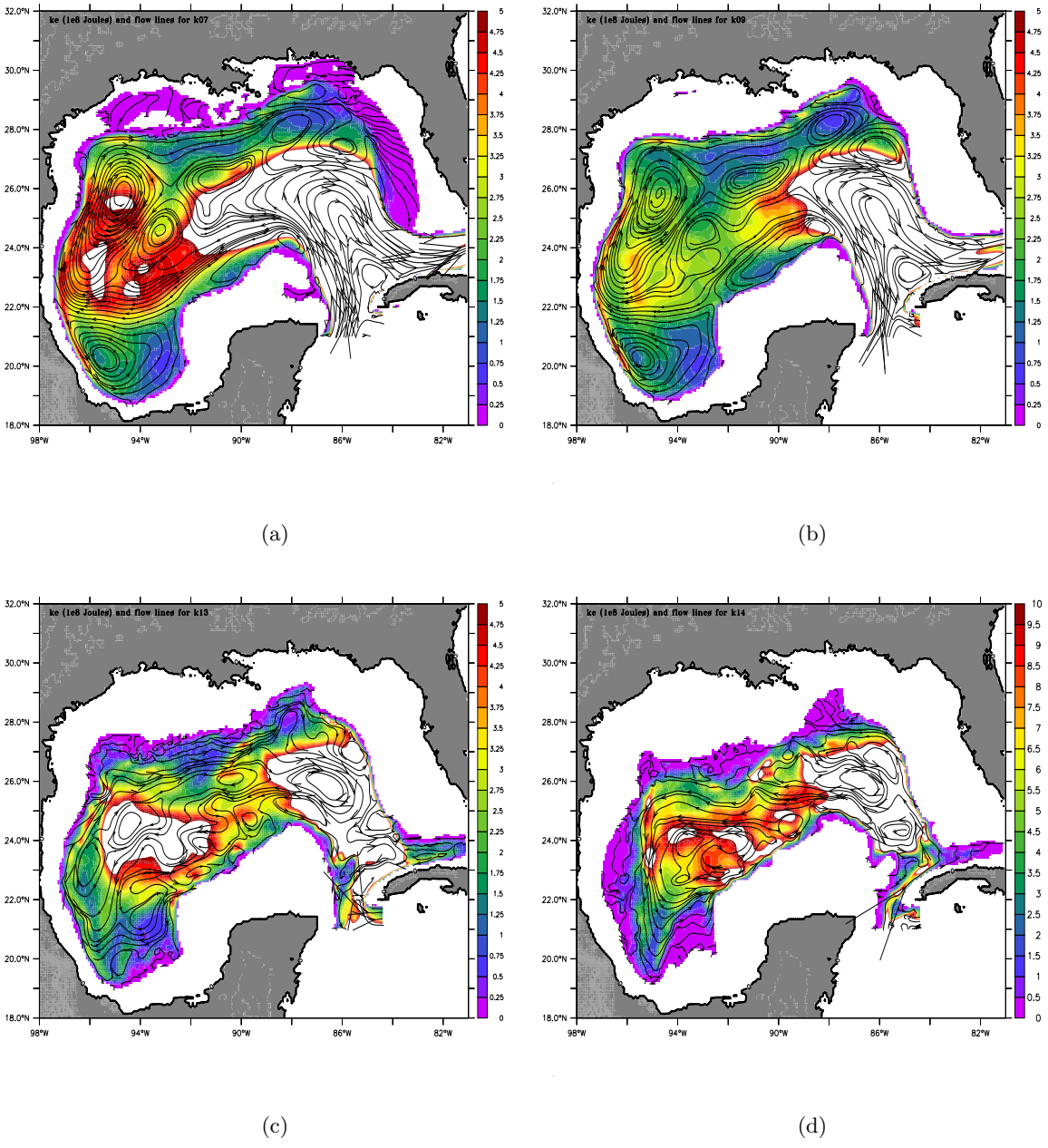

(a) (b)

(c) (d)

Figure 5.4: 7years-averaged, volume-integrated mean kinetic energy of the eddy flow, KE, at four model layers (10^8 Joules).(a) Layer 7 (∼300m depth), (b) layer 9 (∼700m depth), (c) layer 13 (∼1700m depth), and (d) layer 14 (below 2000m in average).

5.3 Eddy-mean flow interaction in the Western Boundary Current

5.3.1 KE sources

On the basis of the energy scheme (Figure 2.2) there are four sources/sinks for KE in the isopycnic Gulf of Mexico: $CKMKE$, $KEDIV$, $RSFDIV$, and $CPEKE$, the latest being the most energetic. Figure 5.5 shows the distribution of $CPEKE$ and $\overline{u'v'}$ at different layers. At surface waters (layer 7, Figure 5.5a) there are two local sources of KE due to baroclinic transfers nearby the Western Boundary Current ($CPEKE > 0$). One is located at the northeastern edge of the Western Anticyclone (25-27N/94-95W), and the second at the southeastern corner of the Bay of Campeche. In these regions (in the time-mean) the available potential energy is released to strengthen the horizontal mixing of momentum. Since no local sources for KE ($CPEKE > 0$) are observed along the path followed by the westward-propagating LC rings at surface waters, thus the high levels of KE in Figure 5.4a are due to energy advection. Compared to Figure 5.5a, in Figure 5.5b the baroclinic transfers are stronger, thus the induction of horizontal mixing of momentum ($CPEKE > 0$) is bottom intensified. Figure 5.5b suggests that $CPEKE > 0$ is the local energy source for the coastal band of KE in Figure 5.4b at sub-surface waters in the western Bay of Campeche. However, Figure 5.5b does not reveal any local source for the high levels in KE along the WBC in Figure 5.4b. Thus the KE source for the sub-surface waters in the WBC has to be remote (energy advection).

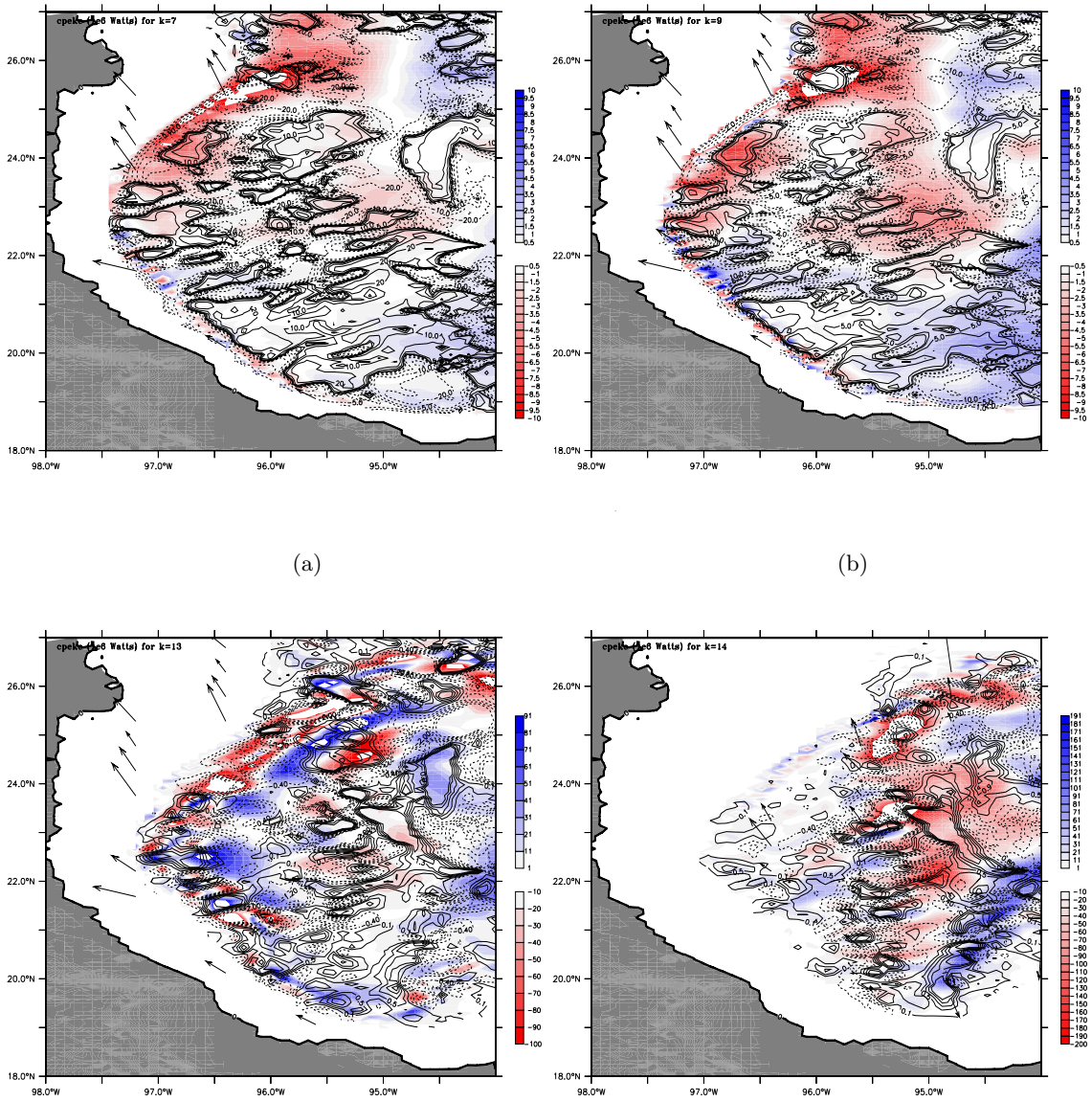

Figure 5.5: 7years-averaged $CPEKE$ (color scale in 10^6 Watts) and Reynolds stress (contours) at the Western Boundary Current in the Mexican shelf. The arrows indicate the orientation of the local β-north. (a) Layer 7 ($\sim$300m depth), (b) layer 9 ($\sim$700m depth), (c) layer 13 ($\sim$1700m depth), and (d) layer 14 (below 2000m in average).

At intermediate layers several local sources for KE develop along the WBC and the Campeche Bay ($CPEKE > 0$, Figure 5.5c). This may explain the presence of the pool of high levels in KE in Figure 5.4c, since advection of KE from the Loop Current region is not apparent. In fact, the flow lines in Figures 5.4b and 5.4c suggest the presence of strong vertical shears in the region. Finally, Figure 5.5d shows that at depth the largest baroclinic transfers take place at the southeastern corner of the Campeche Bay, where strong vertical shears are expected since the flow lines are anticyclonic at layer 13 and cyclonic in the layer underneath (Figures 5.4c and 5.4d).

5.3.2 KE sinks

Figure 5.5 shows that the most energetic contribution from the kinetic energy of the fluctuating flow to the western GOM is to build up pressure gradients ($CPEKE < 0$) along the Western Boundary Current (Figures 5.5a,b,c) and along the deep WBCC (Figure 5.5d). In the four layers the distribution of $CPEKE < 0$ mostly coincide with negative values in Reynolds stress, which, on the basis of the orientation of the local β-north, indicates polarization of the Reynolds stress in the second and/or fourth quadrants. Therefore, the local pressure gradients are mainly due to perturbations propagating along a SE-NW axis respect to the local β-north.

5.3.3 Mean flow rectification

Figures 5.6a,b show high rectification along the WBC at surface and sub-surface waters ($CPEKM > 0$). The rectification region coincide with the negative values in the Reynolds stress in the two layers. Both $CPEKM > 0$ and the Reynolds stress extend over the region of maximum intensity in the mean flow (Figures 5.3a,b), suggesting that the perturbation PE is fed into the mean flow. The negative Reynolds stress suggest a source for the perturbation PE located to the SE or to the NW of the WBC. However, Figures 5.6a,b show that the magnitude of the Reynolds stress decreases from SE to NW respect to the local β-north, which indicates that the source is at the Western Anticyclone and that momentum is lost to the mean flow in the NE direction. Therefore, this pattern suggests that the mean flow at the WBC is rectified by a perturbation pressure field sustained by the Western Anticyclone at surface and sub-surface waters. At intermediate waters in the WBC (layer 13, Figure 5.6c) the picture is not so clear, since the Reynolds stress does not vanish in the NW direction nor in the SE, which suggest that PE is not fed into the mean flow. Therefore the alternate patterns in $CPEKM$ in intermediate waters should be capturing a wave pattern superimposed on the background flow. Since the wave pattern is captured by the averaging procedure, its residence time at the WBC should be large and its frequency higher. This features, together with the negative values in the Reynolds stress suggest shorter planetary waves reflected from the western boundary (source for the fluctuations at the NW). At depth (Figure 5.6d), the $CPEKM$ distribution exhibits a wavy pattern following the topography everywhere, and sinks in the Reynolds stress are not evident. Thus the deep WBCC is not driven by rectification due to the fluctuating pressure field.

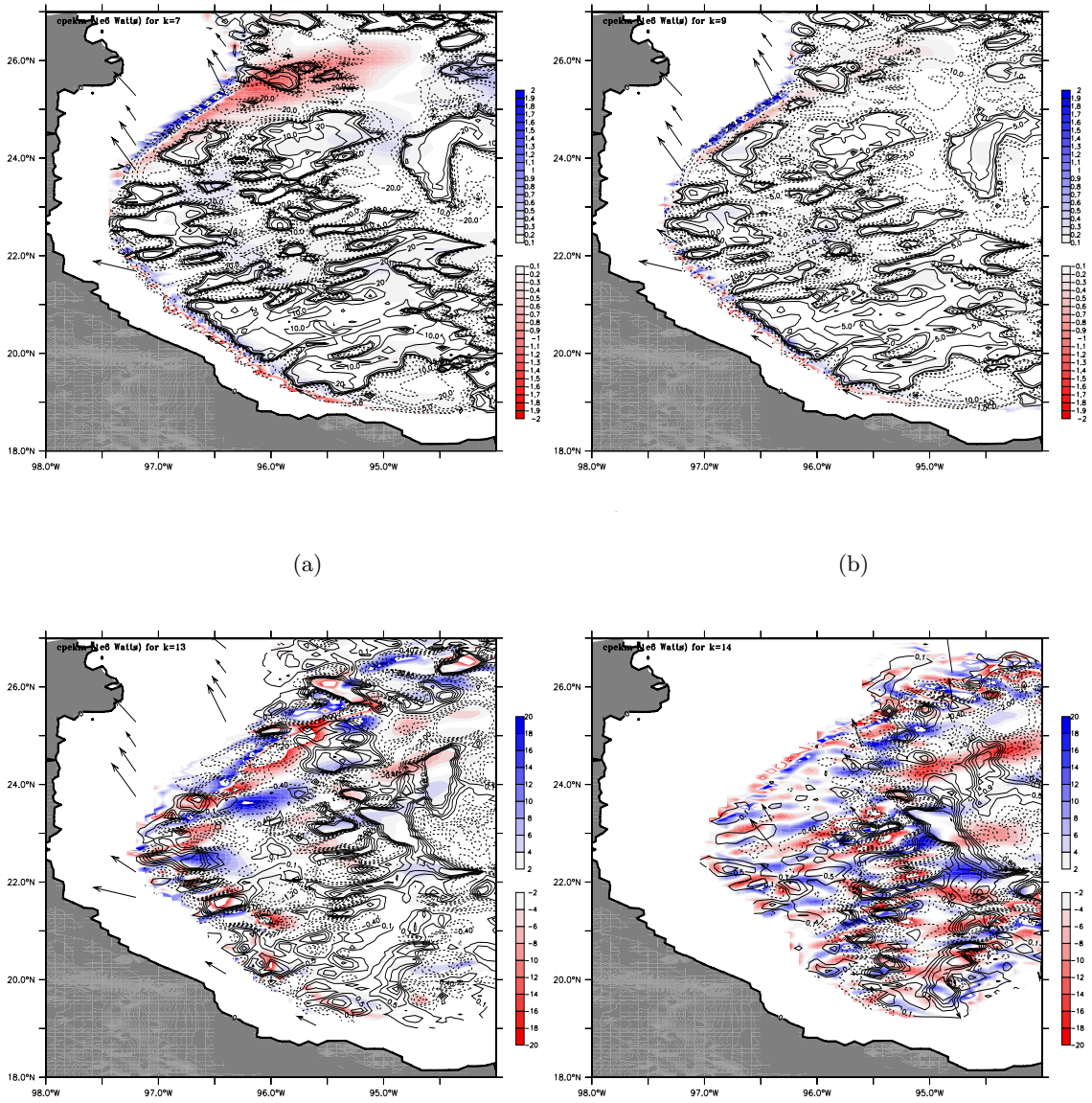

Figure 5.6: 7years-averaged $CPEKM$ (color scale in 10^6 Watts) and Reynolds stress (contours) at the Western Boundary Current in the Mexican shelf. The arrows indicate the orientation of the local β-north. (a) Layer 7 ($\sim$300m depth), (b) layer 9 ($\sim$700m depth), (c) layer 13 ($\sim$1700m depth), and (d) layer 14 (below 2000m in average).

At the Bay of Campeche the distribution of $CPEKM > 0$ along the southward WBC coincides with negative values in Reynolds stress, both at surface and sub-surface waters (Figure 5.6a,b). The orientation of the local β-north suggest a source for the fluctuations at the western shelf (NW quadrant) or at the cyclonic circulation (SE quadrant). However, the Reynolds stress vanishes from SE to NW, indicating that the source is at the cyclonic gyre, and that momentum is fed into the mean flow. The increased mean flow builds up a pressure gradient along the western shelf ($CPEKM < 0$, Figures 5.6a,b).

5.4 Eddy-mean flow interaction in the Northern Gulf of Mexico

For the sake of completeness in this subsection the NE corner of the Gulf of Mexico is added to the investigation, since there is an increasing scientific and economical interest in that area.

5.4.1 KE sources

Figure 5.7 shows the distribution of $CPEKE$ at different depths for the northern Gulf of Mexico. Figures 5.7a,b show two main local sources for KE ($CPEKE > 0$). One is located in the Texas shelf along the northern edge of the Western Anticyclone. The orientation of the local β-north in this region, and the positive values in Reynolds stress suggest an energy source at the SW quadrant, probably due to the interaction of the WAC with the topography. The second source for KE is located to the north of 27.5N, along

the western Florida shelf. In this case the orientation of the local β-north and the positive values in Reynolds stress suggest an energy source associated to the cyclone-anticyclone pair located on the northern edge of the Loop Current (Figures 5.4a,b and 5.7a,b). Secondary local sources for $CPEKE > 0$ extend along the Texas-Louisiana-Mississippi-Alabama shelf, to the south of a band of negative $CPEKE$ (Figures 5.7a,b). At intermediate waters (Figure 5.7c) the $CPEKE$ pattern is more complicated. However the alternate pattern of positive/negative values reveals a wave-like pattern along the topography. Finally, at depth (Figure 5.7d), an intense band of $CPEKE > 0$ runs along a SW-NE axis, associated to strong vertical shears due to the reversal in the circulation, form anticyclonic at intermediate layers, to cyclonic in waters underneath (Figures 5.4c,d).

5.4.2 KE sinks

Figures 5.7a,b show that the fluctuating velocity builds up a pressure gradient along the northern shelf of the Gulf of Mexico at surface and sub-surface waters ($CPEKE < 0$). Negative values in Reynolds stress along the Mississippi-Alabama-Florida shelf, together with the local orientation of the β-north suggest that the fluctuating velocity comes from the north of the Loop Current, where a cyclone-anticyclone-cyclone triad interacts with the local topography (Figures 5.4a,b). Figures 5.7a,b show negative values in Reynolds stress along the Louisiana-Texas shelf, which suggests that the fluctuating velocity originates at the SE or is reflected from the boundary (NW source). Finally, at depth waters (Figure 5.7d) the eddy velocity builds up a pressure gradient along a NE-SW axis that originates underneath the LC, and it is associated to the trajectory of westward-propagating eddies.

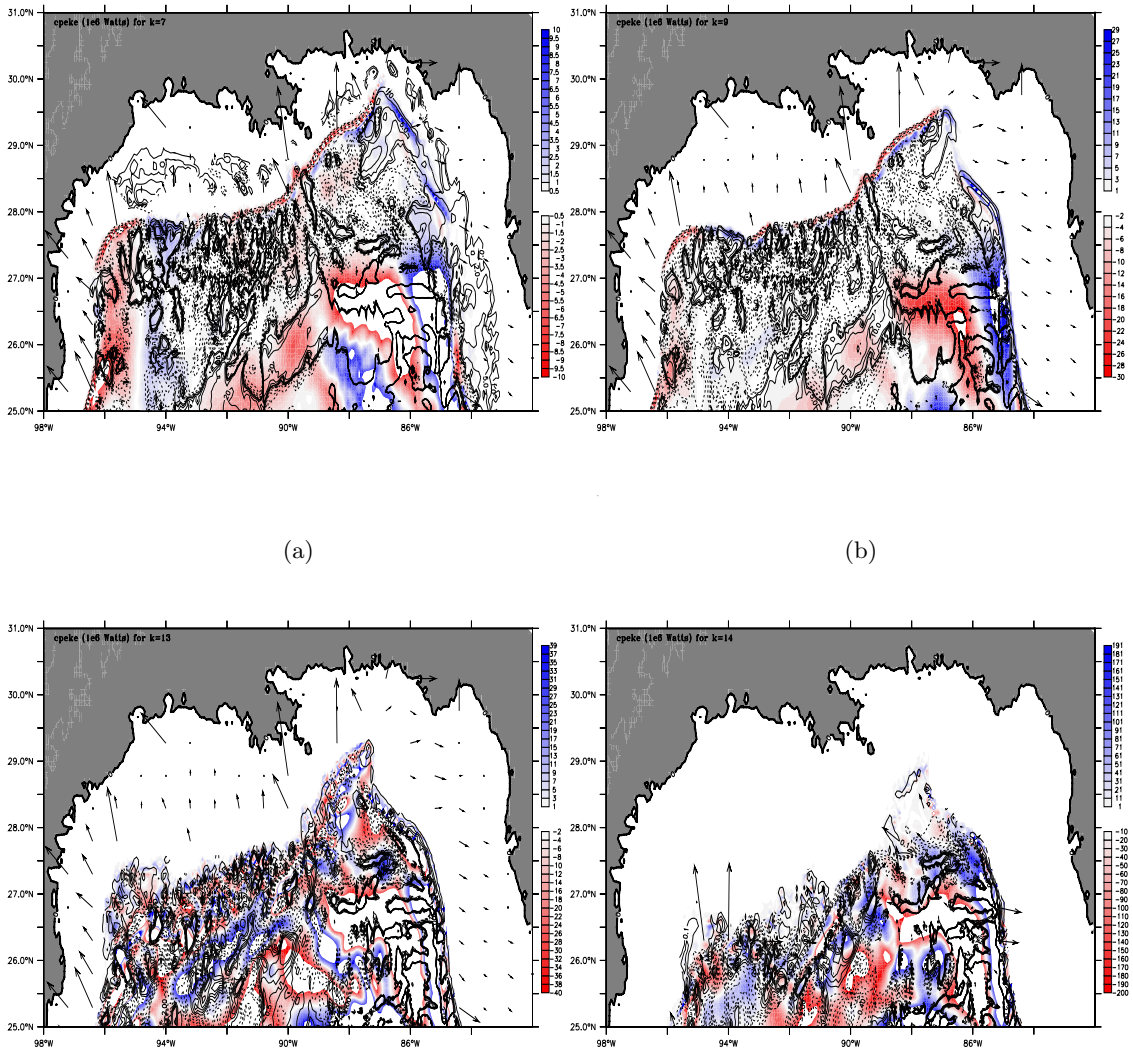

(a) (b)

(c) (d)

Figure 5.7: 7years-averaged $CPEKE$ (color scale in 10^6 Watts) and Reynolds stress (contours) at the Northern Gulf of Mexico. The arrows indicate the orientation of the local β-north. (a) Layer 7 (∼300m depth), (b) layer 9 (∼700m depth), (c) layer 13 (∼1700m depth), and (d) layer 14 (below 2000m in average).

5.4.3 Mean flow rectification

Figures 5.8a,b show a band of high rectification extending along the northern boundary of the Gulf of Mexico, both at surface and sub-surface waters ($CPEKM > 0$). The tendency in the Reynolds stress to diminish from SE to NW respect to the local β-north indicates that a transfer of energy from the perturbation pressure to the mean flow takes place. In fact, the distributions of $CPEKM > 0$, vanishing values in negative Reynolds stress, and high levels in KM are clearly correlated along the northern GOM (Figures 5.3a,b and 5.8a,b), though the KM belt is wider. In regards to the western Florida shelf, the distribution of $CPEKM$ along the shelf exhibits alternate bands of negative/positive values, and there is not a clear tendency for the Reynolds stress to diminish from SW to NE respect to the local β-north, which would imply a transfer of momentum from the perturbation pressure to the mean flow. Therefore, the mean flow is not rectified there. This idea is supported by the fact that KM (Figures 5.3a,b) does not show high energy levels where the $CPEKM$ belts extend along the western Florida shelf.

At intermediate and deep waters (Figures 5.8c,d) it is difficult to distinguish a rectification process, since the alternate values in $CPEKM$ evidence a wave-like distribution. Moreover, the Reynolds stress does not exhibit a tendency to vanish where the mean flow is increased (compare Figures 5.3c with 5.8c, and 5.3d with 5.8d). In fact, the $CPEKM$ transfer term is capturing the low-frequency waves superimposed on the mean flow, as discussed in section 2.6.3. The exchange of energy between the two flow forms is not evident.

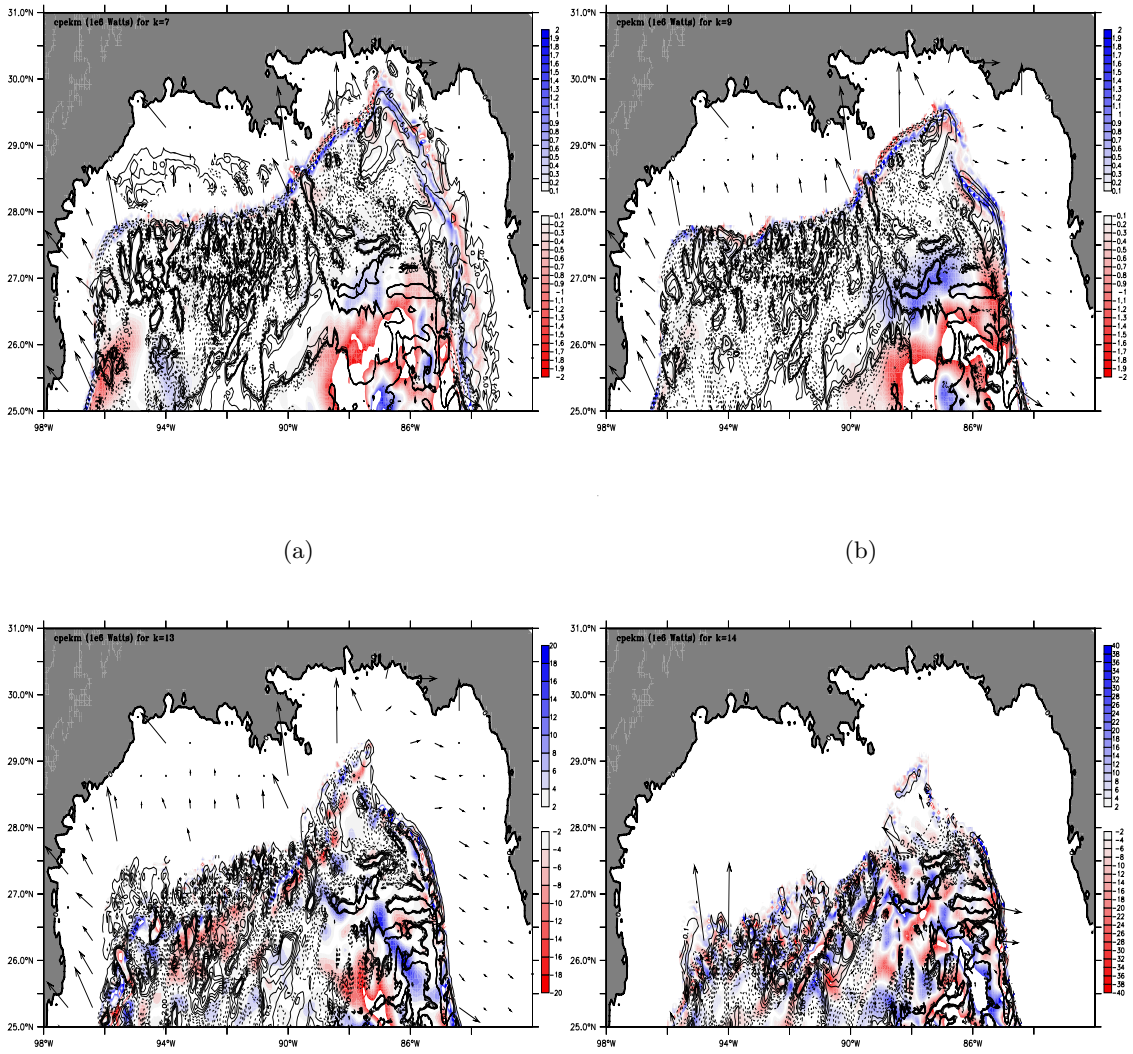

(a) (b)

(c) (d)

Figure 5.8: 7years-averaged $CPEKM$ (color scale in 10^6 Watts) and Reynolds stress (contours) at the Northern Gulf of Mexico. The arrows indicate the orientation of the local β-north. (a) Layer 7 (∼300m depth), (b) layer 9 (∼700m depth), (c) layer 13 (∼1700m depth), and (d) layer 14 (below 2000m in average).

5.5 Discussion

5.5.1 The baroclinic transfer and the energy cascade

The advection of potential energy by the mean flow, $PEDIV$, across 89W is the main energy supply to the Gulf of Mexico circulation. The baroclinic transfer is the mechanism driving the energetic adjustment within the western Gulf, in which the inflow of potential energy is fed into mean, but mostly into eddy horizontal flows. Thus the baroclinic transfer modulates the energy levels by increasing the horizontal mixing of momentum, which causes the western Gulf of Mexico to be energetically conservative. Therefore, it is of great interest to identify the regions where the PE is fed into the perturbation velocity, since this mechanism accounts for the creation of horizontal mixing of momentum.

Figure 5.9 shows the 7years-averaged, volume-integrated distribution of $CPEKE$ at the four vertical sections. In the four layers the induction of horizontal mixing of momentum ($CPEKE > 0$) take place mostly along the Campeche Bank and at the Bay of Campeche. In the northern Gulf another band of $CPEKE > 0$ extends zonally at sub-surface, intermediate, and deep waters. By comparing the flow lines between the layers, it is easy to identify vertical shears along the bands of $CPEKE > 0$, which are bottom-intensified. Therefore, the blue scale in Figure 5.9 highlights the regions where the horizontal mixing of momentum is enhanced. This process represents the pathway for the PE to degenerate during the energy cascade, which brings the system to the energy equilibrium.

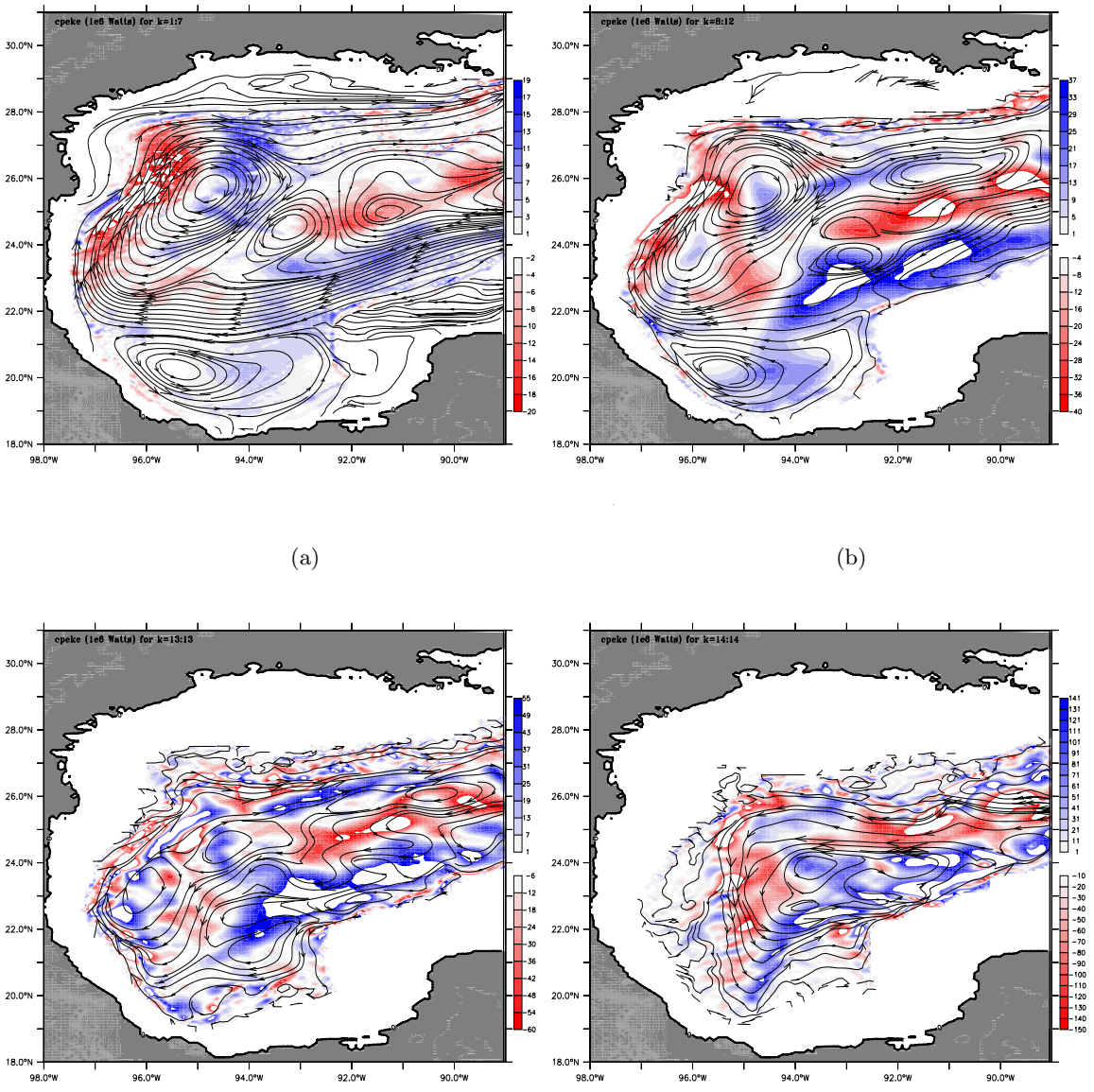

(a) (b)

(c) (d)

Figure 5.9: 7years-averaged $CPEKE$ (color scale in 10^6 Watts) and flow lines at the western Gulf of Mexico. (a) Surface waters, (b) sub-surface waters, (c) intermediate waters, and (d) deep waters.

5.5.2 The driving of the Western Boundary Current

The investigation of the eddy-mean flow interaction in the WBC revealed that the mean flow is rectified there along a narrow band (for example Figure 5.6a), though the current is wider (Figure 5.3a). Therefore it is important to clarify if the rectification process can be accounted for maintaining the mean flow in the WBC. Figure 5.10 shows the zonal structure of the mean flow at the WBC for layer 7 (25N). The width of the current is ∼200 km, in agreement with *Sturges* [1993]. The positive peak in $CPEKM$ at ∼96.6W corresponds to the rectification band in Figure 5.6a. Within the span of this peak the Reynolds stress vanishes from east to west, confirming an energy transfer from PE to KM. With exception of this peak, $CPEKM$ is negative or negligible within the WBC. Thus it is unlikely for $CPEKM$ to drive the WBC. In contrast, the dynamical length of $CPEKE$ is consistent with the scale of the mean flow. Actually, the higher intensity in KM at the western side of the current seems to be related to the intense negative peak in $CPEKE$. In addition, the magnitude in KM decreases from the core of the current to the east, in coincidence with the depletion of $CPEKE$ in the eastward direction.

To understand this result one should recall that $CPEKE$ has a twofold nature, since it can be accounted for as an energy transfer process, and as mechanism to detect wave activity (section 2.6.3). Therefore, the high correlation between KM and $CPEKE$ suggests that the WBC is mostly driven by the pressure field associated to perturbations sustained by the Western Anticyclone (see the sign of the Reynolds stress within the WBC in Figure 5.6a). Since $CPEKE$ does not have a direct energy pathway to KM, one can conclude that the the WBC is not sustained by energy extracted from the eddies. Instead, the WBC

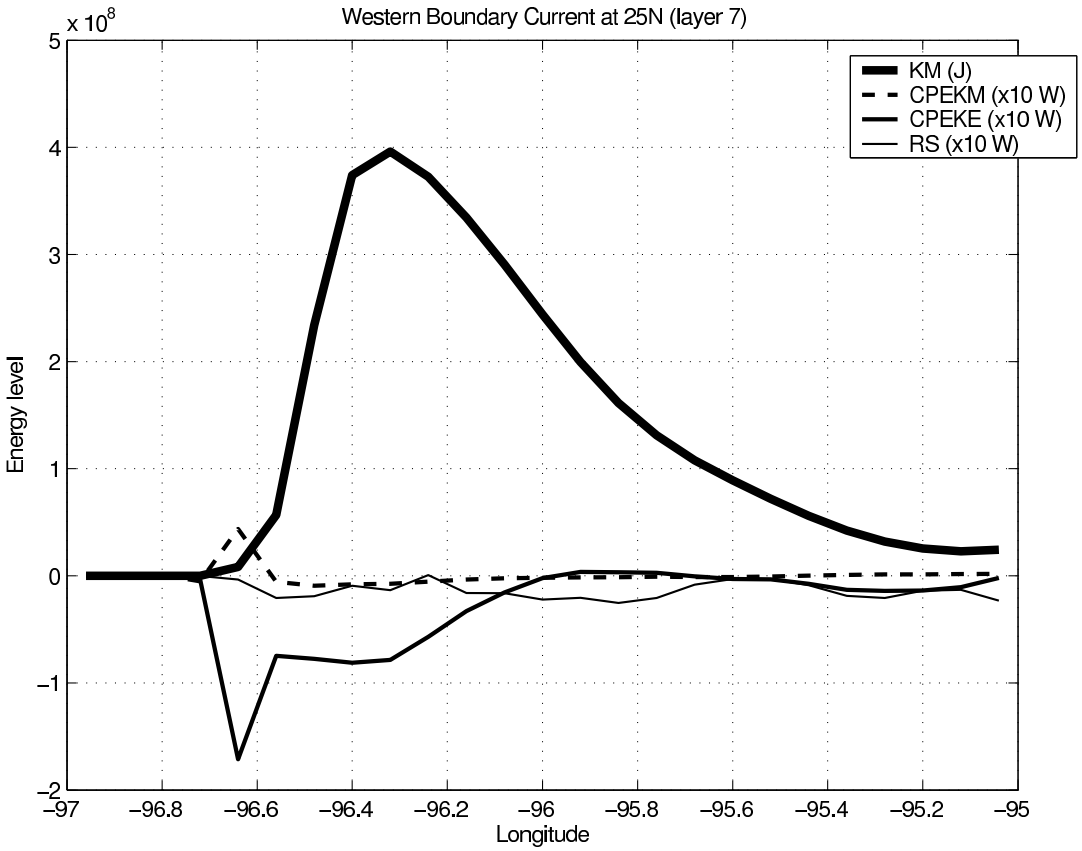

Figure 5.10: Zonal structure of the Western Boundary Current at 25N, layer 7.

adjust to the pressure field created by the eddies. In fact, this conclusion can be extended to the other marginal flows in the Bay of Campeche and the Northern Gulf of Mexico, since the dynamical length of $CPEKE$ –rather than $CPEKM$–, is in agreement to the mean flow width.

Figure 5.11 shows the distribution of the terms in the KM equation along the Western Boundary Current. The sum of the terms is positive only within the narrow rectification band, mainly due to $CPEKM$. Outside the rectification band the mean flow loses energy mainly by pushing down the density interfaces ($CPEKM < 0$ and $CPMKM < 0$). This may explain the depletion in the KM levels in the eastern side of the WBC. With exception of the baroclinic transfer terms the other terms in the KM equation are negligible.

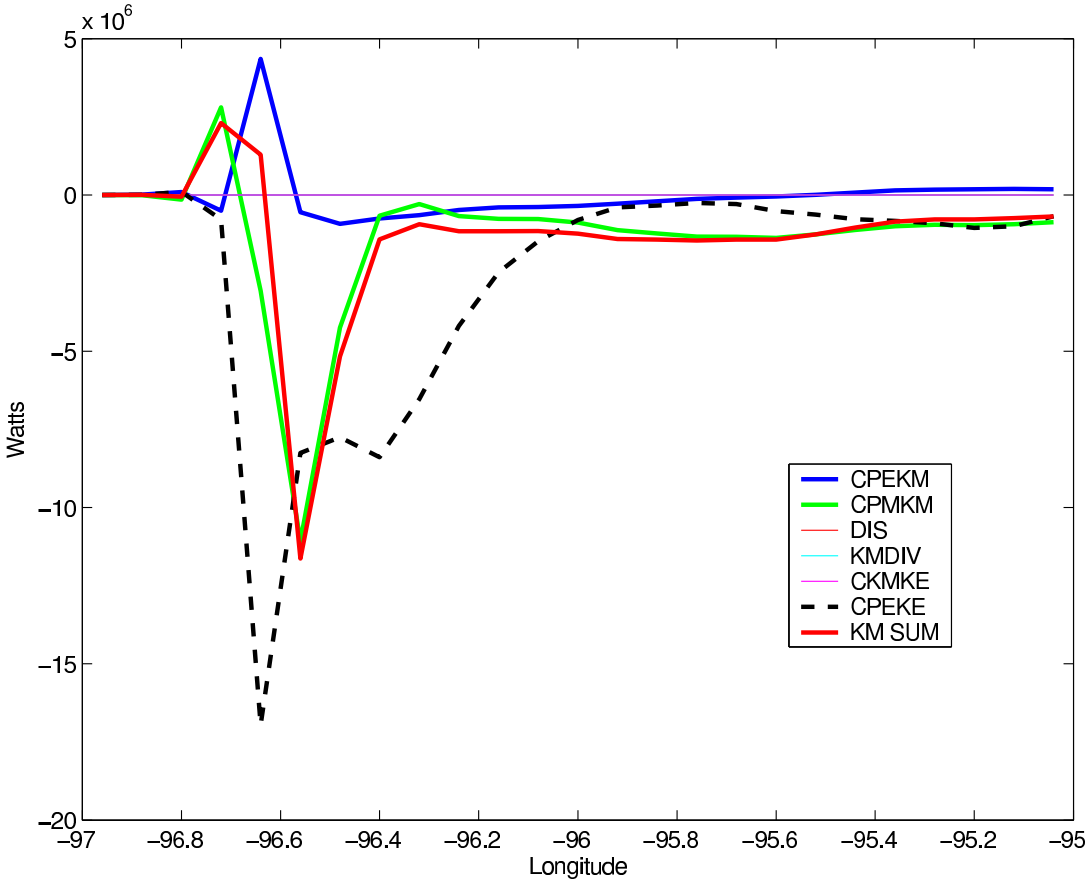

Figure 5.11: Zonal distribution of the terms in the KM equation along the Western Boundary Current at 25N, layer 7. The thicker red line is the sum of all the terms, whereas the thicker dashed line is $CPEKE$ from the KE equation.

5.5.3 The driving of the deep circulation

Sturges et al. [2004] posed the hypothesis that the deep mean circulation in the Gulf of Mexico could be determined –among other mechanisms–, by rectification driven by topographic Rossby waves (TRWs). However, the $CPEKM$ and the Reynolds stress analysis indicate that the waves in the model do not exchange energy with the mean flow in significant amounts (Figures 5.3c,d and 5.6c,d). Therefore it is of interest to clarify if the marginal waves in the model exhibit characteristics of TRWs. Figure 5.12 shows the power spectrum for $CPEKM$ at two places with intense wave-like activity, one at layer 13 and the other at layer 14. The spectra for the two layers show intense activity at periods similar to those reported previously for TRWs in the northern GOM [*Hamilton*, 1990; *Oey and Lee*, 2002]. The presence of TRWs in the model is also illustrated by the Reynolds stress analysis, since the technique enables to identify propagation characteristics for TRWs in terms of the polarization of the perturbation velocity. For example, the predominantly negative values in Reynolds stress along the norther boundary at layer 13, together with the local orientation of β-north (Figure 5.8c), indicate that the TRWs originate along the northern edge of the LC, and from the NE-SW axis followed by the deep eddies during their westward-propagation, in agreement with the findings of *Oey and Lee* [2002].

Figure 5.13 shows the vertical distribution of KE along two meridional sections at 90W and 88W. Figures 5.13a,b show that KE is bottom intensified in deep waters. The two Figures also illustrate the two separated tongues of KE at surface and deep waters, since at mid-depths the energy content vanishes. Figure 5.13a shows an small patch of bottom intensified KE at about 27.25N. In fact the spectrum in the left panel in Figure

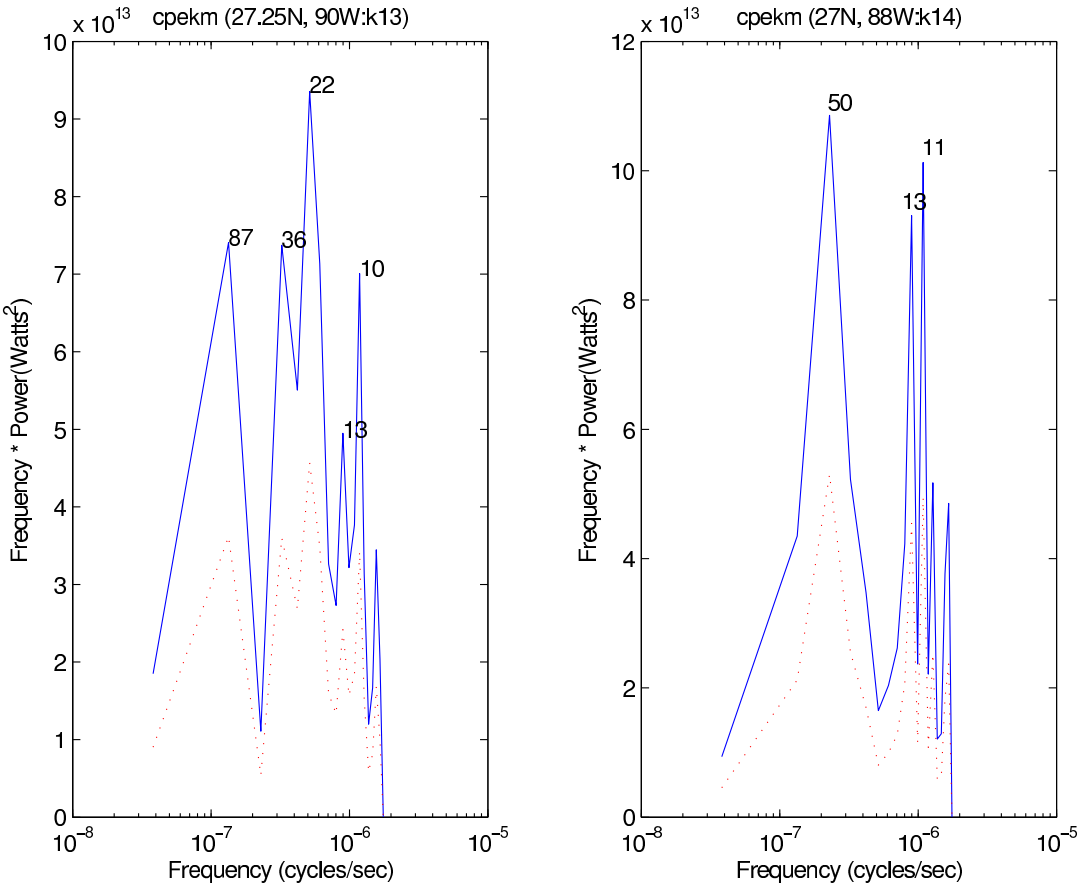

Figure 5.12: Spectra for $CPEKM$ at 27.25N/90W (layer 13) and 27N/88W (layer 14). The numbers in the spectra are days. The dotted line represents the lower limit of the 95% confidence level with 20 degrees of freedom.

5.12 corresponds to that place. In contrast, in Figure 5.13b it is difficult to identify the bottom-intensified KE for the location of the second spectrum in Figure 5.12 (27N/88W), since the energy levels in the center of the basin are higher. Figure 5.13 illustrates that the most energetic processes in the deep Gulf of Mexico take place underneath the surface LCR, and apparently are associated to deep eddies. Therefore, on the basis of this result it is unlikely that the TRWs in this model can drive the deep cyclonic flow.

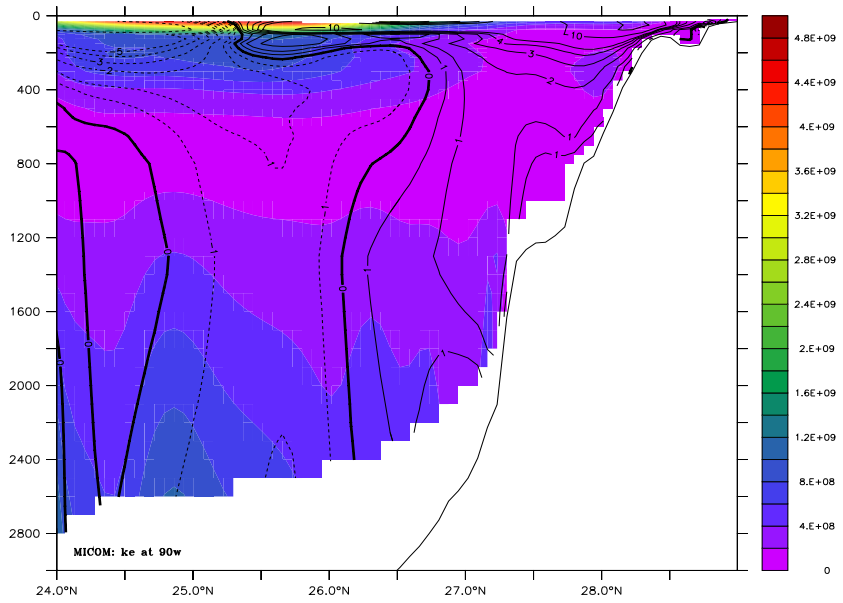

(a)

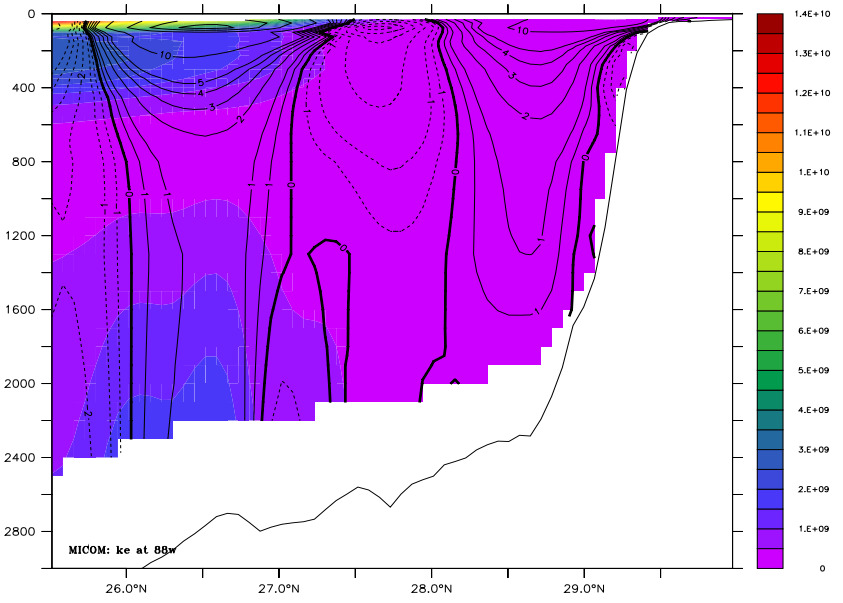

(b)

Figure 5.13: Time-averaged flow structure at 90W and 88W. Solid(dashed) contours are for eastward(westward) zonal velocities (cm/s). Color is volume-integrated mean kinetic energy in the eddy flow (J).

5.6 Summary and conclusions

In this section the energy cycle, and the eddy-mean flow interaction were investigated in the western Gulf of Mexico, at surface, sub-surface, intermediate, and deep waters.

The mean advection of potential energy across 89W is the main energy supply to maintain the Gulf of Mexico circulation, namely Loop Current intrusions, westward-propagating Loop Current rings and deep eddies. The baroclinic transfer emerges as the mechanism driving the energetic adjustment within the western Gulf, in which the inflow of potential energy is fed into mean and eddy flows.

At surface waters, the LC rings are the source for the eddy kinetic energy in the western GOM. At sub-surface and intermediate waters the LCR supply for KE vanishes in the western GOM. Thus local sources develop due to baroclinic transfers. At deep waters, the main energy source for KE is advection due to westward-propagating eddies. Secondary sources for KE are perturbations with characteristics of topographic Rossby waves.

The mean flow is rectified at surface and sub-surfaces waters along the southward jet of the Bay of Campeche Cyclone, the Western Boundary Current, and the northern boundary. However, the rectification is not strong enough to drive the mean flows within the Gulf. In fact, the perturbation velocity builds up pressure gradients along the margins of the Gulf of Mexico. There is a strong association of increased mean flows with the perturbation pressure gradients.

The Western Anticyclone sustains perturbations that build up a pressure gradient along the WBC. On the basis of our energetic formalism, this pressure gradient emerges as the leading mechanism driving the Western Boundary Current. Thus the decay of the Western

Anticyclone could be the process driving the WBC. This result should be verified with potential vorticity analysis.

Wave patterns with properties of topographic Rossby waves were identified at intermediate and deep waters. Both the energy transfer terms and the Reynolds stress analysis did not identified any significant energy exchange between the waves and the mean flow. Thus, the deep cyclonic circulation is unlikely to be driven by those waves.

Chapter 6

Thesis summary and conclusions

The main objective of this thesis was to study the role of the wind and the Loop Current in driving the circulation of the Gulf of Mexico. To this end, the dynamical adjustment under the influence of the two forcing mechanisms was investigated for the western Gulf of Mexico in terms of eddy-mean flow interactions. The subject was approached from an energetic point of view, thus model outputs from MICOM were decomposed into eulerian mean and eddy components, and their interaction was investigated in the energy domain. The model outputs came from a high-resolution, wind-forced, isopycnic numerical simulation of the North Atlantic Ocean, which included the Gulf of Mexico. This experiment incorporated the basin-scale variability into the Gulf through the Yucatan Channel, which allowed to reproduce realistic dynamics within the basin. This choice, however, imposed the computation of energy transfers in open domains, because the Gulf of Mexico has two open boundaries that connect it with the rest of the computational domain. Therefore, it was necessary to review the energetics in idealized closed and open systems with the

aim of defining an energy scheme suitable to investigate the eddy-mean flow interaction in isopycnic open domains.

In chapter 2 the energetics in closed and open systems was investigated in terms of the equation of conservation of total energy, and by means of a numerical experiment in which a double-gyre circulation was spun-up by a steady wind in a 2-layer, isopycnic square ocean. The analysis revealed that the conventional definition of the barotropic transfer terms cannot be applied directly in open systems, since the two barotropic terms differ by the divergence term, $\partial/\partial x_j \left(\overline{u'_\lambda u'_j}\overline{u}_\lambda\right)$, which vanishes upon volume integration over the whole domain, but has to be taken into account during the analysis of energetics in open domains. The divergence term was incorporated to the definition of an energy scheme that enables to investigate "eddy, time-mean" interactions in isopycnic open systems. Under this approach all the energy conversion terms canceled identically. However, the introduction of the divergence term complicated to identify barotropic energy conversion from the perturbation energy flux. The subregional energetic analysis showed that when a subregion is exposed to external boundary forcing, under inviscid and adiabatic conditions the subregion conserves energy only when the total energy content in the inflows balances the total energy content in the outflows. Opposite dynamics must work in the different subregions for the whole system to satisfy this condition and become energetically conservative. The equilibrium state was reached and kept as long as the energy transfers operated oppositely in the subregions. The investigation also revealed that the box diagrams commonly used to summarize the energetics in a closed system can be misleading, preventing to asses properly the relative contribution of the barotropic and baroclinic energy transfers during the onset of instabilities in the flow. Given the limitations to interpret energy transfers in open

domains, a technique was developed in which the baroclinic transfer terms $CPEKM$ and $CPEKE$, in conjunction with the Reynolds stress, allowed a heuristic description of "eddy, time-mean" interactions in isopycnic coordinates. The technique was applied to identify sources of Rossby waves in the double-gyre experiment, as well as regions where the mean flow is rectified by the eddies.

Chapter 3 provided a description of the numerical simulation of the North Atlantic and the processing of model outputs. In addition, the model outputs were compared with the available observations.

In chapter 4 the wind and LC-driven forcing mechanisms were investigated in terms of energy budgets and the Sverdrup balance (vorticity balance), to evaluate their relative contribution in driving the circulation in the western Gulf of Mexico. The energetic analysis revealed that mean advection of eddy potential energy ($PEDIV$) is the leading energy contribution to the western Gulf of Mexico. At surface waters, 50% of the variability of the PE flux across 89W is associated to the growing of the LC extension and LCR shedding; other 30% of the variability is associated to baroclinic transfers triggered within the Loop Current at periods between 20-100 days. At deep waters, ∼87% of the variability of the PE flux is related to the growing of the LC extension and LCR shedding. The energy budget in the western Gulf of Mexico indicated that the energy wind contribution is negligible compared with the advection of eddy potential energy across 89W. However, the Sverdrup balance showed that the wind-driven return flow at the WBC represents about 64% of the net return transport in the model. Our investigation showed that in the model boundary layer the nonlinear and viscous effects are equally important, indicating that the anticyclonic recirculation in the western Gulf of Mexico might be driven by the LC rings.

A vorticity analysis is required to evaluate the contribution of the eddy fluxes of vorticity to the vorticity balance in the boundary layer.

In chapter 5 the energy cycle and the eddy-mean flow interaction were investigated for different depths in the western GOM. Baroclinic energy transfers emerged as the mechanism driving the energetic adjustment within the western Gulf, in which the inflow of potential energy was fed into mean and eddy flows. Vertical shears along the Campeche Bank, the Bay of Campeche, and the northern Gulf, were associated to the baroclinic energy transfers. The LC eddies were identified as the source of KE in surface waters of the western GOM. In contrast, at mid-depths, the advection of KE due to westward-propagating LC rings vanished, and local baroclinic transfers were the source of KE. At deep waters, perturbation flows associated to ring shedding were identified as the main source of KE; secondary sources were associated to perturbations with characteristics of topographic Rossby waves (TRWs). The energy analysis revealed that although the mean flow was rectified at surface and sub-surfaces waters along the margins of the Gulf of Mexico, the rectification was weak and could not account for driving the large scale mean flows within the basin. In contrast, the perturbation velocity built up pressure gradients along the boundaries where the mean flow was increased. In particular, it was noticed that the Western Anticyclone sustained perturbations that built up a pressure gradient along the Western Boundary Current, which suggested that the decay of the Western Anticyclone is the process driving the Western Boundary Current. Moreover, wave patterns with properties of TRWs were identified at intermediate and deep waters. The energy and Reynolds stress analysis did not identified any significant energy exchange between those waves and the background flow, which indicated that other mechanisms should drive the deep cyclonic flow.

The most important limitation of this investigation is that the scarcity in oceanographic observations collected so far in the Gulf of Mexico prevents to verify our results. At the moment, these results can be verified only by applying our energy scheme to outputs from other models, or by comparison with potential vorticity balances. Nevertheless, under this scenario we still depend on approximations to the reality. Thus the challenges are to increase the number of oceanographic surveys in the Gulf, and to install an oceanographic data-collecting network, specially at deep waters and the western Gulf.

On the basis of the results of this investigation new research lines can be proposed. In particular, the interaction of the wind with the LC and its rings requires a deeper and more specific treatment, since this process may explain the observed seasonal variability in the transport across the Florida Straits, which is not apparent in the transport across the Yucatan Channel. This is an important issue since the wind stress may determine the place and rate of release of available potential energy within the Gulf, thus influencing the horizontal mixing of heat and momentum.

In contrast, our results suggest that the investigation of the nature of the deep cyclonic circulation should focus on other mechanisms rather than topographic Rossby waves. Therefore, the other two hypothesis for the deep cyclonic flow proposed by *Sturges et al.* [2004] acquire more relevance, namely, (1) the adjustment in relative vorticity that should result when the denser inflows sink after passing the threshold of the Yucatan Channel, and (2) the tendency for deep denser waters to move with the topography at its right.

In conclusion, it was found in this thesis that the most energetic contribution to the circulation of the western Gulf of Mexico in the MICOM simulation is the boundary flux of eddy potential energy across 89W, due to advection by the background flow. This energy

boundary flux is mostly governed by Loop Current intrusions and westward propagation of LC eddies. Within the basin interior, baroclinic energy transfers redistribute mass horizontally, which drains the external supply of potential energy to fed the mean and eddy horizontal flows. Bands of weak rectification in the mean flow are driven in surface and sub-surface waters by the fluctuating pressure field along the margins of the Gulf of Mexico. However, the boundary mean flows are mostly increased in response to the pressure field created by those perturbations, rather than by energy supply. The results of this investigation indicate that the Western Boundary Current along the Mexican coast is mostly driven at surface and sub-surface waters by a perturbation pressure field sustained by the recirculating Western Anticyclone, which apparently is sustained by incoming LCR. At deeper waters, perturbations with characteristics of topographic Rossby waves are superimposed on the background flow, and the energy exchange between the two flow forms is not apparent. Therefore, TRWs cannot be accounted for driving the mean deep cyclonic flow in the model. Finally, the LC eddies are the main source of eddy kinetic energy for the western Gulf of Mexico, whereas TRWs were a secondary source. At mid-depths, local sources of eddy kinetic energy develop in the western Gulf as a result of baroclinic energy transfers.

Bibliography

Andrews, D.G. (1990), On the forcing of time-mean flows by transient, small-amplitude eddies, *J. Atmos. Sci., 47*, 1837-1844.

Böning, C.W., and R.G. Budich (1992), Eddy dynamics in a primitive equation model: sensitivity to horizontal resolution and friction, *J. Phys. Oceanogr., 22*, 361-381.

Bleck, R. (1978), Finite-difference equations in generalized vertical coordinates. Part I: Total energy conservation, *Contrib. Atmos. Phys., 51*, 360-372.

Bleck, R. (1985), On the conversion between mean and eddy components of potential and kinetic energy in isentropic and isopycnic coordinates, *Dyn Atmos. Oceans, 9*, 17-37.

Bleck, R., and D.B. Boudra (1986), Wind-driven spin up in eddy-resolving ocean models formulated in isopycnic and isobaric coordinates, *J. Geophys. Res.*, 91, 7611-7621.

Bleck, R., and E.P. Chassignet (1994), Simulating the oceanic circulation with isopycnic-coordinate models, in *The Oceans: Physical-Chemical Dynamics and Human Impact*, S.K. Majumdar, E.W. Miller, G.S. Forbes, R.F. Schmalz, and A.A. Panah, Eds., The Pennsylvania Academy of Science, 17-39.

Blumberg, A.F., and G.L. Mellor (1987), A description of a three-dimensional coastal ocean circulation model, in *Three-Dimensional Coastal Ocean Models*, Vol. 4, edited by N. Heaps, pp. 208, American Geophysical Union, Washington, D.C.

Bower, A.S., and N.G. Hogg (1992), Evidence for barotropic wave radiation from the Gulf Stream, *J. Phys. Oceanogr., 22*, 42-61.

Bunge, L., J. Ochoa, A. Badan, J. Candela, and J. Sheinbaum (2002), Deep flows in the Yucatan Channel and their relation to changes in the Loop Current extension, *J. Geophys. Res., 107*(C12), 3233, doi:10.1029/2001JC001256.

Bryan, K. (1963), A numerical investigation of a nonlinear model of a wind-driven ocean, *J. Atmos. Sci., 20*, 594-606.

Brooks, D.A., and R.V. Legekis (1982), A ship and satellite view of hydrographic features in the western Gulf of Mexico, *J. Geophys. Res., 87*(C6), 4195-4206.

Candela, J., J. Sheinbaum, J.L. Ochoa, A. Badan and R. Leben (2002), The potential vorticity flux through the Yucatan Channel and the Loop Current in the Gulf of Mexico, *Geophys. Res. Lett., 29*(22), doi:10.1029/2002GL015587.

Cessi, P.R., G. Ierley, and W. Young (1987), A model of the inertial recirculation driven by potential vorticity anomalies, *J. Phys. Oceanogr., 17*, 1640-1652.

Cochrane, J. D. (1966), The Yucatan Current, *Tech. Report 66-23*, Dept. of Oceanogr., Texas A&M Univ., 14-25.

Cushman-Roisin, B., E.P. Chassignet, and B. Tang (1990), Westward motion of mesoscale eddies, *J. Phys. Oceanogr., 20*, 758-768.

Chassignet, E.P., and D.B. Boudra (1988), Dynamics of Agulhas retroflection and ring formation in a numerical model. Part II. Energetics and ring formation, *J. Phys. Oceanogr., 18*, 304-319.

Chassignet, E.P., and P.R. Gent (1991), The influence of boundary conditions on midlatitude jet separation in ocean numerical models, *J. Phys. Oceanogr., 21*, 1290-1299.

Chassignet, E.P., L.T. Smith, R. Bleck, and F.O. Bryan (1996), A model comparison: Numerical simulations of the North and equatorial Atlantic oceanic circulation in depth and isopycnic coordinates, *J. Phys. Oceanogr., 26*, 1849-1867.

Chérubin, L.M., W. Sturges, and E.P. Chassignet (2005), Deep flow variability in the vicinity of the Yucatan Straits from a high-resolution numerical simulation, *J. Geophys. Res., 110*, C04009, doi:10.1029/2004JC002280.

DeHaan, C.J., and W. Sturges (2004), Deep cyclonic circulation in the Gulf of Mexico, *J. Phys. Oceanogr.*, in press.

Dewar, W.K., and G.R. Flierl (1987), Some effects of the wind on rings, *J. Phys. Oceanogr., 17*, 1653-1667.

Elliot, B.A. (1979), *Anticyclonic rings and the energetics of the circulation of the Gulf of Mexico*, PhD Dissertation, 188 pp. Tex. A&M Univ., College Station, Texas.

Elliott, B.A. (1982), Anticyclonic rings in the Gulf of Mexico, *J. Phys. Oceanogr., 12*(11), 1292-1309.

Gill, A.E. (1982), *Atmosphere-Ocean Dynamics*, Academic Press, pp. 662.

Hallberg, R. (2000), Time integration of diapycnal diffusion and Richardson number-dependent mixing in isopycnal coordinate ocean models, *Mon. Wea. Rev., 128*, 1402-1419.

Hamilton, P. (1990), Deep currents in the Gulf of Mexico, *J. Phys. Oceanogr., 20*(7), 1087-1104.

Harrison, D.E. (1979), Eddies and the general circulation of numerical model gyres: An energetic perspective, *Rev. Geophys. Space Phys., 17*, 969-979.

Harrison, D.E., and A.R. Robinson (1978), Energy analysis of open regions of turbulent flows-mean eddy energetics of a numerical ocean circulation experiment, *Dyn. Atmos. Oceans., 2*, 185-211.

Hofmann, E.E., S.J. Worley (1986), Circulation of the Gulf of Mexico, *J. Geophys. Res., 91*(C12), 14221-14236.

Holland, W.R., and L.B. Lin (1975), On the generation of eddies and their contribution to the oceanic general circulation, *J. Phys. Oceanogr., 5*, 642-669.

Holton, J.R. (1992), *An Introduction to Dynamic Meteorology*, 3rd Edition, Academic Press, pp. 335-343.

Hurlburt, H.E., and J.D. Thompson (1980), A numerical study of loop current intrusion and eddy shedding, *J. Phys. Oceanogr., 10*, 1611-1651.

Hurlburt, H.E., and J.D. Thompson (1982), The dynamics of the Loop Current and shed eddies in a numerical model of the Gulf of Mexico, In *Hydrodynamics of semi-enclosed Seas*, Amsterdam, New York: Elsevier. J.C.J. Nihoul(ed.), 243-298.

Ichiye,T. (1962), Circulation and water-mass distribution in the Gulf of Mexico, *Geofisica Internl., 2*, 47-76.

Johns, W.E., T.L. Townsend, D.M. Fratantoni. and W.D. Wilson (2002), On the Atlantic inflow to the Caribbean Sea, *Deep Sea Res., 49*, 211-243.

Levitus, S. (1982), Climatological atlas of the world ocean, *NOAA Prof. Pap., 13*, U.S. Govt. Print. Off., Washington, D. C.

Lewis, J.K., and A.D. Kirwan (1985), Some observations of ring topography and ring-ring interactions in the Gulf of Mexico, J. Geophys. Res., 90(C5), 9017-9028.

Maul, G.A. (1977), The annual cycle of the Gulf Loop Current, Part I: Observations during a one-year time series, *J. Mar. Res., 35*, 29-47.

Mellor, G.L. (2003), *A three-dimensional, primitive equation, numerical ocean model*, Users Guide, 53 pp., Princeton University, Princeton, NJ.

Merrell, W.J., Jr., and A. Vásquez (1983), Observations of changing mesoscale circulation patterns in the western Gulf of Mexico, *J. Geophys. Res., 88*(C12), 7721-7723.

Molinari, R.L., J.F. Festa, and D.W. Behringer (1978), The circulation in the Gulf of Mexico derived from estimated dynamic height fields, *J. Phys. Oceanogr., 8*, 987-996.

Murphy, S.J., H.E. Hurlburt, and J.J. O'Brien (1999), The connectivity of eddy variability in the Caribbean Sea, the Gulf of Mexico and the Atlantic Ocean, *J. Geophys. Res., 104*, 1431-453.

Nof, D., and T. Pichevin (2001), The ballooning of outflows, *J. Phys. Oceanogr., 31*, 3045-3058.

Oey, L.-Y. (1996), Simulation of mesoscale variability in the Gulf of Mexico: sensitivity studies, comparison with observations, and trapped wave propagation, *J. Phys. Oceanogr., 26*, 145-175.

Oey, L.-Y., H.-C. Lee, and W.J. Schmitz Jr. (2003), Effects of winds and Caribbean eddies on the frequency of Loop Current eddy shedding: A numerical model study, *J. Geophys. Res., 108*(C10), 3324, doi:10.1029/2002JC001698.

Pedlosky, J. (1987), *Geophysical Fluid Dynamics*, 2nd Ed., Springer, pp. 374.

Pedlosky, J. (1996), *Ocean Circulation Theory*, 1st Ed., Springer, pp. 453.

Pedlosky, J. (2003), *Waves in the Ocean and Atmosphere. Introduction to Wave Dynamics*, Springer, pp. 260.

Pichevin, T., and D. Nof (1997), The momentum imbalance paradox, *Tellus, Ser. A, 49*, 298-319.

Plumb, R.A. (1983), A new look at the energy cycle, *J. Atmos. Sci., 40*, 1669-1688.

Plumb, R.A., and R. Ferrari (2005), Transformed eulerian-mean theory. Part I: nonquasi-geostrophic theory for eddies on a zonal-mean flow, *J. Phys. Oceanogr., 35*, 165-174.

Rhines, P. (1977), The dynamics of unsteady currents, In *The Sea*, E.N. Goldberg, Ed., *6*, Wiley-Interscience, 189-318.

Rhines, P., and W.R. Holland (1979), A theoretical discussion of eddy-driven mean flows, *Dyn. Atmos. Oceans, 3*, 289-325.

Robinson, A.R., D.E. Harrison, Y. Mintz, and A.J. Semtner (1977), Eddies and the general circulation of an idealized oceanic gyre: A wind and thermally driven primitive equation numerical experiment, *J. Phys. Oceanogr., 7*, 182-207.

Romanou, A., E.P. Chassignet, and W. Sturges (2004), The Gulf of Mexico circulation within a high-resolution numerical simulation of the North Atlantic, *J. Geophys. Res., 109*, C01003, doi:10.1029/2003JC001770.

Schmitz, W. J., Jr. (1996), On the World Ocean circulation: Volume I, Some Global Features/North Atlantic Circulation, *Tech. Report WHOI-96-03*, 150 pp., Woods Hole Ocean. Inst.

Schmitz, W.J., Jr., and P.L. Richardson (1991), On the sources of the Florida Current, *Deep Sea Res., Part A, 38*, supp. 1, S379-S409.

Sheinbaum, J., J. Candela, A. Badan, and J. Ochoa (2002), Flow structure and transport in the Yucatan Channel, *Geophys. Res. Let., 29*(3), doi:10.1029/2001GL013990.

Smith, D.C., IV (1986), A numerical study of Loop current eddy interaction with topography in the western Gulf of Mexico, *J. Phys. Oceanogr., 16*(7), 1260-1272.

Sturges, W. (1993), The annual cycle of the western boundary current in the Gulf of Mexico, *J. Geophys. Res., 98*(C10), 18053-8068.

Sturges, W., and J.P. Blaha (1976), A western boundary current in the Gulf of Mexico, *Science, 192*, 367-369.

Sturges, W., and R. Leben (2000), Frequency of ring separations from the Loop current in the Gulf of Mexico: A revised estimate, *J. Phys. Oceanogr., 30*(7), 1814-1819.

Sturges, W., E.P. Chassignet, and T. Ezer (2004), Strong mid-depth currents and a deep cyclonic gyre in the Gulf of Mexico. *OCS Report, MMS-2004-40*, U.S. Department of the Interior, Minerals Management Service, Gulf of Mexico OCS region.

Sturges, W., J.C. Evans, S. Welsh, and W. Holland (1993), Separation of warm-core rings in the Gulf of Mexico, *J. Phys. Oceanogr., 23*(2),250-268.

Vázquez de la Cerda, A.M. (1993), *Bay of Campeche cyclone*, Ph.D. Dissertation, 91 pp., Texas A&M Univ., College Station.

Vidal, V.M.V., F.V. Vidal, and J.M. Perez-Molero (1992), Collision of a Loop current anticyclonic ring against the continental shelf slope of the western Gulf of Mexico, *J. Geophys. Res., 97*(C2), 2155-2172.

Vidal, V.M.V., F.V. Vidal, E. Meza, J. Portilla, L. Zambrano, and B. Jaimes (1999), Ring-slope interactions and the formation of the western boundary current in the Gulf of Mexico, *J. Geophys. Res., 104*(C9), 20523-20550.

Welsh, S.E., and M. Inoue (2000), Loop Current rings and the deep circulation in the Gulf of Mexico, *J. Geophys. Res., 105*(C7), 16951-16959.

Wienders, N., A. Romanou, and G. Weatherly (2004), Intermediate-depth circulation in the Gulf of Mexico, *AGU Monograph on circulation in the Gulf of Mexico*, submitted.